Ti(IV) TUNGSTOMOLYBDATE CATION EXCHANGER: APPLICATIONS TO BINARY SEPARATION OF HEAVY METALS, PHOTOCATALYSIS, AND ANTIBACTERIAL ACTIVITIES

MSc THESIS

FEYERA GEDEFA BULTO

AUGUST 2018

HARAMAYA UNIVERSITY, HAREMAYA

Ti(IV) Tungstomolybdate Cation Exchanger: Applications to Binary Separation of Heavy Metals, Photocatalysis, and Antibacterial Activities

A Thesis Submitted to the Department of Chemistry, Postgraduate Program Directorate

HARAMAYA UNIVERSITY

In Partial Fulfillment of the Requirements for the Degree of

MASTER OF SCIENCE IN CHEMISTRY

Feyera Gedefa Bulto

August 2018

Haramaya University, Haramaya

HARAMAYA UNIVERSITY
POSTGRADUATE PROGRAM DIRECTORATE

I hereby certify that I have read and evaluated this Thesis entitled "Titanium(iv) tungsto-molybdate Cation Exchanger: Applications to Binary Separation of Heavy Metals, Photocatalysis and Antimicrobial Activities " prepared under my guidance by Feyera Gedefa. I recommend that it be submitted as fulfilling the thesis requirement.

Abi Taddesse (PhD)	_____	_____
Major Advisor	Signature	Date
Endale Teju (PhD)	_____	_____
Co-Advisor	Signature	Date

As a member of the Board of examiners of the MSc Thesis Open defense examination, I certify that I have read and evaluated the Thesis prepared by Feyera Gedefa and examined the candidate. I recommend that the thesis be accepted as fulfilling the Thesis requirement for the degree of Master of Science in Chemistry.

_____	_____	_____
Chairperson	Signature	Date
_____	_____	_____
Internal Examiner	Signature	Date
_____	_____	_____
External Examiner	Signature	Date

Final approval and acceptance of the Thesis is contingent upon the submission of its copy to the council of Graduate studies (CGS) through the candidate's department or school graduate committee (DGC and SGC).

DEDICATION

This manuscript is dedicated to my beloved families for nursing me with affection and love and for their dedicated partnership in the success of my life.

STATEMENT OF THE AUTHOR

By my signature below, I declare and affirm that this thesis is my own work. I have followed all ethical and technical principles of scholarship in the preparation, data collection, data

analysis and compilation of this Thesis. Any scholarly matter that is included in the Thesis has been given recognition through citation.

This Thesis is submitted in partial fulfillment of the requirement for Master of Science (MSc.) degree at the Haramaya University. The Thesis is deposited in the Haramaya University Library and is made available to borrowers under the rules of the Library. I solemnly declare that this Thesis has not been submitted to any other institution anywhere for the award of any academic degree, diploma, or certificate.

Brief quotations from this Thesis may be made without special permission provided that accurate and complete acknowledgement of source is made. Requests for permission for extended quotation from or reproduction of this thesis in whole or in part may be granted by the Head of the School or the Head of Chemistry Department when in his/her judgment the proposed use of the material is in the interest of scholarship. In all other instances, however, permission must be obtained from the author of the Thesis.

Name : Feyera Gedefa Bulto Signature : _____

Date of submission : August 2018

Place: Chemistry Department

BIOGRAPHICAL SKETCH

The author was born on August 5, 1989 at watiyo kebele , Guduru Woreda, Horo Guduru Wollega Zone in Oromia Regional State. He attended his primary education at Watiyo Elementary School and secondary education at Ambo Comprehensive Senior Secondary School. Later, he joined Addis Ababa University in 2006 and graduated with BEd degree in Chemistry on July 17, 2008. Soon after his graduation, he was employed as Teacher at Adaba preparatory school, west Arsi Zone, in September 2009. He worked there for three years and

then joined School of Graduate studies at Haramaya University, College of Natural and Computational Sciences, Department of Chemistry in 2012 to pursue his MSc.

ACKNOWLEDGMENTS

First, I would like to offer thanks to the Almighty GOD, my LORD and SAVIOR. Once again I bless his Holly name for his plan in my life. I would like to express my deepest and truthful gratitude and respect to my major advisor Dr. Abi Tadesse for his significant observations and direction, invaluable advice, guidance, continuous supervision, encouragement and assistance that greatly encouraged me to accomplish this thesis work. My appreciation and gratitude also go to my co-advisor, Dr. Endale Teju, for his significant observations, direction and

enthusiastic assistance and guidance that he had provided for the successful completion of this thesis work.

I would like to give great respect and thanks to Dr. Ephrem Tadesse (from H.U) for his permission to characterize the as-synthesized sample by PL in his research laboratory. My sincere thanks are also due to Mr. Fituma Diriba who arranged to me an apparatus during the course of this research work. Successfully and timely accomplishment of this study would have been difficult without his cooperation.

I sincerely and gratefully acknowledge the Addis Ababa University, Department of Chemistry for characterization of the material with respect to X-ray Diffractometer (XRD) and Fourier Transform Infrared Spectrometer (FTIR) analysis.

I also appreciate the Haramaya University Laboratory Management Unit for their genuine cooperation that ascertained the accomplishment of all laboratory related works. I am also grateful to Haramaya University, Department of Chemistry for hosting me and Ministry of Education (MOE) for giving me the opportunity to pursue my MSc. and for funding this research work. Lastly, but not least, I would like to thank my family and friends for their support and encouragement throughout my life.

ACRONYMS AND ABBREVIATIONS

ANOVA	Analysis of Variance
BET	Brunauer-Emett-Teller
CB	Conduction Band
CEC	Cation Exchange Capacity
DSC	Differential Scanning Calorimetry
DIW	Deionized water
DMF	Dimethyl Formamide
DMSO	Dimethyl Sulfoxide
DTA	Differential Thermal Analy0sis

EDTA	Ethylene Diammine Tetraacetic Acid
EDX	Energy dispersive x-ray spectroscopy
Eg	Band Gap Energy
EHP	Electron-hole pair recombination
Ev	Electron-Volts
FTIR	Fourier Transform Infrared Spectrometer
FWHM	Full width half maxima
HS&E	Health Safety and Environment
ICP-AES	Inductively Coupled Plasma-Atomic Emission Spectroscopy
ICP-OES	Inductively Coupled Plasma-Optical Emission Spectroscopy
IEC	Ion Exchange Capacity
IIE(s)	Inorganic Ion Exchanger(s)
MB	Methylene Blue
MHA	Mueller Hinton Agar
MOE	Ministry of Education
NF	Nanofiltration
NPs	Nanoparticles
PL	Photoluminescence
PZC	Point of zero charge
R&D	Research and Development
SD	Standard deviation
SEM	Scanning Electron Microscope
STARA	Society for Technology and Action for Rural Advancement

ACRONYMS AND ABBREVIATIONS(continued)

TGA	Thermo Gravimetric Analysis
TMA	Tetra Metal Acid
TTM	Ti(IV) tungstomolybdate
UV	Ultra Violet
UV-Vis	Ultraviolet-Visible
VB	Valance Band
VIS	Visible-Light
WM	Tungstomolybdate
XRD	X- Ray Diffractometer
XRF	X-ray fluorescence

TABLE OF CONTENTS

LIST OF TABLES

Table

page

LIST OF FIGURES

F i g u r e

Page

LIST OF TABLES IN APPENDIX

Appendix Table

Page

LIST OF FIGURES IN APPENDIX

Appendix Figure

Page

Ti(IV) TUNGSTOMOLYBDATE CATION EXCHANGER: APPLICATIONS TO BINARY SEPARATION OF HEAVY METALS, PHOTOCATALYSIS AND ANTIBACTERIAL ACTIVITIES

ABSTRACT

In this work, nano-titanium(IV) tungstomolybdate cation exchanger has been synthesized via sol-gel approach under varying mixing volume ratio (i.e. 2:1:2:3) *with respect to titanium isopropoxide ($(Ti(OCH(CH_3)_2)_4$ in 250 mL of ethanol, 1 mL of concentrated HCl and 2 mL of deionized water), sodium tungstate dihydrate, sodium molybdate dihydrate and urea(NH_2CONH_2) respectively. The samples were calcined at various temperatures: 300 ^0C, 400 ^0C, 500 ^0C and 600 ^0C for 3 h. The sample that was calcined at 600 ^0C showed the maximum ion exchange capacity, IEC (1.34 meq.g^{-1}) with particle size (41.35 nm) and thus selected for the entire study. Physical characterization of nano-titanium (IV) tungstomolybdate: crystal structure, functional groups, band gap energy, and optical properties of the photocatalyst were done by using XRD, FTIR, Uv-vis and PL instruments, respectively. The specific surface area of the cation exchanger was found to be 4.416 ± 0.003 m^2/g as calculated by the Brunauer Emmett-Teller (BET) method. Based on separation factor*

α, binary separations have been carried out for four sets of metal ions: Pb(II)−Ni(II), Pb(II)−Cu(II), Cr(III)−Ni(II) and Cr(III)−Cu(II). Photocatalytic activities and antimicrobial activities of nano-titanium(IV) tungstomolybdate were evaluated using Methylene blue as a model organic pollutant and Gram-negative and Gram-positive bacteria as test microbes respectively. The effect of pH, initial dye concentration, catalyst load and scavengers on the active sites were evaluated using photocatalytic degradation of TTM with optimum mixing volume ratio of 2:1:2:3 indicating the highest value of IEC (i.e. 1.34 meq.g^{-1}). *At the optimum pH = 8, degradation efficiency is 60 %, for optimum initial dye concentration 10ppm, extent to 57.14 % and for optimum catalst load 0.1g, extent to 57.14 %. Effect of scavengers also assure an important species in the degradation process would be (·O_2^-) hole (h^+) and hydroxyl radical (·OH). The sequence of antibacterial efficiency of nano-Ti(IV) tungstomolybdate exchanger for both Gram negative and Gram-positive bacteria was found to be 150 μg/mL > 100 μg/mL > 50μg/mL.* The antibacterial activities of the exchenger is relatively low as compared to the reference drug, Chloramphnicol.

Key words: Cation exchanger, distribution-coefficient, homogeneous precipitation, ion exchenge capacity, nano-titanium(IV) tungstomolybdate, photocatalysis, antimicrobial activities.

1. INTRODUCTION

Heavy metal pollution of water and soil is known to adversely affect the ecology causing health hazards in humans. Unlike organic contaminants, heavy metals are not biodegradable and tend to accumulate in living organisms having toxic or carcinogenic effects. A number of these toxic heavy metals have been discharged to the environment as industrial wastes, causing serious soil and water pollution. Major contributors to environmental pollution with toxic metals are released from anthropogenic sources such as metal plating facilities, mining operations, fertilizer industries, tanneries, batteries, paper industries, pesticides, power regeneration and electronic industries (Bamlaku *et al*., 2016).

Several methods, such as chemical precipitation, electrolysis, membrane separation, and ion exchange are available to remove toxic metals from aqueous waste streams. Among the heavy metal removal processes, ion exchange process is an effective to remove various heavy metals and can be easily recovered and reused by regeneration operation. Thus, it is probably one of the most attractive processes and, consequently, the one commonly used in industry, because of its simple and efficient application as well as cost effectiveness. Inorganic ion exchangers, due to their properties such as chemical and thermal stability, resistance to oxidation, unique selectivity to certain ions, have definite advantages over the well known and traditionally used organic resins. Moreover, inorganic ion exchangers also have advantage in that they have a little tendency to swell in contact with water (Bezabih *et al.,* 2017). Apart from ion exchange applications, nanocrystalline ion exchangers are also being advocated for their sensing, photocatalytic and antimicrobial applications (Pathania *et al.,* 2014).

Large quantities of colored dye effluents discharged from manufacturing and processing in the textile industry, create severe environmental pollution problems due to their negative impact on photosynthetic activity (Zainal *et al*., 2005). Additionally, variety of a wide organic pollutants especially pesticides and dyes are introduced into the water system from various sources such as industrial effluents, agricultural runoff and chemical spills (Cohen *et al*., 1986; Muszka *et al*., 1994). Their toxicity, stability to natural decomposition and persistence in the environment has been the cause of much concern to the societies and regulation authorities around the world. Recently, due to the rapid development of the textile industry more and more new types of dye have been produced, such as methylene blue (Tang

et al., 2003; Jian-xiao *et al.*, 2011). Methylene blue (MB) is one of the thiazine dyes which is hard to be degraded, and it usually acts as the model object of photocatalytic degradation with TiO_2 (Tang *et al.,* 2003) and has harmful effects on living things. For example, during inhalation, it can give rise to short periods of rapid or difficult breathing, while ingestion through the mouth produces a burning sense Caution and may cause nausea, vomiting, diarrhea and gastritis (Abdullah *et al.,* 1990). Therefore, decolorization and detoxicity of these dyes containing effluents have received increasing attention. Conventional methods used to treat dye effluents are classified as physical, biological or chemical methods (Robinson *et al.,* 2001) each having its own drawbacks. Physical methods such as chemical or electro-flocculation, reverse osmosis and adsorption are not destructive and mainly create pollutant concentrates. Activated sludge process does not work efficiently due to high solubility of synthetic dyes and their resistance to aerobic degradation. Furthermore dyes, although not directly toxic, may generate carcinogenic compounds such as aromatic amines from azo dyes during their anaerobic treatment (Ledakowicz *et al.,* 1999). Thus, new treatment methods such as photocatalysis are necessary for the removal of persistent dye chemicals or converting them into harmless compounds in water.

Several semiconducting materials such as TiO_2 (Kiros *et al.,* 2013) and ZnO (Tesfay *et al.,* 2013) in various modifications such as doping (Nibret *et al.,* 2015), coupling (Tedla *et al.,* 2015) and a combination of doping and coupling (Gebru, 2013) have been employed as heterogeneous photocatalysts for degradation of dyes. The use of ion exchangers for photocatalytic application is a recent phenomenon. A number of composite (Gupta *et al.,* 2013; Bushra *et al.,* 2014; Sharama *et al.,* 2014; Akhtar *et al.,* 2015; Pathania *et al.,* 2015) exchangers have therefore been used for this purpose in the last five years. Although relatively good number of reports have been witnessed on the use of the organic-inorganic composite exchangers for photocatalytic applications, similar reports on their inorganic congeners is scant. We reported very recently on the synthesis and characterization of a new inorganic cation exchanger, nano-crystalline titanium(IV) tungstomolybdate cation exchanger for ion exchange applications. The exchanger demonstrated a good ion exchange capacity towards Pb(II), Cr(III) and UO_2^{2+} cations. However up to now no information is available on the application of this exchanger for binary separation of heavy metals, photocatalysis and antimicrobial activities.

Resistance to antibiotics is one of the biggest problems that faces public health (Byarugaba, 2004; Okeke *et al.,* 2005). This problem is a natural consequence of the adaption of infectious pathogens to antimicrobials used in several areas (Bloomfield, 2002; McEwen *et al.,* 2002; Vidaver, 2002; Wise *et al*., 2002). Bacteria have developed resistance to all known antibiotics and, as so, the economic burden associated with these multidrug resistant bacteria is high. In order to find novel antimicrobial agents with new modes of action, photocatalyzed nanomaterials have been explored as sources for the identification of new and effective antimicrobials. Photocatalyzed nanomaterials have received an increasing attention as the treatment methods to inhibit or damage microbial membrane structures and modify bacterial membrane surface. Thus antibacterial activity of titanium(IV) tungstomolybdate nanomaterial with different concentrations was studied against two Gram-positive bacteria(Staphylococcus aureus and streptococcus) and two Gram-negative bacteria (Escherchia coli and salmonella thyphei).

General Objective

To evaluate the photocatalytic and antimicrobial efficiency of Ti(IV) tungstomolybdate Cation-exchanger under visible radiation.

Specific Objectives

- To synthesize nanosized Ti(IV) tungstomolybdate (TTM) *via* sol-gel approach.
- To characterize the as-syntheized TTM Cation-exchanger using XRD, BET FTIR, UV/Vis, SEM-EDX, and PL techniques.
- To evaluate the separation efficiency of Pb(II) and Cr(III) from synthetic binary mixtures of other metal ions.
- To study the photocatalytic degradation and Antimicrobial activity of TTM towards methylene blue and selected microbes, respectively.
- To study the effect of methylene blue initial dye concentration, pH and amount of photocatalyst on photocatalytic activities of Ti(IV) tungstomolybdate (TTM) Cation exchanger for photodegradation of methylene blue.

2. LITERATURE REVIEW

The removal and recovery of toxic/heavy metals is an area of current interest and challenging task for the environmentalists. Major objectives for the removal of metals from aqueous solutions are toxicity removal which entails an environmental aspect and recovery of valuable metals which involves a technological aspect (Thakkar and Chudasama, 2009). Methods such as ion exchange, solvent extraction, reverse osmosis, precipitation and adsorption have been proposed for treatment of wastewater contaminated with heavy metals (Gupta *et al*., 2005). All these approaches have their inherent advantages and limitations. Although filtration and chemical precipitation are low cost and effective in removing large quantities of metal ions quickly, none is capable of removing these at trace levels. Adsorption is also ineffective at very low concentrations (Moller, 2002). Recently, due to its simple and efficient application, ion exchange has been remarkably extended by the invention and application of new organic and inorganic ion exchangers (Zhang *et al*., 2008).

2.1. Ion Exchange Theory

A description of ion exchange process can be cited in the most ancient literature following a paragraph written in Holy Bible. In the Old Testament scribes which says “Moses succeeded in preparing drinking water from brackish water by an ion exchange method” (Exodus 15v25). Nowadays the ion exchange has come to be recognized as an extremely valuable technique. Ion exchange is a process in which an insoluble (or immiscible) material, when comes in contact with an electrolyte solution takes up stoichiometrically ions of positive or negative charge and release other ions of like charge from the exchanger phase into the solution phase. Carriers of these exchangeable ions are called "Ion Exchangers" (Chand *et al*., 2011). Ion exchange was originally discovered in naturally occurring materials such as soils, clays and zeolites. These materials found application as water softeners, but the first commercially available inorganic ion exchangers were amorphous aluminium silicate gels. In spite of their low cost, their industrial use was often difficult (impurities, bad physical properties for packed bed operations) and they sometimes need a chemical or thermal pretreatment. This led to

development and synthesis of organic ion exchange resins in 1930's. However, extensive studies on the synthetic inorganic ion exchangers have proved their potential in solving diverse problems of environmental and analytical chemistries (AbdEl-Latif and El Kady, 2008).

2.1.1. Ion Exchange Processes

An ion exchange reaction may be defined as the reversible interchange of ions between a solid phase (the ion exchanger) and a solution phase, the ion exchanger being insoluble in the medium in which the exchange is carried out. Although ion exchangers comprise a very heterogeneous group of materials, their general structure has one common feature - a framework with surplus electric charge which can bind oppositely charged ions, as well as mobile (charge compensating) counter ions which can be exchanged for a stoichiometric amount of similarly charged ions. Exchangers carrying exchangeable cations (mobile) are called cation exchangers, while carriers of exchangeable anions are referred to as anion exchangers. Certain materials posses the ability to exchange both cations and anions and these are called amphoteric ion exchangers (Hendricks, 2005). If an ion exchanger M^-A^+, carrying cations A^+ as the exchanger ions, is placed in an aqueous solution phase containing B^+ cations, an ion exchange reaction takes place which may be represented by equation (1)

$$\underset{\text{Solid}}{M^- A^+} + \underset{\text{Solution}}{B^+} \leftrightarrows \underset{\text{Solid}}{M^- B^+} + \underset{\text{Solution}}{A^+} \qquad (1)$$

The equilibrium represented by the above equation is an example of cation exchange, where M^- is the insoluble fixed anionic complement of the ion exchanger M^-A^+, often called simply the fixed anion. The cations A^+ and B^+ are referred to as counter-ions, whilst ions in the solution which bear the same charge as the fixed anion of the exchanger are called co-ions. In much the same way, anions can be exchanged provided that an anion-receptive medium is employed. An analogous representation of an anion exchange reaction may be written (Dorfner, 1991):

$$\underset{\text{Solid}}{M^+A^-} + \underset{\text{Solution}}{B^-} \leftrightarrows \underset{\text{Solid}}{M^+ B^-} + \underset{\text{Solution}}{A^-} \qquad (2)$$

A schematic representation of the process of ion exchange is illustrated by Figure 1. A cation exchanger in the form of ‘A’ is placed in a solution of electrolyte ‘BY’. Counter-ions ‘A’ migrate from the exchanger into the solution, while counter ions ‘B’ migrate from the solution into the ion exchanger. Within a certain time span, ion-exchange equilibrium is attained, in which both the ion exchanger as well as the solution contains both counter-ion species ‘A’ and ‘B’. However, the pores of the ion exchanger are occupied not only by charge compensating ions(counter-ions), but also by solvent and ions (solutes) which may enter the pores when the ion exchanger is in contact with the solution. Solvent uptake may result in “swelling” of the ion exchanger while ion (solute) uptake is usually referred to as sorption (Hendricks, 2005*)*.

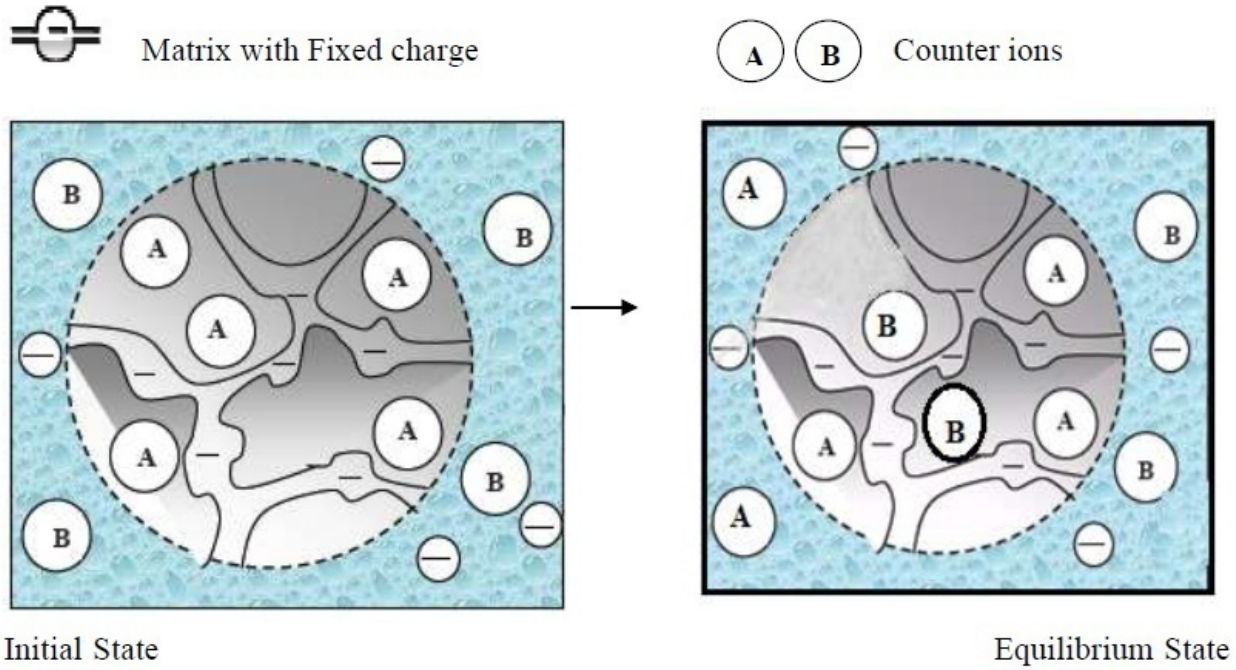

Figure 1. Schematic representation of ion exchange process within a solution. A cation exchanger containing counter ions ‘A’ is placed in a solution containing counter ions ‘B’(left). The counter ions are redistributed by diffusion until equilibrium is attained (right) (Helfferrich, 1962).

The unique characteristic properties of ion exchangers can be attributed to a distinctive feature in their structure. They consist of a framework, held together by chemical bonds or lattice energy and the framework carries a positive or negative electric surplus charge, which is compensated by ions of opposite sign, also referred to as counter-ions. The counter-ions are mobile thus able to move within the framework and can be replaced by other ions of the same sign. However, electro-neutrality must be preserved, *i.e.,* the electric surplus charge of the ion exchanger must be compensated at any time by a stoichiometrically equivalent number of counter-ions within the pores. A counter-ion can subsequently leave the framework, only when, simultaneously, another ion enters and takes over the task of contributing its share to the compensation of the framework charge (Helfferrich, 1962; Hendricks, 2005). The process of ion exchange can be carried out in a variety of ways with different main objectives (Hendricks, 2005):

- **Substitution:** A valuable ion can be recovered from solution and replaced by a valueless one. Similarly, a toxic ion (*e.g.*, mercury) can be removed from solution and replaced by a nontoxic ion.
- **Separation:** A solution containing a number of different ions passes through a column with beads of ion exchange resin. The ions are separated and emerge in order of increasing affinity for the resin.
- **Removal:** By using a combination of cation (in the H^+ form) and anion resin (in the OH^- form), all ions are removed and replaced by H^+ and OH^- ions, the solution is thus demineralized.

2.1.2. Classification and Properties of Ion Exchangers

By definition, ion exchangers are insoluble solid materials carrying exchangeable cations or anions, which can be exchanged stoichiometrically with equivalent amount of other ions of the same sign when the ion exchanger is in contact with an electrolyte solution. There are various natural and synthetic products exhibiting ion exchange properties, however, ion exchange materials comprise two main groups: organic and inorganic exchangers.

2.1.2.1. Organic ion exchange resins

Organic ion exchangers are broadly classified in to natural organic ion exchangers and synthetic organic resins. A large number of natural organic materials exhibit ion exchange properties. These include polysaccharides (such as cellulose, algic acid, straw and peat),

proteins (such as casein, keratin and collagen) and carbonaceous materials (such as charcoals, lignites and coals). Of these, only charcoals, coal, lignite and peat are used commercially. Although they exhibit a very low ion exchange capacity compared with synthetics, they are widely available at a very low cost. They are normally used as general sorbents, with their ion exchange properties being a secondary consideration (IAEA, 2002). The main limitations of natural organic ion exchangers include the followings.

- Their low exchange capacity compared with other materials,
- Their excessive swelling and tendency to peptize,
- The very limited radiation stability of cellulosic and protein materials,
- Their weak physical structures,
- Their non-uniform physical properties,
- They are non-selective,
- They are unstable outside a moderately neutral pH range.

2.1.2.2. Inorganic ion exchangers

Inorganic ion exchangers (IIE) are a vast field for study. They are supposed to contain ions that are exchangeable with others present in a solution in which it is considered to be insoluble (El-Naggar *et al*., 2007). Inorganic materials can act as ion exchangers if their structure bears an electrical surplus charge. This charge can be caused by two phenomena (Helfferich, 1962; Clearfield, 1982).

I. In the lattice M^{n+} ions are replaced by $M^{(n-1)+}$, which results in the ion of minor valence acquiring a negative charge. The charge has to be balanced by mobile cations (counter-ions).

II. Chemical groups are situated on the surface functional groups of inorganic exchangers which can be ionized due to protonation or de-protonation. The resulting electrical charges also have to be compensated by counter-ions. Amongst the synthetic inorganic ion exchangers, tetravalent metal acid (TMA) salts are gaining importance due to their excellent thermal stability and chemical resistivity. TMA salts materials with varying water content, composition, ion exchange capacity and crystallinity can be obtained by varying the synthesis

parameters such as stoichiometry and concentration of the reagents used, temperature at which they are mixed, rate of addition, mode of mixing and pH (Moller, 2002).

New mixed materials of this class with cation substitution are of interest since they show improved ion exchange properties and selectivity for particular metal ions in comparison to their single salt counter parts, because cation substitution alters the properties, composition and dimensions of the structure. It has been reported that the affinity of antimony silicate towards cesium can be improved by doping with Ti^{IV}, Nb^{V}, Mo^{VI} or W^{VI} in different mole ratios and it was found that cesium selectivity in acid increased with a ternary Sb-Si-W system (Moller, 2002). Preparation and characterization of sodium iron titanate ion exchanger and its application in heavy metal removal from waste waters has also been reported (Akieh *et al.*, 2008).

2.1.2.2.1. Natural inorganic ion exchangers

Natural inorganic exchangers can be classified into three main categories (Hendricks, 2005):

- zeolites, with reference to those found in nature, which falls under the banner of mineral ion exchangers;
- oxides and
- clay minerals, such as smectite clays: $Zr(HPO_4)_2 \cdot H_2O$, $Sn(HPO_4)_2 \cdot H_2O$.

Zeolites (aluminosilicates) are crystalline microporous silica based solids, which are used extensively in adsorption and catalytic processes (Sepehrian, 2010). Increasing the Al content gives a negative net charge to the framework, and by varying the Si/Al ratio, zeolites with different capacities and selectivities may be obtained.

The rigid three-dimensional structure, with cavities and tunnels of 4-7 Å in size, often acts as an ‘ion sieve’ and it structurally separates ions according to size (Moller, 2002). Natural zeolites such as clinoptilolite, chabazite and mordenite have been extensively studied for applications in nuclear and heavy metal waste treatment, and zeolites were the first materials to be used in large-scale processes to treat these wastes. They have also been used as water softeners in detergents (exchange of Ca^{2+} and Mg^{2+}) for many decades. Their ion exchange properties have been thoroughly investigated and the regular structures are well suited for many ion exchange modeling purposes (Fletcher and Townsend, 1981).

2.1.2.2.2. Synthetic inorganic ion exchangers

Synthetic inorganic ion exchange sorbents have been used more extensively in the past two decades. Synthetic ion exchanger may be classified in the following categories (Naushad, 2009):

- Polybasic acid salts
- Hydrous metal oxides
- Synthetic zeolites
- Metal ferrocynides
- Insoluble ion exchange materials and hetropolyacids.

They are distinguished by their greater thermal stability at elevated temperatures, resistance to high radiation fields and their selectivity to certain ions which are properties the organic resins tend to lack. They also have a high chemical stability and compatibility with final waste forms. Some of the inorganic ion exchangers have proved to have greater selectivity for trace radionuclides compared to organic ion exchangers, and much better operation over a wide pH range (Harjula and Lehto, 1987; Lehto *et al*., 1987; Leenen *et al*., 1996).

2.2. Background of Nanotechnology

Commercial interest in nanotechnology is growing exponentially across a range of industries. Many potential new users have little or no experience of handling nano materials, which can have very different physical and chemical properties from traditional chemicals (Anischik *et al*., 2008). Small and medium enterprises who wish to use nano technology may not have extensive Health Safety and Environment (HS&E) resources available in house. Separate but related to the above, there is a high level of interest in nanotechnology in both the popular and scientific press (Borisenko *et al.,* 2008). The general tenor is that nanotechnology offers major potential benefits but there is a lot we do not yet know from a human and environmental safety stand point. In net, it is very important that those wishing to deploy nanotechnology develop HS&E capability before moving ahead. Not only do they need to develop capability to ensure worker and environmental safety, they also need to be able to demonstrate capability to internal and external stakeholders including workers, shareholders and public interest groups.

This is an important aspect of Product Stewardship and miss-steps by a few companies could jeopardize the wider community's right to practice.

2.2.1. Nanomaterials

The term 'nanomaterial' is now frequently used for a variety of materials. It usually refers to materials with any external dimensions, or an internal structure, in the nanoscale or having internal structure or surface structure in the nanoscale that exhibit additional or different properties and behavior as compared to coarser materials with similar chemical composition. The term nanoscale refers to the size of the particles, with at least one dimension range from approximately 1 nm to 100 nm (Lovestam *et al*., 2010).

Nanophase materials can be organic or inorganic and essentially of any composition. Organic molecules in the nanometer dimension are the basis of life. The nanocrystalline materials can be zero (clusters), one (lamellar), two (filamentary) or three (equiaxed particles) dimensional in nature and can be obtained by a number of techniques (Sumej and Raveendran, 2008).

Intense research activity is seen in recent years in advancing the synthesis and functionalization of various sizes and shapes of semiconductor and metal nanoparticles. The most fundamentally important theme of this field is that the nanoscale building blocks, because of their sizes below about 100 nm, impart the new and improved properties and functionalities to the nanostructures created from them heretofore unavailable in conventional materials and devices. The reason for this is that materials in this size range can exhibit fundamentally new behavior when their sizes fall below the critical length scale associated with any given property. Thus, essentially any material property can be dramatically changed and engineered through the controlled size-selective synthesis and assembly of nanoscale building blocks (Hu *et al*., 1999). The exotic properties of nanoparticles have been considered in applications such asoptoelectronics, catalysis, photochemical and non-linear optical devices. Quite recently, nanoscale matter has been looked at with interest for potential applications in nanocomputers, synthesis of advanced materials for energy storage devices, chemical and biosensors as well as biomedical devices. They are also used as substrates for high temperature superconducting devices (Sumej and Raveendran, 2008). Research in nanostructured materials is motivated by the belief that ability to control the building blocks or nanostructure of the materials can result in enhanced properties at the macroscale: increased hardness, ductility, magnetic coupling, catalytic enhancement, selective absorption, or higher efficiency electronic or optical behavior (Kamat and Meisel, 2002). Every property has a critical length scale, and if a nanoscale

building block is made smaller than that critical length scale, the fundamental physics of that property starts to change. By altering the sizes of those building blocks, controlling their internal and surface chemistry, and controlling their assembly, it is possible to engineer properties and functionalities in unprecedented ways (Hu *et al*., 1999).

2.2.1.1. Nanotechnologies in the water sector

A range of water treatment devices that incorporate nanotechnology are already on the market, with others either close to market launch or in the process of being developed. Various examples of nanotechnology in water treatment and purification and detoxification are:

- Nanofiltration membranes
- Attapulgite clays, nonporous Zeolites, and nanoporous Polymers
- Nanoparticles for catalytic degradation of water pollutants
- Magnetic nano particles
- Nanosensors *etc* (STARA, 2010).

Nanofiltration (NF) membrane technology is widely applied for removal of dissolved salts *(i.e*., desalination) from salty (*i.e*., brackish) water, removal of micro pollutants (*e.g*., arsenic and cadmium), water softening (i.e., removal of Ca^{2+} and Mg^{2+} ions), and wastewater treatment. The main advantages of the membrane process for water treatment is that it does not require chemicals, requires relatively low energy, and is easy to operate and maintain. NF membranes using carbon nanotubes and alumina fibers are already being used to remove dissolved salts and micro-pollutants, soften water and treat wastewater (STARA, 2010).

The membranes act as a physical barrier, capturing particles and micro-organisms bigger than their pores, and selectively rejecting substances. NF water treatment plants typically consist of two types of treatment stages in series. These are the pre-treatment and membrane systems. The pre-treatment system removes particulate matter; in particular, suspended solids. The membrane removes some soluble substances and minute substances that were not rejected by the pre-treatment system. NF membranes selectively reject substances. The characteristic selectivity of NF has advantages because it enables the retention of nutrients present in water that are required for the normal functioning of the body. For example, calcium ions are

necessary for the healthy development of bones (Thembela *et al*., 2006). A study using attapulgite clay membranes to filter wastewater from a milk factory in Algeria has shown they can economically and effectively reduce whey and other organic matter in wastewater, making it safe to drink (Khider *et al*., 2004). Nanotechnology also utilizes the existence of nanoscopic pores in zeolite filtration membranes. Zeolites are microporous, aluminosilicates minerals commonly used as commercial adsorbents. They can be used to separate harmful organics from water and to remove heavy metal ions (STARA, 2010).

Nanocatalysts could make heavily polluted water fit for drinking, sanitation and irrigation. Nanocatalysts owe their better catalytic properties to their nanosize or to being modified at the nanoscale. They can chemically degrade pollutants instead of simply moving them somewhere else, including pollutants for which existing technologies are inefficient or prohibitively expensive. Immobilization is a good technique since it would keep water free of nanoparticles during and after water treatment. Researchers at the Indian Institute of Science, in Bangalore, are developing such a technique for degrading organic molecules using nano-titanium dioxide (Raichur, 2009). Magnetic nanoparticles can be used to bind with contaminants like arsenic or oil. Magnetic nanoparticles have large surface areas relative to their volume and can easily bind with chemicals. Then they can be removed using a magnet. Scientists at Rice University in the United States are using magnetic "nanorust" to remove arsenic from drinking water. Size 12nm particles can remove up to 99.2% arsenic from solution. They are developing a way of creating nanorust from inexpensive household items. This could significantly reduce production costs, making it a viable product for communities throughout the developing world (Yavuz *et al*., 2006). Nanosensors for the detection of contaminants and pathogens can improve health, maintain a safe food and water supply, and allow for the use of otherwise unusable water sources. They can detect single cells or even atoms, making them far more sensitive than counterparts with larger components. Detection technology for water purification would allow people to more quickly find out what the contaminants are, without having to send samples to laboratories for testing. Nanosensors, such as those based on titanium oxide nanowires or palladium nanoparticles are used for analytical detection of contaminants in water samples (STARA, 2010).

2.3. Principles of Photocatalysis

Photocatalysis is a reaction which uses light to activate a substance which modifies the rate of a chemical reaction without being involved itself. Photocatalysis is a process by which a

semiconductor material absorbs photon of energy equal to or greater than its band gap energy, there by generating electrons and holes at conduction and valence band, respectively, which can further generate free hydroxyl radicals in the system. The resulting free radicals are very efficient oxidizers of organic molecules (Pouretedal *et al*., 2009). The photocatalyst is the substance which can modify the rate of chemical reaction using light irradiation.

Dyes are important class of aquatic pollutants and are becoming a major source of environmental contamination. As the international environmental standards are becoming more stringent, many research studies have been focused on the treatment of colored wastewater. However, because of the complexity and variety of dyestuffs employed in the dyeing process, it has become rather difficult to find a unique treatment procedure that entirely covers the effective elimination of all types of dyes. Particularly, biochemical oxidation suffers from significant limitations since most dyestuffs commercially available have been intentionally designed to resist aerobic microbial degradation and are converted to toxic or carcinogenic compounds. Physical methods such as flocculation, reverse osmosis and adsorption on activated charcoal are non-destructive and merely transfer the pollutants to other media, thus causing secondary pollution (Belver *et al.,* 2006). Photocatalyst particles' band structure is composed of a low energy valence band (VB) filled with electrons and an empty high energy conduction band (CB), which are separated by forbidden band. When exposed to radiation of energy equal or more than the forbidden band gap, VB electrons on the surface may absorb the light energy to transit to the CB. Then the CB gets electrons with reducibility, and the VB produces holes possessing oxidizability. These electrons and holes can move to the surface of the catalyst under suitable light energy, and can react with other substances adsorbed at photocatalyst surface.

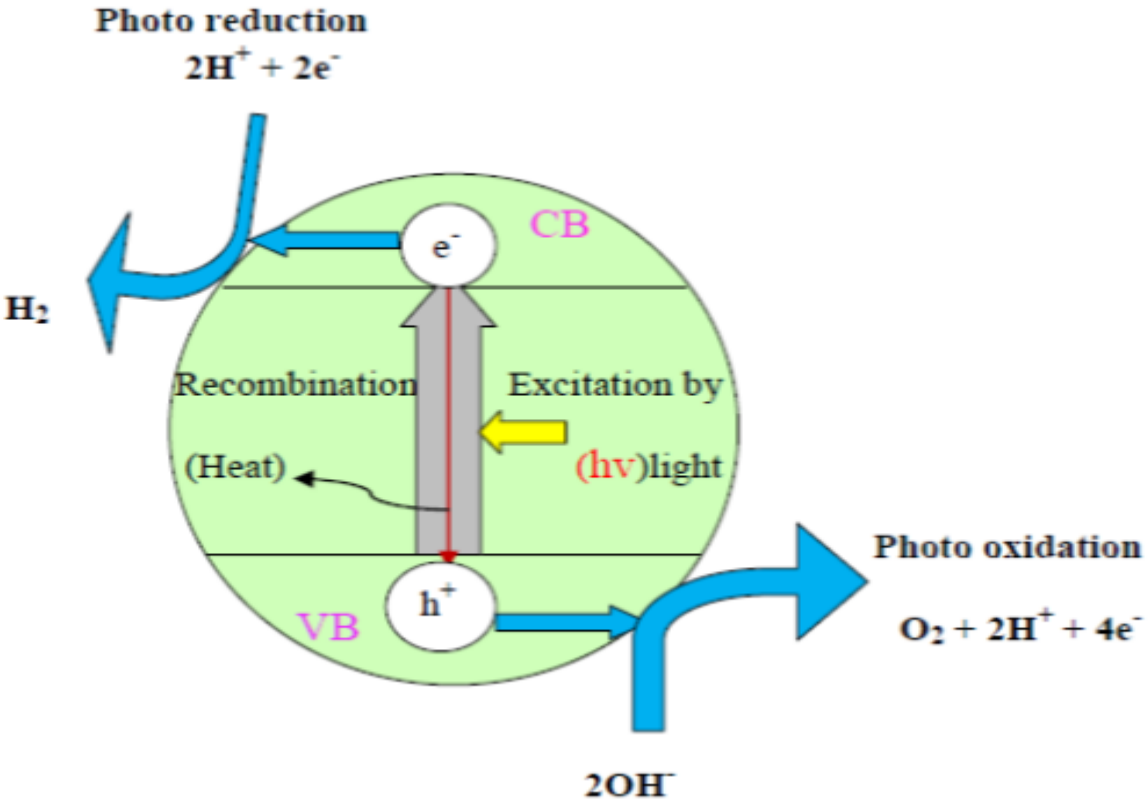

Figure 2. Schematic diagram of photocatalytic process initiated by photon acting on the semiconductor (Ahmed *et al*., 2010).

The absorption of photons with lower energy or longer wavelengths than band gap energy usually causes energy dissipation in the form of heat. The positive hole oxidizes either pollutant molecules directly or water to produce OH^- radicals, whereas the electron in the conduction band reduces free oxygen adsorbed on the surface of the photocatalyst (Ahmed *et al*., 2010). The activation of nanophotocatalyst by visible light can be represented by the following steps.

$$\textbf{Photocatalyst} + h\nu \rightarrow e^- \textbf{CB} + h^+ \textbf{VB} \qquad \textbf{(3)}$$

$$e^- CB + O_2 \rightarrow {}^{\bullet}O_2^- \quad (4)$$

$${}^{\bullet}O_2^- + H^+ \rightarrow HO_2^{\bullet} \quad (5)$$

$$2HO_2^{\bullet} \rightarrow H_2O_2 + {}^{\bullet}O_2 \quad (6)$$

$$H_2O_2 + hv \rightarrow 2\ {}^{\bullet}OH \quad (7)$$

Where, *hv* is photon energy required to excite the semiconductor photocatalyst electron from filled valence band (VB) to empty conduction band (CB). In this reaction, h^+ and e^- are powerful oxidizing and reducing agents, respectively. The oxidation and reduction steps are described below:

Oxidation Reaction:

$$h^+ + dye \rightarrow Dye^* \quad (8)$$

$$h^+ + H_2O \rightarrow {}^{\bullet}OH + H^+ \quad (9)$$

Reduction reaction:

$$Dye^* + {}^{\bullet}OH \rightarrow CO_2 + H_2O + \text{non toxic minerals} \quad (10)$$

In the degradation of organic pollutants, the hydroxyl radical which is generated from the oxidation of adsorbed water is the primary oxidant and the presence of oxygen at CB prevents the electron-hole pair recombination (Ahmed *et al*., 2010).

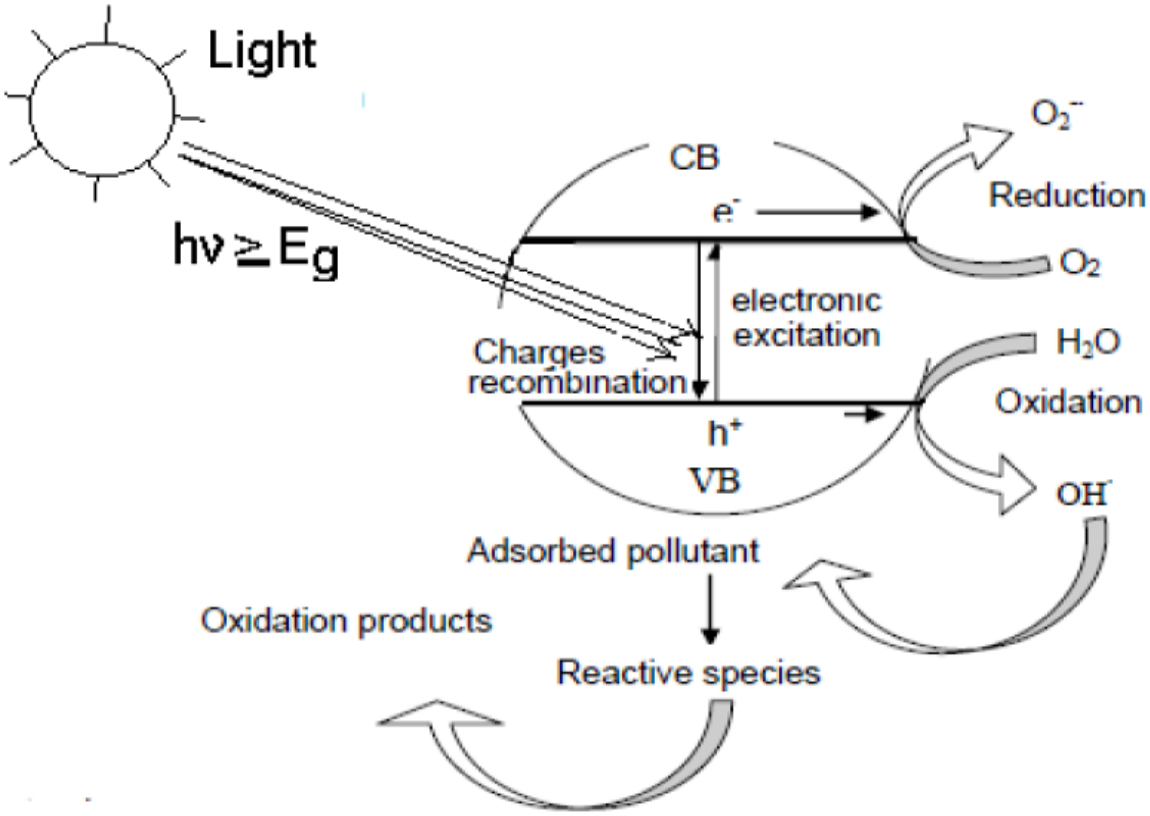

Figure 3. Schematic mechanism of photocatalytic degradation of organic dye by Ti(IV) tungstomolybdate under visible light.

2.3.1. Electron-Hole Pair Recombination

The absorption of a photon with sufficient energy of the catalyst leads to a charge separation due to promotion of an electron from valance band to the conduction band of the semiconducting materials. This excited electron in conduction band comeback across a band gap into the empty state represented by hole in the valence band (Linsebigler *et al*., 1995), this process is known as electron-hole pair recombination (EHP). Recombination of the photoexcited electron-hole pair needs to be retarded for an efficient charge transfer on the photocatalyst surface. Charge carrier trapping would be suppressing the recombination and

increase the lifetime of the separated electron and hole, which improve the photocatalytic efficiency (Jing *et al*., 2006; Hamadanian *et al*., 2010). The oxygen molecule over the TTM photocatalyst surface traps the electrons, that present in the conduction band (e^- CB) and generate the superoxide radical anion ($\cdot O_2^-$) which prevents the recombination of electron-hole pairs (Ilisz *et al*., 1997).

2.4. Methods of Synthesis of Nano-Inorganic Ion Exchanger Materials

Synthesis routes play a crucial role in preparing the target product and determining its properties. To obtain nano-crystalline powders with high homogeneity and uniform structure, many techniques have been provided (Rashad *et al*., 2009). There are so many kinds of processes related to soft solution processing, and the important ones are: sol-gel precipitation, co-precipitation, conventional solid state method, modified emulsion precipitation, hydrothermal technique, soft solution electrochemical process, liquid phase deposition, emulsions (aerogel methods), low temperature combustion methods, solvothermal, wet-chemical processing, templating, *etc* (Byrappa and Yoshimura, 2001). Generally, the first three techniques (sol-gel precipitation, co-precipitation and hydrothermal) were most frequently used for preparation of nano-inorganic materials (Abd El-Latif and El Kady, 2011).

2.4.1. Sol-gel Method

The sol-gel process also known as chemical solution deposition is a wet chemical technique widely used in the fields of materials science and ceramic engineering. This method is also one of the most popular processes for producing nanophotocatalyst. Over the years, solution precipitation and sol–gel processing have come to be used interchangeably, mostly by people on the fringes of the technical community. There are distinct differences between the two methods, as will be made clear below. Metal alkoxides have been widely used as a precursor in sol-gel preparations because they are commercially available in high purity and their solution chemistry has been documented (Bradley, 1989). Sol gel method needs a low-temperature chemical precursors to produce fine particles with desired structural characteristics such as compositional homogeneity, grain size, particle morphology and porosity, high purities, able to control the particle size in nanometric range (Buasri *et al.*, 2008; Wang *et al*., 2010). In sol gel method, appropriate precursors (such as metal salts or metal organic compounds) will be added into water and alcohol under controlled temperature and pH which to form sol followed by conversion into homogeneous oxide networks (gel) after hydrolysis and condensation.

2.4.1.1. Principles of sol gel method

Sol gel process involves the formation of sol followed by gel formation. Sol is liquid suspensions of solid particle in range of nanometer obtain by hydrolysis and condensation of precursors.

$$\mathbf{M\text{-}OR + HOH \rightarrow M\text{-}OH + ROH} \quad \mathbf{(11)}$$

$$\mathbf{M\text{-}OH + R\text{-}OM \rightarrow M\text{-}O\text{-}M + ROH} \quad \mathbf{(12)}$$

$$\mathbf{M\text{-}OH + HO\text{-}M \rightarrow M\text{-}O\text{-}M + HOH} \quad \mathbf{(13)}$$

There are four steps in sol gel preparation as follows: formation of a gel, aging of gel, removal of solvent and heat treatment. The gel formation is initiated by hydrolysis to obtain reactive M-OH groups and then condensation occur leading to the formation of Metal-oxygen-Metal bonds (M-O-M). Aging step is between the gel formation and solvent removal. Drying and subsequent calcination of the drying gel yields to a metal oxide product. After calcination, the organic group (R) is removed from the gel and leaving metal oxides. High temperature calcination leads to sintering and consequently decreases in surface area of catalyst.

2.4.2. Co-precipitation (Homogenous precipitation)

The chemical co-precipitation method ensures proper distribution of the various metal ions resulting in stoichiometric and smaller particles size product, compared to the other methods. In co-precipitation processes, the metal precursors(salts like chlorides) are dissolved in an appropriate solvent and a precipitating agent (*e.g.* NH_4OH, urea, *etc.*) is added to precipitate the exchanger materials (Kooti and Matturi, 2011). The co-precipitation method requires that all the components have roughly the same solubility. Otherwise, when the precipitating agent is added, the less soluble components will precipitate out as a separate phase (Lalena *et al.*, 2008). Moreover, the chemical co-precipitation method is a low-cost technique and suitable for mass production. Furthermore, the molecular level mixing and the tendency of partially hydrolyzed species to form extended networks, facilitate the structure evolution and thereby lowering the crystallization temperature of the prepared inorganic exchanger material. The main drawback is that this process is difficult to control and the particle size is not, relatively, monodispersed enough for specific applications like recording media applications (Rashad *et al.*, 2009).

2.4.3. Hydrothermal Method

Nanoparticles can also be synthesized by this technique which is also known as solvo-thermal technique (Wang *et al.*, 2009). The reactions are carried out in an autoclave at a pressure of 2000

pounds per square inch and a temperature of 200 °C or higher. Nanoparticles prepared by this method show better crystallinity and grain size. Nano photocatalyst with specific sizes and morphology can be synthesized by continuous hydrothermal technique. Reaction kinetics can be increased by microwave heating during hydrothermal technique (Komarneni *et al*., 2002). Microwave hydrothermal technique needs lower temperature as 150 °C and shorter time as 25 minutes as compare to conventional hydrothermal technique.

2.4.4. Impregnation Method

Catalyst support is the material, usually a solid with a high surface area, to which a catalyst is affixed. The activity of heterogeneous catalysts and nanomaterial-based catalysts occurs at the surface atoms. Consequently, great effort is made to maximize the surface area of a catalyst by distributing it over the support. The support may be inert or participate in the catalytic reactions. Typical supports include various kinds of carbon, alumina, silica and organic polymer (Zhen and Francisco, 2006). In impregnation techniques, the support is contacted with a precursor solution, in other word impregnation is related to ion exchange (adsorption processes) and the interaction with the support is dominant. Thus, low loadings, often for precious metals, are achieved by adsorption of the precursor molecules onto surface groups of the support (ion adsorption) or through the exchange of ions in, for example, zeolites (ion exchange), after which excess precursor is removed. When higher loadings are required, the washing step is skipped and the support is directly dried, so that all precursor ends up on the support (impregnation and drying). Impregnation can be performed to incipient wetness, whereby the pores of the support are filled with precursor solution, to prevent deposition on the external surface of the catalyst grains and to limit waste (Munnik *et al.,* 2015).

2.5. Characterization of Inorganic Ion Exchangers

2.5.1. Chemical Characterization

In order to characterize a new substance as an inorganic ion exchanger, its utility in various fields and its limitation, the following properties may be studied as per given order of preference(Naushad, 2009; Fisseha, 2010).

- Ion exchange capacity
- Chemical and thermal stability

- Composition
- Structural studies
- Selectivity
- Specific Surface area(SSA)

2.5.1.1. Ion exchange capacity (IEC)

The IEC of an exchanger is a measure of its content of exchangeable ions and is conventionally expressed in terms of the total number of equivalents of ion per kilogram (milli-equivalents per gram) of the exchanger in its dry state and in a given univalent ionic form. Zeolite minerals used in water softening, for example, have a large capacity to exchange sodium ions (Na^{+}) for calcium ions (Ca^{2+}) of hard water (Clive, 1994). Hence, the IEC (Q, meq g^{-1}) is a term which describes the quantity of uptake of exchangeable ions under specific conditions. The theoretical capacity is often higher than the apparent capacity, which strongly depends on solution concentration and pH. In addition, the framework of the exchanger may create circumstances in which the access of larger ions and hydrated cations is prevented, and therefore, the experimentally obtained maximum uptake may not represent theoretical capacity (Moller, 2002).

Table 1. Ion exchange capacity of some inorganic ion exchangers

S.No	Ion exchange Materials	IEC (meq/g)	References
1	cerium(IV) iodotungstate	0.86	Dhara *et al*., 2009
2	Zirconium(IV) iodotungstate	0.68	Nabi *et al*., 2009
3	Titanium oxide	2.00	Naushad, 2009
4	Titanium(IV) molybdosilicate	0.74	Nabi *et al*., 2007b
5	Zirconium(IV) tungstoiodophosphate	2.20	Siddiqui and Khan, 2007

6	Titanium (IV) tungstosilicate	0.44	Siddiqi and Pathania, 2003
7	Titanium(IV) tungstophosphate	0.80	Siddiqi and Pathania, 2003
8	Zirconium(IV) selenomolybdate	0.94	Gupta *et al*., 2000

2.5.1.2. Chemical and thermal stability

Chemical and thermal stability of the exchanger is another important parameter. This is mainly because industrial waste waters mostly contain complex mixtures and alkalinity or acidity (Moller, 2002). Hence the exchanger should be stable in these conditions without losing its ion exchange capacity. A good deal of interest has grown in the last decades in synthetic inorganic ion exchangers, because of certain advantages over organic resins such as resistance towards high ionizing radiation, stability at higher temperatures and selectivity towards certain metal ions (Akieh *et al.*, 2008). The chemical stability of the material can be determined using instruments like Uv-vis spectrophotometer, inductively coupled plasma (ICP) *etc*. whereas the thermal stability of the exchanger can be determined using thermo gravimetric analysis (TGA), differential thermal analysis (DTA) and differential scanning calorimetry (DSC) (Fisseha, 2010).

Table 2. Thermal and chemical stability of some inorganic ion exchangers

S.No.	Ion exchange Materials	Thermal stability	Chemical stability	References
1	ZrSi	Stable up to 850 ^{o}C	Difficult to dissolve in 5 M mineral acids	El-Naggar *et al*., 2007
2	TiMoSi	Stable up to 700 ^{o}C retaining 85% of IEC	Stable in 0.1M acids and bases	Nabi *et al*., 2007b
3	TiMoP	Stable up to 750 ^{o}C retaining 85 % of IEC	Stable in 1 M acid and 0.4 M base	Yavari *et al*., 2009
4	SnSiMo	Stable up to 800 ^{o}C	Stable up to 1M alkalis and fairly stable in acid	Nabi and Khan, 2006

2.5.1.3. Composition

The composition of constituting elements of the ion exchanger is another factor which determines the properties of cation exchanger. Many inorganic ion exchangers are not stochiometrically produced and depend on the condition of their synthesis (Naushad, 2009). For example, a cation exchanger with hydrogen form, the cation exchange capacity of the exchanger increases with the increase of the anionic part (Nabi *et al.*, 2007a). This is because the exchanging ions are attached to the oppositely charged parts. The composition of the ion exchanger can be determined using ICP- AES, ICP- OES, and XRF.

Table 3. Compositions of some inorganic cation exchangers

S.No	Ion exchange Materials	Composition	References
1	Cerium phosphosilicate	Ce:Si:P=2:5:4	Naushad, 2009
2	Titanium(IV) molybdosilicate	Ti:Mo:Si = 1:1:3	Nabi *et al*., 2007b
3	Silico-antimonate	Si: Sb = 1:4	Abou-Mesalam, 2003
4	Cerium(IV) iodotungstate	Ce: IO_3:W= 1:3:3	Dhara *et al*., 2009
5	Titanium(IV) arsenophosphate	Ti: As: P = 1:1:3	Airoldi and de Oliveira, 1992

2.5.1.4. Structural studies

Inorganic ion exchangers can be produced as crystalline structure or amorphous materials. Though structures of crystalline materials are well known, they are not found to be suitable in column operations as they are obtained in powder forms. Amorphous materials on the other hand can be prepared easily and obtained in granular form, very suitable for column operations (Gupta *et al*., 2005; Maheria and Chudasama, 2006). The structure of the ion exchange material is usually determined using X- ray diffraction spectroscopy (XRD).

Table 4. Structure and use of some inorganic ion exchangers

S.No.	Ion exchange Materials	Structure	Used in	References
1	Aluminum oxide	Crystalline	B.P	Zhang *et al*., 2008
2	Titanium(IV) molybdophosphate	Amorphous	C.O	Yavari *et al*., 2009
3	Tin(IV) tungstoselenate	Crystalline	B.P	Naushad, 2009
4	Zirconium(IV) iodotungstate	Amorphous	C.O	Nabi *et al*., 2009
5	Zirconium titanium phosphate	Amorphou	C.O	Thakkar and Chudasama, 2009

C.O- column operation; B.P- batch process

2.5.1.5. Selectivity

Selectivity is a term used to describe the affinity of the material for limited number of ions.

The relative selectivity of ion exchange materials is determined by distribution studies in a suitable solvent. Accordingly, the ion exchanger is said to be highly selective towards some metal ions when the value of distribution coefficient (*Kd*) in a specific type of solvent concentration yields relatively larger value. In order to use inorganic ion exchanger for specific application, they have to be selective for the ions under study. Most of industrial wastes may contain interfering complex inactive components (Moller, 2002). Hence, the ion exchanger should selectively remove toxic substances from these waste waters containing inactive components. Many selective inorganic ion exchange materials have been synthesized during the last four decades (Claudia *et al.*, 2005).

Table 5. Selective properties of some inorganic ion exchangers

S. No	Ion exchange Materials	Selectivity	References
1	Zirconium(IV) iodotungstate	Hg^{2+} and Pb^{2+}	Nabi *et al*., 2009
2	Titanium phosphosilicate	Zr^{4+}, Nb^{5+}, Cs^{+}	Naushad, 2009
3	Titanium(IV) arsenophosphate	Hg^{2+} and Pb^{2+}	Airoldi and de Oliveira, 1992
4	Zirconiu(IV) selenoiodate	Pb^{2+}	Gupta *et al*., 2005
5	Zirconium arsenophosphate	Rb^{+}, Ag^{+}, Ti^{+}	Singh and Tando, 1979
6	Titanium molybdophosphate	Cs^{+}, Sr^{2+}, Ba^{2+}, Ti^{+}, UO_2^{2+}, Pb^{2+}, Zn^{2+}, Rb^{2+} and Zr^{4+}	Yavari *et al*., 2009

2.5.1.6.Specific surface area

Specific surface area is a property of semiconductor which improve the adsorption capability of semiconductor for organic pollutants. Nanoparticles have large specific surface areas when

compared with the bulk material (Tachikawa *et al*., 2011). Thus, the nanoadsorbents with higher specific surface area have superior adsorption capacity(Wang *et al*., 2009). In particular, nanosized adsorbents (ion exchangers) are believed to be promising scavengers toward adsorbates as they have greater surface area (Michael *et al.,* 2009). The specific Surface area of as synthesized particular solid materials can be determined either by nitrogen absorption Brunauer-Emett-Teller(BET) method or Sears' method (Sears, 1956; Al-Qodah and Shawabkah, 2009; Chen *et al*., 2011). In general it can be concluded that the most important features characterizing an ideal exchanger are:

- A hydrophilic structure of regular and reproducible form.
    - Controlled and effective ion exchange capacity.
    - Rapid rate of exchange.
    - Chemical and thermal stability.
    - Physical stability in terms of mechanical strength and resistance to attrition.
    - Consistent particle size and effective surface area compatible with hydraulic design and requirements for large scale plant (Clive, 1994).

2.6. Antimicrobial Activities

In recent years, a lot of titanium dioxide nanoparticles (TiO_2-NPs) have been developed and extensively studied for prospective and safe antimicrobial application in daily life, medicine, laboratories, food and pharmaceutical industry, waste water treatments and in development of new self-cleaning and antimicrobial materials, surfaces and paints. Antibacterial activity of titanium dioxide nanoparticles (TiO_2-NPs) has received significant interest worldwide particularly by the implementation of nanotechnology to synthesize particles in the nanometer region. Particular emphasis was given to bactericidal and bacteriostatic mechanisms which focus on generation of reactive oxygen species including hydrogen peroxide (H_2O_2), ·OH (hydroxyl radicals), and $\cdot O_2^-$ (peroxide). The irradiation of TiO_2 with visible light, leads to generation of an electron-hole pair on the TiO_2 surface. The electrons and holes react on the surface and convert water and oxygen into reactive oxygen species such as hydroxyl radicals (·OH), superoxide ion ($\cdot O_2^-$) and hydrogen peroxide (H_2O_2) (Srinivasan *et al.,* 2003). Those reactive species can bind to the surface. Consequently, microbial cells that adhere to the

surface of the TiO_2 catalyst react with the free radicals causes the loss of membrane integrity (Gogniat *et al.,* 2006).

One functional application of the titanium dioxide (TiO_2) is widely utilized as a self-cleaning and self disinfecting material for surface coating in many applications. It has a more helpful role in our environmental purification due to its nontoxicity, photo induced super-hydrophobicity and antifogging effect (Haghi, *et al.,* 2012). The antimicrobial activity of TiO_2 has been assayed in several bacteria and yeasts including *Escherichia coli* (Matsunaga *et al.,* 1985; Ditta *et al.,* 2008; Coleman *et al.,* 2005; Maness *et al.,* 1999; Bonetta *et al.,*2013; Kuhn *et al.,* 2003), *Lactobacillus acidophilus* (Matsunaga *et al.,* 1985), *Bacillus subtilis*, *Pseudomonas putida*, *Staphylococcus aureus*, *Listeria innocua* (Bonetta *et al.,* 2013), *Enterobacter cloacae* (Ibanez *et al.,* 2003), *Candida albicans*(Kuhn *et al.,* 2003), and Saccharomyces cerevisiae (Matsunaga *et al.,* 1985).

3. MATERIALS AND METHODS

3.1. Experimental Site

Synthesis of nanosized-Ti(IV) tungstomolybdate, photocatalytic experiment and partial characterization of the as-synthesized nanomaterial by UV-Vis and PL were carried out at Haramaya university research laboratory. The antimicrobial properties of the as-synthesized titanium(IV) tungstomolybdate was conducted in the School of Plant Sciences. FTIR and X- ray diffraction(XRD) patterns of the nanomaterial were conducted at AAU, Chemistry Department Research Laboratory. SEM-EDX was conducted at the Institute of Catalysis and Petroleum Chemistry (CSIC), in Madrid Spain.

3.2. Materials and Apparatus

3.2.1. Instruments and Apparatus

The instruments and apparatus used include: XRD, UV-Visible spectrophotometer, SEM-EDX, BET, Reactor tube, Analytical balance, pH meter, Hot plate, Furnace, Ceramic crucible, Agate mortar, Centrifuge, Thermometer, Volumetric flasks, Pipettes, Graduated cylinders, Magnetic stirrer, Test tubes, and beakers.

3.2.2. Chemicals and Reagents

Chemicals used include: Sodium tungstate dihydrate ($Na_2WO_4 \cdot 2H_2O$, MW: 329.84 g/mol, BDH, England), Sodium molybdate dihydrate ($Na_2MoO_4 \cdot 2H_2O$, MW : 241.9452 g/mol Fisher scientific, India), Titanium isopropoxide (($Ti(OCH(CH_3)_2)_4$, MW : 189.68 g/mol), Urea ($CO(NH_2)_2$, MW : 60.06 g/mol, Abron chemical, India), Nitric acid (HNO_3, MW : 63 g/mol, Breackland scientific supplies, UK), Hydrochloric acid (HCl, MW : 36.5 g/mol, Blulux, India), Ethanol (CH_3CH_2OH, MW : 46 g/mol) and Methylene blue ($C_{16}H_{18}N_3SCl$, MW : 319.50 g/mol), Sodium bicarbonate ($NaHCO_3$, MW : 84 g/mol), Methanol (CH_3OH, MW : 32 g/mol) and Silver nitrate ($AgNO_3$, MW : 137 g/mol), Sodium chloride (NaCl, MW : 58.5 g/mol), Sodium nitrate ($NaNO_3$ MW : 85 g/mol). The following chemicals were also employed in the work: Cupper(II) sulphate pentahydrate ($CuSO_4.5H_2O$, MW : 249.68 g/mol, SD fine chemicals, India), Lead nitrate ($Pb(NO_3)_2$, MW:331.209g/mol), Chromium(III) sulfate hexahydrate (($Cr_2(SO_4)_3.6H_2O$, MW:500.25 g/mol), Nickel(II)chloride hexahydrate ($NiCl_2.6H_2O$, MW : 237.69 g/mol), Sodium hydroxide (NaOH, MW:40 g/mol), Phenolphthalein (($C_{20}H_{14}O_4$), MW:318.328 g/mol, BDH,UK), Disodium salts of EDTA (($C_{10}H_{16}N_2O_8$), MW : 292.24 g/mol, BDH, England).

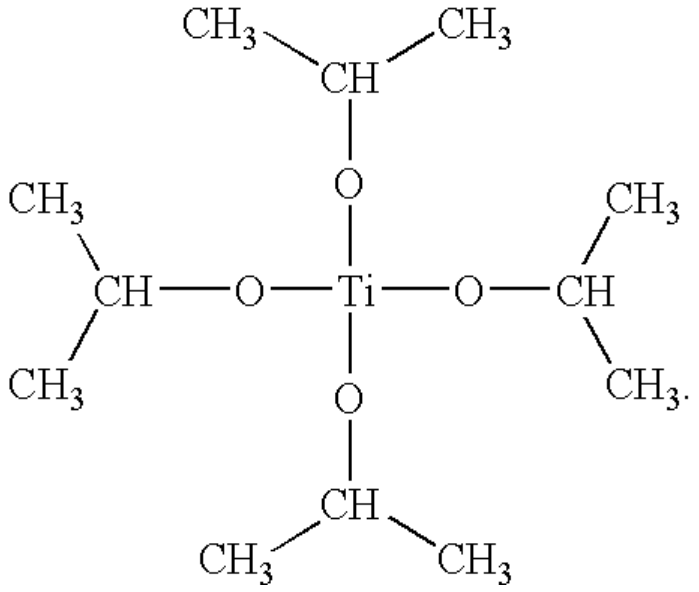

Figure 4. Chemical structure of titanium isopropoxide

3.2.3. Preparation of Reagents

Solution of 0.1 M titanium isopropoxide ($Ti(OCH(CH_3)_2)_4$ was prepared (i.e 30 mL of $(Ti(OCH(CH_3)_2)_4$ was dissolved in 250 mL of ethanol, 1 mL of concentrated HCl as a catalyst and 2 mL of deionized water to avoid a solid formation) (Karkare, 2014). 0.1 M Sodium tungstate dihydrate ($Na_2WO_4.2H_2O$) and 0.1 M sodium molybdate dihydrate ($Na_2MoO_4.2H_2O$) solutions were prepared in deionized water (Bezabih *et al,* 2017).

3.3. Synthesis of Nano-titanium(IV) tungstomolybdate Cation Exchenger

Nano-titanium(IV) tungstomolybdate was prepared by urea hydrolysis homogeneous precipitation technique. The conditions used for the preparation have considerable effect on the degree of hydration and the composition of the exchanger. These two factors are responsible for the shape and size of cavities inside the ion exchanger and for other properties of the exchanger resulting in their unusual ion exchange behavior (Yavari *et al.*, 2009). Ti(IV) tungstomolybdate was prepared by mixing sodium tungstate dihydrate, sodium molybdate

dihydrate and titanium isopropoxide ($Ti(OCH(CH_3)_2)_4$ solutions gradually with continuous stirring of the mixture in varying mixture solutions. This was done by varying volume ratio of the solutions of ($Ti(OCH(CH_3)_2)_4$ (30 mL dissolved in 250 mL of ethanol), 30 mL of 0.1 M ($Na_2WO_4 \cdot 2H_2O$) and 60 mL of 0.1M ($Na_2MoO_4 \cdot 2H_2O$) and 80 mL of Urea (0.31M) added drop wise with continuous stiring with magnetic stirrer in different volume ratio.

The mixtre was stirred for 1 h to get a precipitate of Ti(IV) tungstomolybdate. The desired pH of the solution was maintained with constant stirrng by magnetic stirrer and it was then heated at 90 ^{0}C for 1 h to decompose the excess urea (Bezabih *et al,* 2017). Finally milky white color of nano-Ti(IV) tungstomolybdate was formed. The resultant mixture were kept for 24 h at room temperature for the polymerization of the mixture to obtain a cross-linked network. The precipitate of Ti(IV) tungstomolybdate thus formed was filtered out and washed continuously with deionized water twice until filtrate became colorless to remove traces of acid, HCL or base, NaOH ion and then dried at 40 ± 1^{0}C for 24 h. It was ground and calcined at various temperatures (300 ^{0}C, 400 ^{0}C, 500 ^{0}C, and 600 ^{0}C) for 3 h. The powder obtained was immersed into 1M nitric acid for 24 h with occasional shaking using mechanical shaker at the speed 100 rpm in order to transform the cation exchanger into its hydrogenated form. The IEC was calculated using the equation below:

$$\mathbf{IEC(meq/g) = V_{NaOH} \times (C_{NaOH}/W_d)} \qquad \mathbf{(14)}$$

Where V_{NaOH}, C_{NaOH} and W_d are the volume of NaOH in liter, the concentration of NaOH in milliequivalents per liter and the weight of the dry exchanger sample in g, respectively (Abd El-Latif *et al*, 2011).

In order to determine the optimum mixing volume ratio of the precursors two samples with varying calcination temperatures were prepared keeping other parameters constant (Appendix Table 1). The optimum mixing volume ratio was found to be 2:1:2:3. with respect to titanium isopropoxide, sodium tungstate dihydrate and sodium molybdate dihydrate and urea respectively.

3.4. Evaluation and Characterization of the as-Synthesized Titanium(IV) tungstomolybdate

3.4.1. Evaluation of Ti(IV) tungstomolybdate Cation exchanger

3.4.1.1. Ion exchange capacity (IEC)

The IEC of the as-synthesized cation exchanger was determined by acid-base titration. The weighed sample that is 0.5g in its H^+ form, was soaked in 50 mL of 1 M NaCl solution for 12 h with shaking at ambient temperature. The ion exchanged solution was titrated against 0.1 M NaOH solution to the phenolphthalein end point.

3.4.1.2. Determination of point of zero charge (pHpzc)

Point of zero charge (pzc) of Ti(IV) tungstomolybdate cation exchanger was determined using the method described by Rao *et al*., (2011). The pHp_{zc} of the as-synthesized cation exchanger was determined by adding 0.1g of the cation exchanger into 250 mL beaker. 50 mL of 0.001 M $NaNO_3$ was added and adjusted to various pH ranging from 1 to 11 using dilute 1M HNO_3 or 1 M NaOH solutions. The solution was equilibrated for 60 minutes in a mechanical shaker to determine the initial pH. Then, 1g of $NaNO_3$ was added to the above solution and further equilibrated for another 60 minute after agitation to measure the final pH. A plot of $pH_{final-initial}$ (Y-axis) versus pH_{final} (X-axis) was used to determine the point of zero charge where the graph intersects the X-axis.

3.4.2. Physical Characterization of Ti(IV) tungstomolybdate Cation exchanger

3.4.2.1. X-ray diffraction study

For X-ray diffraction analysis, the X-ray diffractometer with Cu Kα radiation of wavelength (λ = 0.l5406 nm) operating at 40 kV and 30 mA at 298 K was used (Nabi and Naushad, 2008; Abd El-Latif and El Kady, 2011).

3.4.2.2. Fourier-transformed infrared study

Fourier-transformed infrared (FT-IR) spectroscopic measurement was used to identify the functional groups within the compounds in the mid infrared region which covers the frequency from 400-4,000 cm^{-1}. Titanium(IV) tungstomolybdate calcined at 600 ^oC was thoroughly mixed with KBr and the mixture was ground and pressed into a disk of standard diameter.

FTIR absorption spectrum was scanned and recorded in the region 4000–400 cm^{-1} (Abd El-Latif and El Kady, 2011).

3.4.2.3. UV-Vis diffuse absorption edge determination

For the estimation of absorption edge of the as-synthesized photocatalyst, UV–Vis diffuse absorption was measured using SP65 spectrophotometer at Haramaya University research laboratories, scanning over 200-800 nm. Band gap energy of the as-synthesized photocatalyst was obtained using the relation (Cao *et al*., 2012) given bellow.

$$\mathbf{E_g = 1240/ \lambda_{max}} \qquad \mathbf{(15)}$$

Where, E_g is band gap energy and λ is maximum wavelength (nm) corresponding to absorption edge of nanoparticles.

3.4.2.4. Scanning electron microscope study

Scanning electron microscope (SEM) was used to investigate the morphologies and particle sizes of the photocatalyst samples using Hitachi TM1000 attached with EDX detector to do the elemental analysis.

3.4.2.5. Photoluminescence spectroscopy

The energy levels in a semiconductor quantum well structure are investigated using the technique of photoluminescence (PL). Thus, luminescence is analyzed with a spectrometer and the peaks in the spectra represent a direct measure of the energy levels in the semiconductor. Electrons having energies above a certain value are referred to as conduction electrons, while electrons having energies below a certain value are referred to as valence electrons. This is where they are labeled as conduction and valence bands. The word band is used because the electrons have a multiplicity of energies in either band. Furthermore, there is an energy gap between the conduction and valence electron states. Under normal conditions electrons are forbidden to have energies between the valence and conduction bands. However, if a light particle (photon) has energy greater than the band gap energy, then it can be absorbed and thereby raise an electron from the valence band up to the conduction band across the forbidden energy gap. In this process of photo excitation, the electron generally has excess energy which it loses before coming to rest at the lowest energy in the conduction band. At this point the electron eventually falls back down to the valence band. As it falls down, the

energy it loses is converted back into a luminescent photon which is emitted from the material (Katsumata *et al.,* 2014). Thus, the energy of the emitted photon is a direct measure of the band gap energy, Eg. The process of photon excitation followed by photon emission is called photoluminescence.

3.4.2.6. BET specific surface area

The specific surface area of the sample was determined by physical adsorption of nitrogen gas on the surface of the solid and by calculating the amount of adsorbate gas corresponding to a monomolecular layer on the surface (Mohanty, 2012). The determination is usually carried out at the temperature of liquid nitrogen. The amount of gas adsorbed can be measured by either volumetric or continuous flow procedure. The data were treated according to BET adsorption isotherm equation:

(16)

Where, P = partial vapour pressure of adsorbate gas in equilibrium with the surface at K (B.P of liquid nitrogen), in Pascal

P_o = Saturated pressure of adsorbate gas, in Pascal

V_a = Volume of gas adsorbed at standard temperature and pressure (STP) [273.15 K and atmospheric pressure (1.013×10^5 Pa)], in milliliters

V_m = Volume of gas adsorbed at STP to produce an apparent monolayer on the sample surface, in milliliters

C = The adsorbate gas on the powder sample

3.5. Binary Separation

3.5.1. Quantitative Separation of Metal Ions from Binary Mixtures of other Metal Ions

Quantitative separations of some important metal ions of analytical utility were achieved on nano-Ti(IV) tungstomolybdate loaded columns (Juang *at el.,* 2006). In this method, 0.5 g of the acidified exchanger in H^+ form was packed in a glass column of 0.9 cm internal diameter with a glass wool support at the end. The column was washed 2–3 times with deionized water and the binary mixture (2.0 mL) was then poured on to the top of the column and the solution was left to flow slowly (8–10 drops min^{-1}) through the column until a small amount remained above the surface of the resin. The mixture was recycled at least three to four times through

the column to ensure complete adsorption of metal ions. The column was then rinsed with deionized water so that the metal ions, which were not exchanged, could be removed. Individual metal ions adsorbed on the exchanger, were then eluted using the appropriate eluting reagents. The effluent collected were titrated against the standard solution of 0.01 M di-sodium salt of EDTA.

3.6. Photocatalytic Activities

The photocatalytic activities of Ti(IV) tungstomolybdate photocatalyst was evaluated for the photocatalytic degradation of MB dye. A fluorescent lamp that predominantly emit at 360 nm with the definite power 40 W, 100 Volts and 50 Hz frequency was employed as source of visible radiation and positioned parallel to the reactor. Batch tests were performed as per the following procedure: An appropriate amount of Ti(IV) tungstomolybdate photocatalyst was added in to the solution of MB in a beaker and the mixture was stirred in dark for 30 minutes to allow the physical adsorption of dye molecules on catalyst particles reaching the equilibrium. Subsequently, the mixture was poured in to the photocatalytic reactor. The reaction solution was purged with air. Reaction samples were collected at regular intervals and immediately centrifuged to remove suspended particles before recoding absorbance. The concentration of MB was determined by measuring the absorption intensity at maximum absorbance wavelengths of 664nm by using a UV–Vis spectrophotometer (Lambda 17, PerkinElmer) with a 1cm path length spectrometric quartz cell. The percentage of degradation was calculated from the following equation (Hong *et al.,* 2009):

$$\textbf{\% Degradation} = [(A_0 - A_t)/ A_0]x100 \qquad (17)$$

Where A_0 is absorbance of dye at initial stage, A_t is absorbance of dye at time "t".

3.6.1. Effect of Various Operational Parameters on Photocatalytic Activities of Ti(IV) tungstomolybdate.

The oxidation rates and efficiency of the photocatalytic system are highly dependent on a number of operational parameters that govern the photodegradation of Methylene Blue (Chong *et al.,* 2010).

3.6.1.1. Effect of amount of photocatalyst

Dye degradation is influenced by the amount of the photocatalyst and aggregation of catalyst particles in high amounts of catalyst. The dye degradation increases with increasing catalyst

concentration (Rauf and Ashraf, 2009). Beyond a certain limit of catalyst amount, the solution becomes turbid and therefore percentage degradation starts decreasing (Sun *et al*., 2008). The effect of amount of photocatalyst on the rate of photocatalytic degradation of methylene blue was carried out to by taking different amounts of Ti(IV)tungstomolybdate; 0.05, 0.1, 0.2, 0.3 and 0.4g keeping other factors constant.

3.6.1.2. Effect of pH of the solution

The effect of pH on the rate of photocatalytic degradation of MB was investigated in the pH range of 2 to 12 (Pouretedal *et al*., 2009). The pH was maintained each time by using 1 M HCl or 1 M NaOH and measured using a pH meter (Mettler Toledo MP220).

3.6.1.3. Effect of concentration of methylene blue

The effects of methylene blue concentrations on the rate of their photocatalytic degradation was observed by taking different concentrations of methylene blue. Moreover, the high concentration of pollutants in water saturates on the catalyst surface and hence reduces the photonic efficiency and deactivates the photocatalyst efficiency (Saquib and Muneer, 2003). The extent of dye adsorption depends on the dye initial concentration. The percentage degradation of Ti(IV) tungstomolybdate was determined by varying the amount of dye concentration, from 10 ppm to 30 ppm while keeping a fixed amount of catalyst load (0.1g) and pH (8).

3.6.1.4. Effect of scavenger

To investigate the mechanism for photodegradation of the MB, the influence of active species such as superoxide radical ($\cdot O_2^-$), hole (h^+) and hydroxyl radical ($\cdot OH$) in the process were studied. Different scavengers were employed individually to remove the corresponding active species so that the function of different active species in the photodegradation process based on the change of photocatalytic conversion of MB was understood. The scavengers used in this study were $NaHCO_3$ for h^+, CH_3O/H_2O for $\cdot OH$ and $AgNO_3$ for superoxide radical ($\cdot O_2^-$) (Liu *et al*, 2013).

The reaction of $\cdot OH$ with methanol proceeds by abstraction of a hydrogen atom at either the methyl or the hydroxyl site (Xu and Lin, 2007).

$$\bullet OH + CH_3OH \quad CH_2OH + H_2O \qquad (18)$$

$$\bullet OH + CH_3OH \quad CH_3O. + H_2O \qquad (19)$$

However, this reaction is not a single step and it consists of three elementary reactions:

$$\bullet OH + CH_3OH \rightarrow C \quad (20)$$

$$C \rightarrow \bullet OH + CH_3OH \quad (21)$$

$$C \rightarrow \text{products (either } CH_2OH + H_2O \text{ or } CH_3O. + H_2O) \quad (22)$$

where C is the pre-complex reaction.

- Proposed mechanism for the reaction of bicarbonate with h^+, follows the steps:

Illumination:

$$\text{Photocatalyst} + hv \rightarrow \text{Photocatalyst*} (e^- \text{ CB} + h^+ \text{ VB}) \quad (23)$$

Oxidation:

$$H_2O \xrightarrow[\text{Photocatalyst*}]{h^+} H^+ + {}^\bullet OH \quad (24)$$

Reduction:

$$HCO_3^- \xrightarrow[\text{Photocatalyst*}]{e^-} HCO_3^{2-} \quad (25)$$

$$HCO_3^{2-} \xrightarrow[\text{Photocatalyst*}]{H^+ + e^-} HCO_2^- + H_2O \quad (26)$$

- Proposed mechanism for the reaction of silver cation with $\cdot O_2^-$, follows the steps:

$$Ag^+ + \cdot O_2^- \rightarrow Ag \text{ Photocatalyst} \quad (27)$$

$$\cdot O_2^- \rightarrow O_2 \ (e^- \text{ charged Ag Photocatalyst formed}) \quad (28)$$

3.7. Antibacterial Activity of Ti(IV) tungstomolybdate Cation Exchanger

Paper disk-diffusion method was employed to investigate the antimicrobial activity of Ti(IV) tungstomolybdate photocatalyst against two Gram-positive bacteria (*Staphylococcus aureus* and *streptococcus*) and two Gram-negative bacteria (*Escherchia coli* and *Salmonela thyphei*) (Gebru *et al*., 2003).

3.7.1. Antimicrobial Study

The antimicrobial screening tests were conducted against four important bacteria, two Gram-positive bacteria (*Staphylococcus aureus* and *streptococcus*) and two Gram- negative bacteria (*Escherchia coli* and *Salmonela thyphei*) using paper disk-diffusion method (Gebru *et al*., 2003) and administered with titanium(IV) tungstomolybdate photocatalyst. The antibacterial activity of Ti(IV) tungstomolybdate was tested using nutrient agar medium. Chloramphnicol, a standard antibiotic drug was used as a reference in bacteriacidal studies. From the diameters of inhibition zones the effectiveness of the compound was critically examined.

3.7.1.1. Preparation of media

Two Gram-positive bacteria (*Staphylococcus aureus* and *streptococcus*) and two Gram-negative bacteria (*Escherchia coli* and *Salmonela thyphei*) were transferred from the stock cultures and streaked on Mueller Hinton Agar (MHA) plates and incubated for 24 h at 37 ^{o}c. The Bacteria were transferred to the autoclave MHA and cooled at about 45 ^{o}C in water bath and mixed by gently swirling of the flasks. The medium was poured to sterilized petri dishes. Lastly, the media containing different concentrations of titanium(IV) tungstomolybdate (50,100, and150 µg/mL) spore suspension were poured to sterilized plates, solidified and used for the biotest under visible light illumination (Koseki *et al.* 2009).

3.7.1.2. Procedure for antibacterial activity test

A 6mm diameter paper discs of Whatmann No.1 filter paper was pierced with office puncture and the disc was sterilized in an oven at 180 ^{o}c for 1 hour and a 30 µL of solutions of nanoparticle were pipette on the discs in three replications. Finally, the samples were transferred with sterile forces on the impregnated disc paper on to nutrient agar plate seeded with bacteria and incubated at 37 ^{o}c for 24 h.

4. RESULTS AND DISCUSSION

4.1. Characterization of as-Synthesized Cation Exchanger

4.1.1. X-ray Diffraction Analysis

The XRD patterns of the as-synthesized cation exchanger calcined at 600 ^{o}C is shown in Figure 5. The exchanger exhibited tungstomolybdate of the form $Mo_{8.5}W_{1.5}O_{29}$ (96-153-4278) at diffraction peaks, 2 theta: 22.30^{o}, 24.70^{o} and 25.41^{o} and a mixed oxide of the form $Mo_{8.8}W_{1.2}O_{29}$ (96-153-0708) at diffraction peaks, 2 theta: 22.30^{o} and 25.41^{o} indicating the presence of monoclinic structure. The remaining is attributed to the rutile phase of TiO_2 (96-900-9084) representing the presence of tetragonal structure at diffraction peaks, 2 theta: 27.42^{o}, 36.09^{o}, 41.25^{o} and 54.32^{o}. A sharp and intense peaks observed from the XRD patterns indicated a well-ordered crystal structure.

The average crystalline size of the as-synthesized titanium(IV) tungstomolybdate cation exchenger was calculated using the Debye-Scherrer's formula;

$$\mathbf{D =} \qquad \mathbf{(29)}$$

Where, D = crystalline size in nm, K = the shape factor constant taken as 0.9; β is the full width at half maximum (FWHM) in radians, λ is the wave length of the X-ray (0.15406 nm) for Cu target $K\alpha_1$ radiation and θ_{max} is the diffraction angle. The average crystalline size calculated by Scherrer's equation (Sasirekha *et al*., 2009) considering the most intense peak using equation 29 was found to be 41.35 nm.

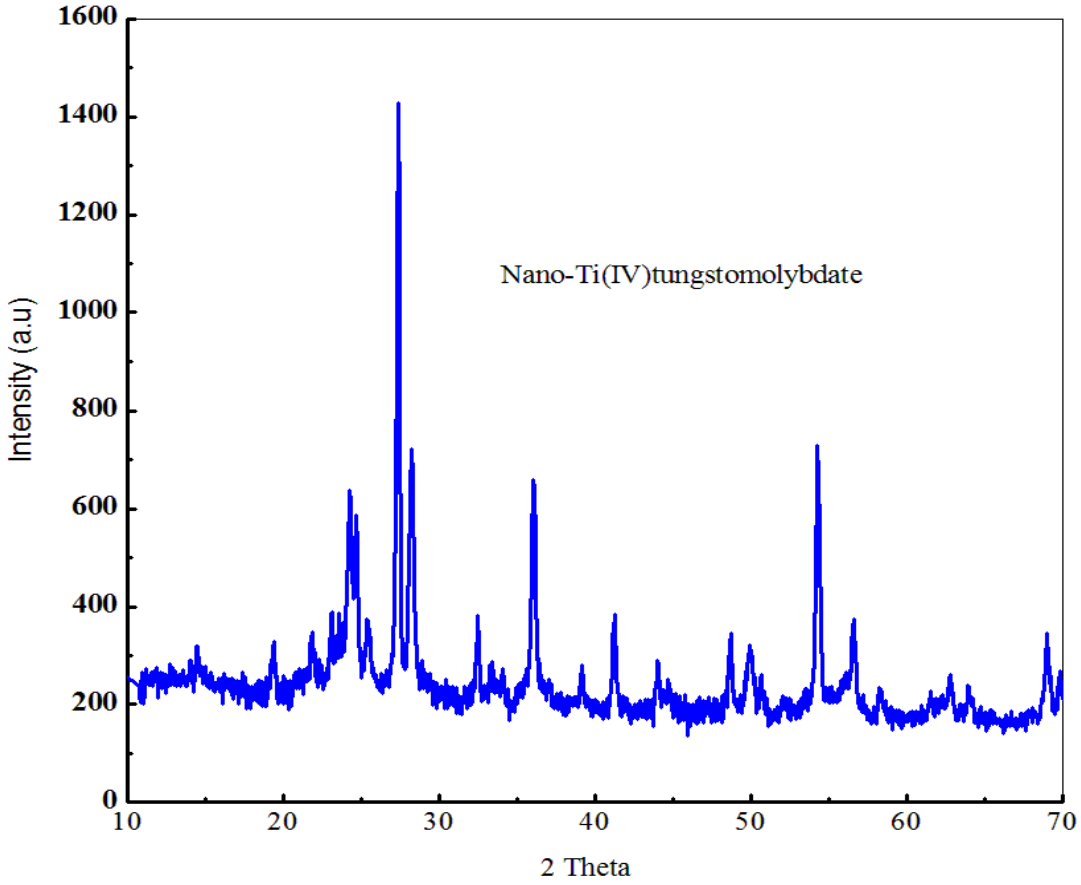

Figure 5. The XRD pattern of as-synthesized titanium(IV) tungstomolybdate cation exchanger pre-calcined at 600 ^{O}C for 3 h

Table 6. Calculated crystal sizes of as-synthesized titanium(IV) tungstomolybdate cation exchanger pre-calcined at 600 ^{O}C for 3 h

Sample	Temp. (^{0}C)	FWHM β(degree)	β(radian)	2θ (degree)	COSθ (radian)	Particle size D(nm)	Band gap(Eg) (eV)
TTM	600	0.1977	0.00345	27.42	0.971508	41.35	3.25

4.1.2. Fourier Transform Infrared Spectroscopic Analysis

The FTIR spectra of the as-synthesized nano sized titanium(IV) tungstomolybdate cation exchanger is presented in Figure 6. A broad band in the region 3500-3000 cm^{-1} is due to the O-H stretching vibration of the water bonded to TiO_2 (Binti-Jubri *et al*., 2007; Nabi *et al*., 2009; Nakamoto, 2009). A peak around 1630 cm^{-1} corresponds to the deformation or bending vibration of water molecules (*v*H−O−H). A band at ~ 1384 cm^{-1} is also ascribed to the presence of C=O residue probably due to atmospheric CO_2 (Chira *et al*., 2011). Finally, bands at around 900, 606 and 409cm^{-1} may be due to the presence of M−O bonds (Nawar and Hosny, 2000; Preethaand Janardanan, 2010).

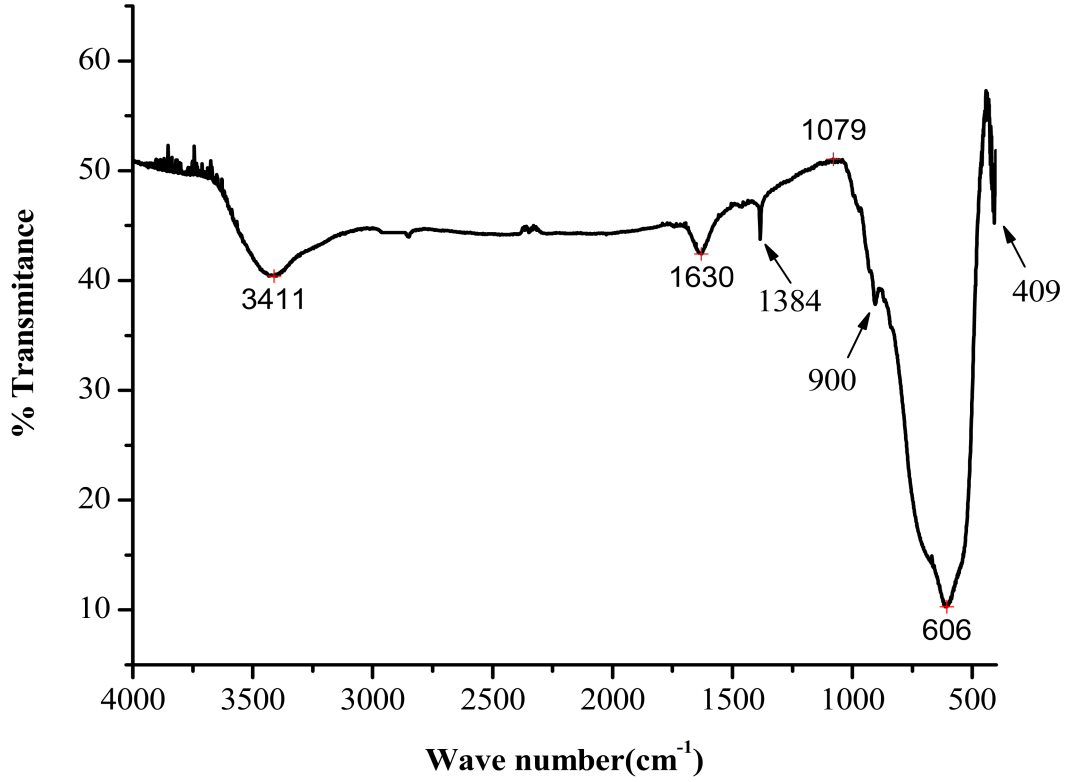

Figure 6. FTIR spectra of nano-titanium(IV) tungstomolybdate

4.1.3. UV-Visible Spectra of the as-Synthesized Photocatalyst

Uv-visible diffuse absorption spectra of the as-Synthesized titanium(IV) tungstomolybdate cation exchenger material is displayed in Figure 7. The intercept of the tangent line on the descending part of the absorption peak at the wavelength axis of the plot gives the value of diffuse absorption edge (nm). However, estimation of band gap energy using the above mentioned approach sometimes may not provide clear tangential line when the peak is not well resolved for a given sample. To overcome these challenges, it is possible to use diffuse

absorption spectroscopy data and then transform the data obtained using Kubelka Munk equation (Kubelka and Munk, *et al.,* 1931).

$$\alpha h\nu = A(h\nu - Eg)^{n/2} \qquad (30)$$

Where α, hν, Eg and A represent optical absorption coefficient, the photonic energy, band gap and proportionality constant, respectively. In this equation, n decides the type of the transition in a semiconductor (n = 1, direct absorption; n = 4, indirect absorption). By applying n = 1, the direct band gap of the prepared photocatalyst was determined from the plot of $(\alpha h\nu)^2$ vs. hν as indicated in Figure 6. Such transformation suppresses the band gap estimation obtained from plot of absorbance against wavelength using equation (Cao *et al*., 2012). Accordingly, the estimated band gap by drawing the straight line to the x-axis for titanium(IV) tungstomolybdate was found to be 3.25 eV.

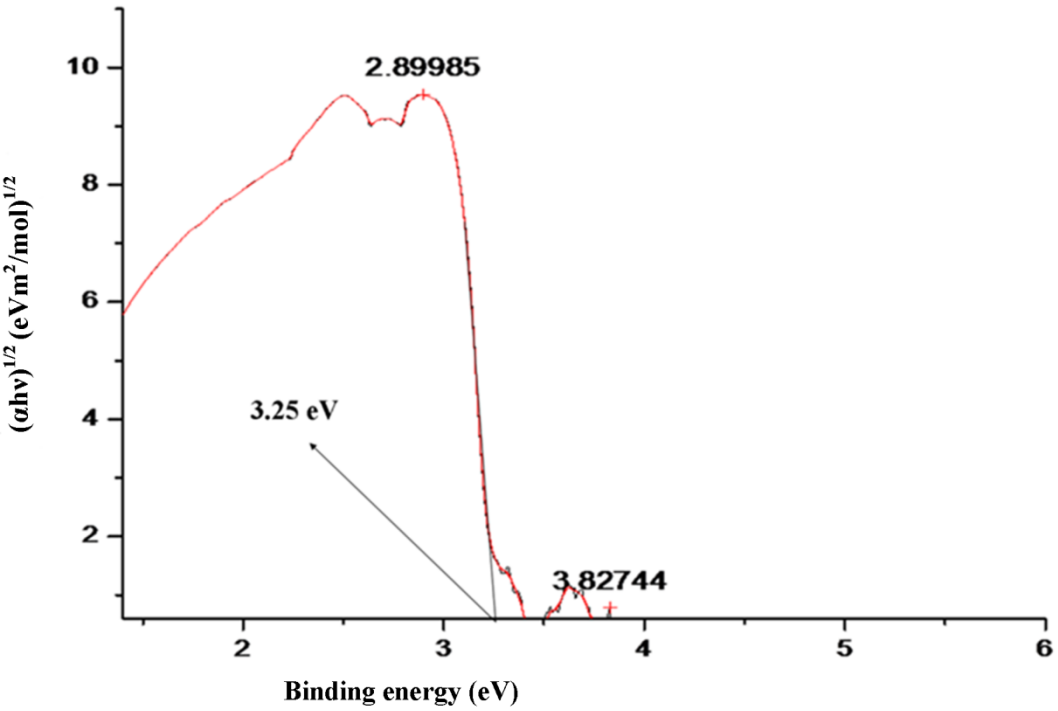

Figure 7. UV-Visible absorption spectra of nano-titanium(IV) tungstomolybdate using Kubelka-Munk

4.1.4. UV-Visible Absorption Spectra of MB Dye

UV-visible absorption spectra of MB is shown in Figure 8. Two peaks are observed, one in the UV range at λ = 296 nm. This is due to n→π* transition in C=N chromophore at λ = 296 nm and the other in the visible range at λ = 664nm. This band is most likely associated with the resonance of the pi electrons from the sulfur resonating with those from the C's in thiazinic center. This is due to n→π* transition in C=S Chromophore and hence maximum absorption

of visible light at 664 nm. Therefore, all spectroscopic measurements of MB concentration have been carried out at λmax = 664 nm.

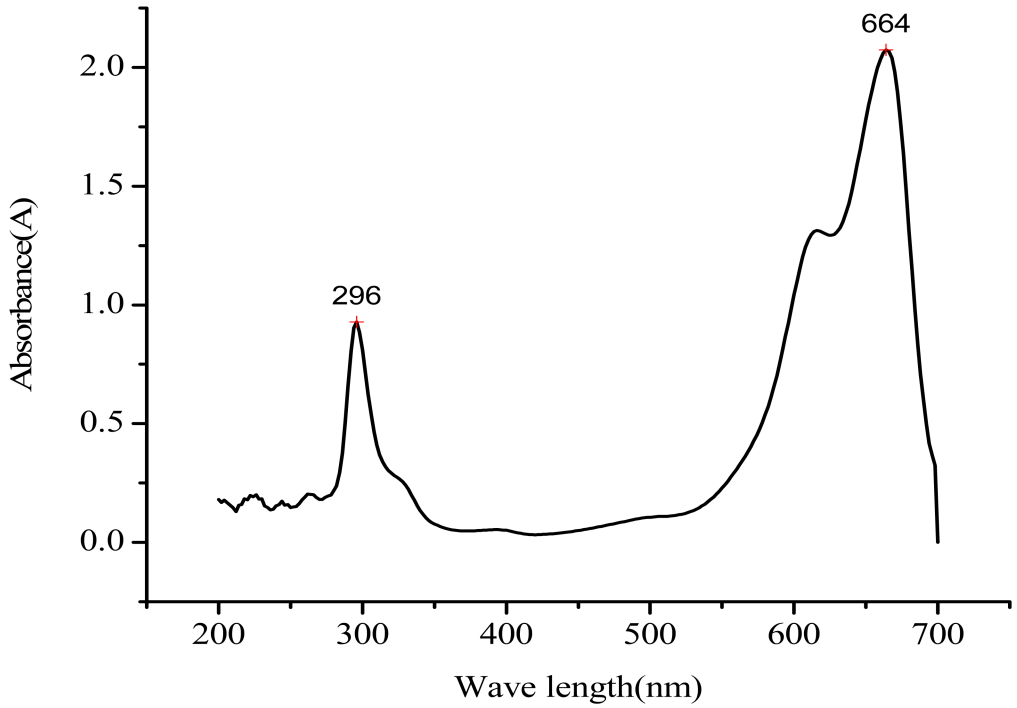

Figure 8. UV-visible absorption maxima of aqueous MB solution

4.1.5. SEM-EDX Analysis

Microscopic morphology of the as-synthesized nano-titanium(IV) tungstomolybdate was determined using scanning electron microscope (SEM) image. The SEM micrograph of the inorganic exchanger fired at 600 ^{0}C calcination temperature showed aggregates of particles, which is may be due to the high extent of branching and cross-linking of the inorganic (TTM) polymer which determined by the relative rates of hydrolysis and condensation reaction (Livage*, et al.,* 1988). When the condensation reaction is relatively faster than the hydrolysis reaction, the resulting sol-gel is highly branched and the corresponding gel is more

mesoporous in structure. On the contrary, if the hydrolysis reaction is relatively faster than the condensation reaction, the resulting sol-gel is weakly branched. However, a closer look at the image of this exchanger at magnification of 300x showed deposition of brighter spots correspond to either W or Mo atoms randomly distributed in the structure whereas a darker spots highly dispersed due to the presence of TiO_2 (Figure 9A). On the other hand, the estimated percent chemical distribution gradients across the surface of the sample (w/w%) were determined from results of energy dispersive X-ray (EDX) analysis in conjunction with SEM. The data generated by EDX analysis consist of spectra showing peaks corresponding to the elements that makeup composition of the sample being analyzed (Tables 7) and that of the corresponding map (Figures 9B), respectively, both indicating the existence of all chemical compositions.

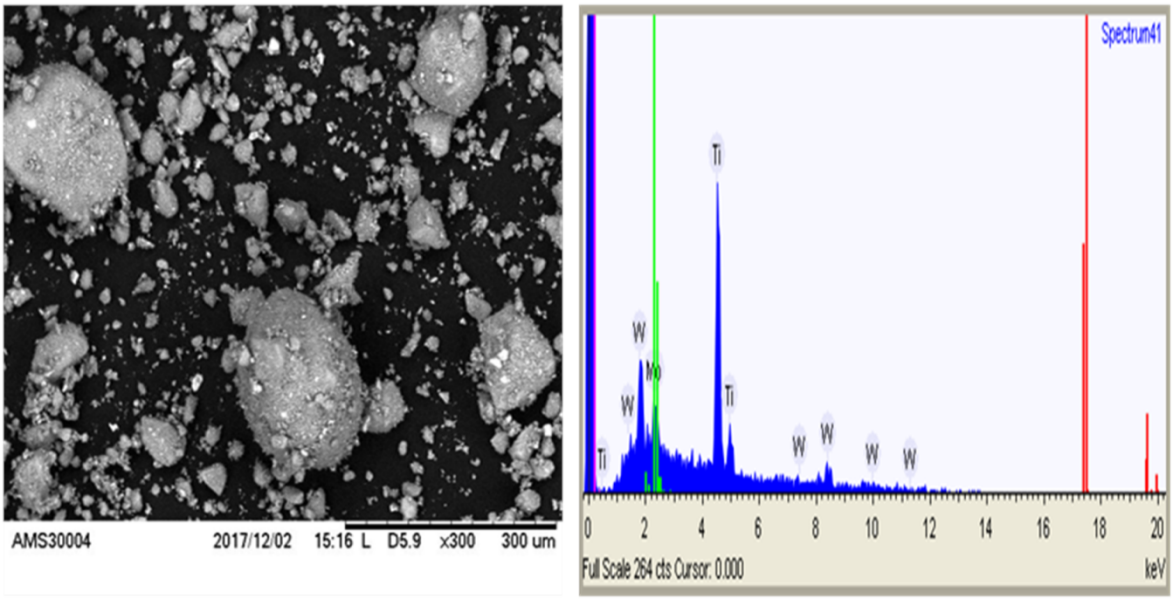

(A) (B)

Figure 9. SEM image (A) and EDX spectra (B) of the as-synthesized nano-TTM

Table 7. Elemental compositions obtained by SEM/EDX analysis (w/w%) of nano-TTM

Element	Weight %
Titanium	65.5
Molybdenum	10.3
Tungsten	24.2

4.1.6. PL Analysis

Photoluminescence (PL) emission spectra were used to investigate the efficiency of charge carrier trapping, immigration, transfer and the fate of electron-hole pairs in semiconductor particles. It is well known that the recombination of electron hole pairs can release energy in the form of PL emission. The intensity of the peaks in the PL spectra indicate the degree of recombinations: the higher the peak intensity, the faster the recombination process. The relatively lower peak intensity demonstrates the relatively slower recombination process; a phenomenon that plays positive role in enhancing the photocatalytic activity of the exchanger provided that other factors in the catalytic process play likewise.

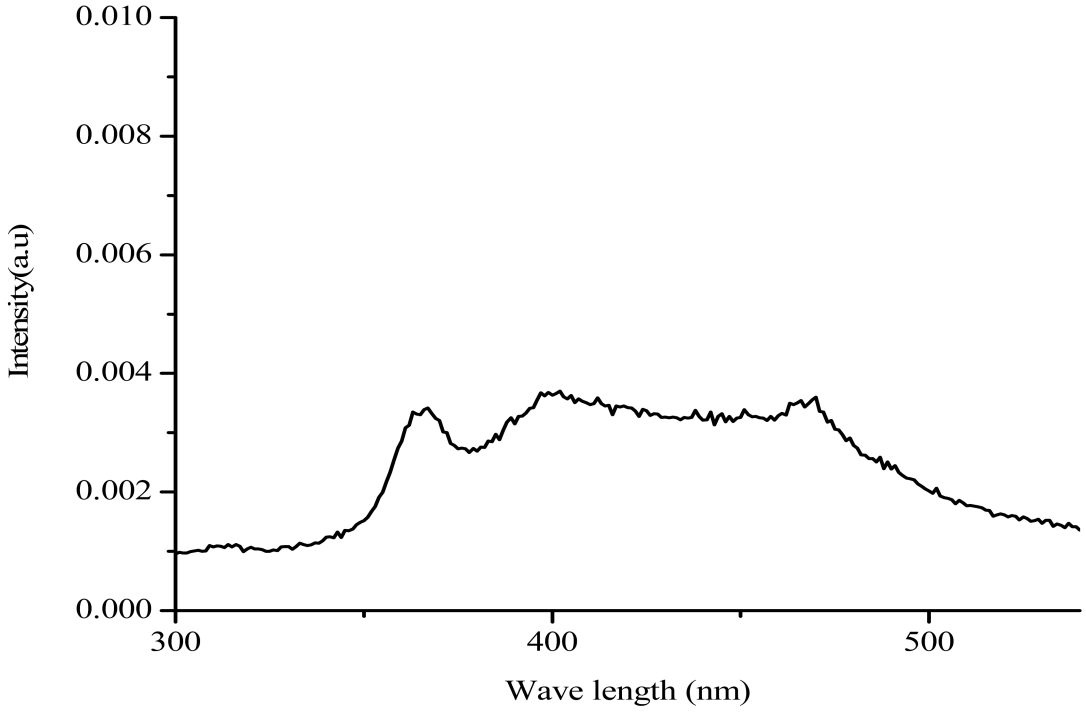

Figure 10. The PL emission spectra of nano-titanium(IV) tungstomolybdate(Excitation Wavelength = 290 nm)

4.1.7. BET Analysis

The average specific surface area of the as-synthesized titanium (IV) tungstomolybdate cation exchange material calcined at 600 ^{0}C was found to be 4.416 ± 0.003 m^2/g. The as-synthesized exchanger showed low specific surface area possibly due to the high crystallinity of the nanomaterial as evidenced by the XRD result.

4.2. Evaluation of Titanium(IV) tungstomolybdate Cation Exchanger

4.2.1. Ion Exchange Capacity (IEC)

The cation exchange capacity of nano-titanium(IV) tungstomolybdate for Na^+ was done by batch equilibrium method under pre-optimized conditions: [NaCl] = 1.0 M; agitation speed = 100 rpm; contact time = 12 hrs. The IEC for Na^+ ion of the samples calcined at varying temperatures is depicted in Appendix Table 1. The relatively higher value of IEC observed was 1.34 meq.g^{-1} for the exchanger sample calcined at 600 ^oC for 3hr. The relatively lower value of IEC (0.38 meq.g^{-1}) was obtained for the sample calcined at 300 ^oC for 3 hr. The value of IEC increases with decrease of exchanger particle size due to enhanced specific surface area. The value of IEC-the exchanger particle size relationship was not agree with the data reported by Bezabih *et al.* (2017). This may be due to the kinetic complexities during the phase trans- formation of TiO_2 and other factors like geometrical effect which leads to the increase in the number of nucleation sites per unit volume as crystal size decrease (Li *et al*., 2002). Similar pattern of particle size - calcination temperature relationship was reported by Li and co-workers (Li *et al*., 2002). According to these scholars, the anatase nanoparticle size decreases slightly with the increase of substrate temperature until the transition temperature. Above the transition temperature, particle size increases with the appearance of the rutile phase.

4.3. Binary Separation Studies of Nano-titanium(IV) tungstomolybdate

Based on the distribution coefficient (Kd) values adopted from Bezabih *et al.* (2017), the separation capability of the material has been demonstrated by undertaking different types of binary systems of some metal ions. The sequential elution of ions through column depends upon the metal-ligand stability. The distribution coefficients were calculated using equation (31) (Nabi and Shalla, 2009; Chand *et al*., 2011):

$$\mathbf{K_d = [(I- F)/F] [V/M]} \qquad \mathbf{(31)}$$

Where: F = final concentration of metal ion (mgL^{-1})

I = initial concentration of metal ion (mgL^{-1})

V = volume of the solution (mL)

M = the dry mass of the cation exchanger (g)

Based on separation factor, α as guiding measures for separations, binary separations have been carried out for four sets of metal ions: Pb(II)-Ni(II), Pb(II)-Cu(II), Cr(III)-Ni(II) and Cr(III)-Cu(II). The details of these separation studies are presented on Table 8. To elute Pb(II) from Pb(II)-Ni(II) binary system, 0.1 M CH_3COOH was preferably used. This was due to the fact that low Kd value of the metal Pb(II) in 0.1 M CH_3COOH enables quantitative elution than 0.05 M HCOOH that gives highe Kd value of the metal Pb(II). To elute Ni(II) from Pb(II)-Ni(II) binary system, 0.05 M HCOOH was preferably used than 0.05 M DMF that gives relatively high Kd value of the metal Ni(II). To elute Cr(III) from Cr(III)-Ni(II) binary system, 0.3 M HCOOH was preferably used as compared to 0.05 M HCOOH that gives relatively high Kd value of the metal Cr(III). This was due to the fact that low Kd value of the metal Cr(III) in 0.3 M HCOOH enables quantitative elution. 0.1 M CH_3COOH was used to elute Ni(II) from Cr(III)-Ni(II) mixture. This was due to low Kd value of the metal Ni(II) in 0.1 M CH_3COOH enables quantitative elution than 0.05 M DMF that gives relatively high Kd value of the metal Ni(II). For Cr(III)-Cu(II) binary system, 0.05 M DMF was used to elute Cu(II) from Cr(III)-Cu(II) binary system. This was due to the fact that low Kd value of the metal Cu(II) in 0.05 M DMF enables quantitative elution than 0.1 M DMSO that gives relatively high Kd value of the metal Cu(II). For Pb(II)-Cu(II) binary system, 0.05 M DMF was used to elute Cu(II) from Pb(II)-Cu(II) binary system. The selection of solvents were done based on the Kd values of both metal ions. Nano-titanium(IV) tungstomolybdate is found to exhibit a separation efficiency ranging from 54.32 % to 85.22 % for these metal ions.

Table 8. Binary separation of metal ions achieved on nano-TTM columns

Separation achieved	Separation factor (α)	Eluent used	Amount of metal ion(mg)		% Recovery
			Loaded	Found	
Pb(II)-Ni(II)	91.24	0.05M HCOOH Ni(II)	10.00	6.13	61.30
		0.1M CH_3COOH Pb(II)	9.46	5.17	54.65
Pb(II)-Cu(II	307.62	0.05M DMF Cu(II)	22	18.75	85.22
		0.1M CH_3COOH Pb(II)	9.83	5.34	54.32
Cr(III)-Ni(II)	100	0.1M CH_3COOH Ni(II)	10.00	6.00	60.00
		0.3M HCOOH Cr(III)	9.46	5.14	54.33
Cr(III)-Cu(II)	337.14	0.05M DMF Cu(II)	22	18.75	85.22
		0.3M HCOOH Cr(III)	9.83	5.41	55.03

Note: $\alpha = Kd_1/Kd_2$, where Kd_1 and Kd_2 are Kd values of metal 1 and metal 2 in aqueous media. % Recovery = (concentration of metal ion eluted/concentration of metal ion loaded) ×100.

4.4. Photocatalytic Studies

To test the photocatalytic efficiency of the prepared photocatalyst, photocatalytic degradation of MB was carried out under visible irradiations as well as in the dark. The percentage degradation of MB was measured at every 20 minutes interval for over 2 hours (i.e. methylene blue dye was photocatalytically degraded after two hours exposure). The percent degradation was calculated for each case using the above equation 18.

4.4.1 Effect of Operating Parameters

4.4.2. Effect of Catalyst Load on Photocatalytic Activities

The amount of photocatalyst is one of the main parameters for the degradation of substrate from economical point of view. In order to avoid the use of excess photocatalyst, it is necessary to find out the optimum loading of photocatalyst for efficient removal of dye (Sakthivel *et al*., 2003). Hence, a series of experiments were carried out to find the optimum amount of the photocatalyst by varying titaniumi(IV)tungstomolybdate; 0.05, 0.1, 0.2, 0.3 and 0.4g keeping other factors constant. The degradation efficiency of the dye versus time by varying the photocatalyst load is recorded on Appendix Table 2 and the corresponding plot is depicted in Figure 11. The observed dependence of reaction rate on the amount of photocatalyst can be explained in terms of the availability of active sites at the adsorbent

surface and the level of light penetration in the reaction medium (Goncalve *et al*., 1999). The photodegradation of MB is found to be 28.57 %, 57.14 %, 40 %, 26.66 %, and 20 % when the catalyst load is 0.05, 0.1, 0.2, 0.3 and 0.4g respectively. This indicates that an increase in the adsorbent total surface area increases the number of active sites available for the photocatalytic reaction. However, excess photocatalyst above 0.1 g, would induce more aggregation (particle-particle interactions) of photocatalyst making a significant fraction of the catalyst in accessible either to the adsorbing dye or to the radiation (Wong and Chu, 2003). The degradation efficiency decreases from 57.14 % to 20 % after the optimum photocatalyst load (0.1 g) is achieved. Therefore, 0.1 g of the photocatalyst was selected as the optimal amount of photocatalyst for the subsequent experiments.

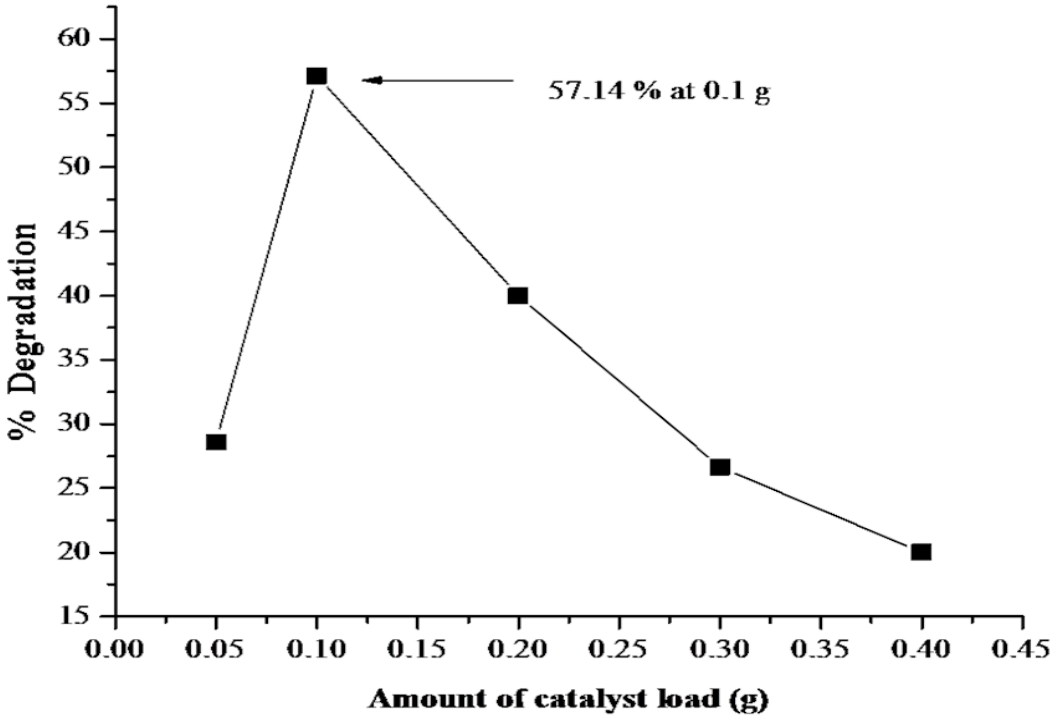
57.14 % at 0.1 g
% Degradation
Amount of catalyst load (g)

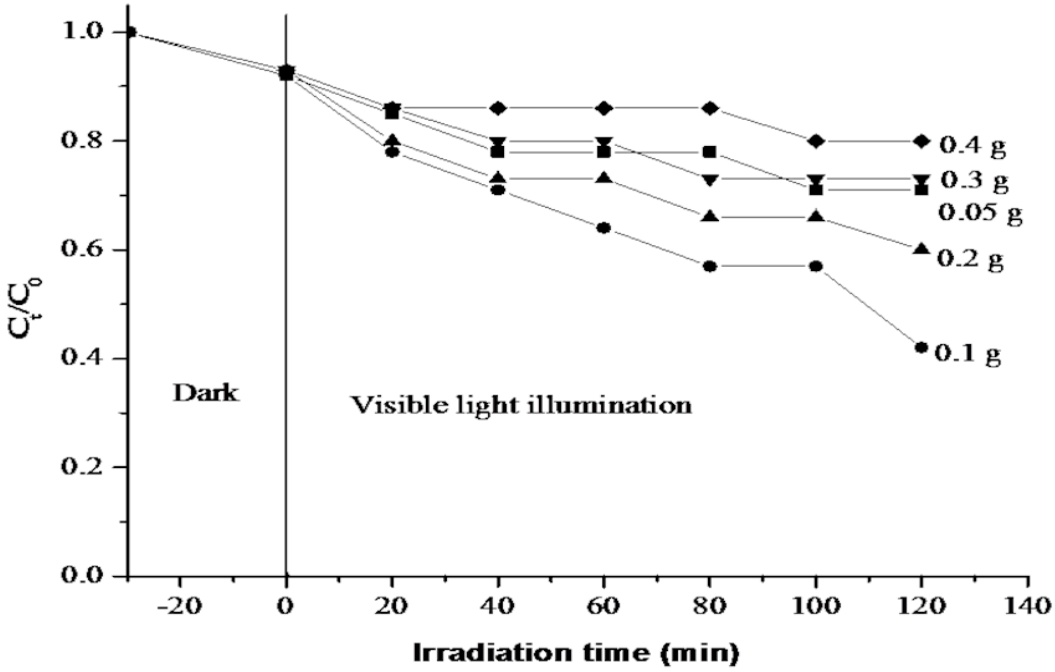
0.4 g
0.3 g
0.05 g
0.2 g
0.1 g
Dark
Visible light illumination
C_t/C_0
Irradiation time (min)

Figure 11. Plot of C_t/C_0 as a function of time for photocatalyzed degradation of MB dye by varying the amount of photocatalyst and keeping both dye concentration and pH constant (pH = 8, 10 ppm MB and λmax= 664nm)

4.4.3. Study of Point of Zero Charge of TTM Cation Exchenger

The P_{ZC} is a point at which the surface charge of the photocatalyst is zero or neutral that lies in the pH range of 4.5 to 7.0, depending on the catalysts used. Due to the absence of any electrostatic force between photocatalyst and dye particles, the interaction (adsorption) and photocatalytic processes are very less at P_{ZC}. When the pH of the system is less than the P_{ZC}, the surface charge of the photocatalyst is positive and interaction with the anionic dye is higher and the adsorption and photocatalysis are higher. But when the pH of the system under study is higher than the P_{ZC}, the photocatalyst surface is negatively charged and the repulsion between the photocatalyst and anionic dye particles is higher and adsorption and photocatalysis will be less. If the dye is cationic (MB) at pH greater than the P_{ZC}, interaction and photocatalysis is higher but at pH less than the P_{ZC} of the photocatalyst the repulsion is higher and the photocatalysis is lesser (Mahmood, 2011). As illustrated in Figure 11, the point of zero charge of TTM was investigated between pH of 1.0 and 11.0. The P_{ZC} of the photocatalyst was found to be 6.12, which was expected to be the point at which the surface charge of TTM was found to be neutral. The photodegradation result revealed that higher percent degradation was obtained at pH greater than the P_{ZC} of the photocatalyst, which is pH = 8.0 with 60 % as indicated in Figure 13. This is due to the higher interaction between the negatively charged surface of the photocatalyst particles and the positively charged (cationic) MB molecules at this pH. The values of initial pH (pH_i), final pH (pH_f) and pH_{f-i} were depicted on Appendix Table 3. The plot of pH_f versus pH_{f-i} was shown in Figure 12. The P_{ZC} value for adsorbent/photocatalyst shows that the cation exchanger has acidic nature below 6.12, basic nature above 6.12 and neutral at pH = 6.12.

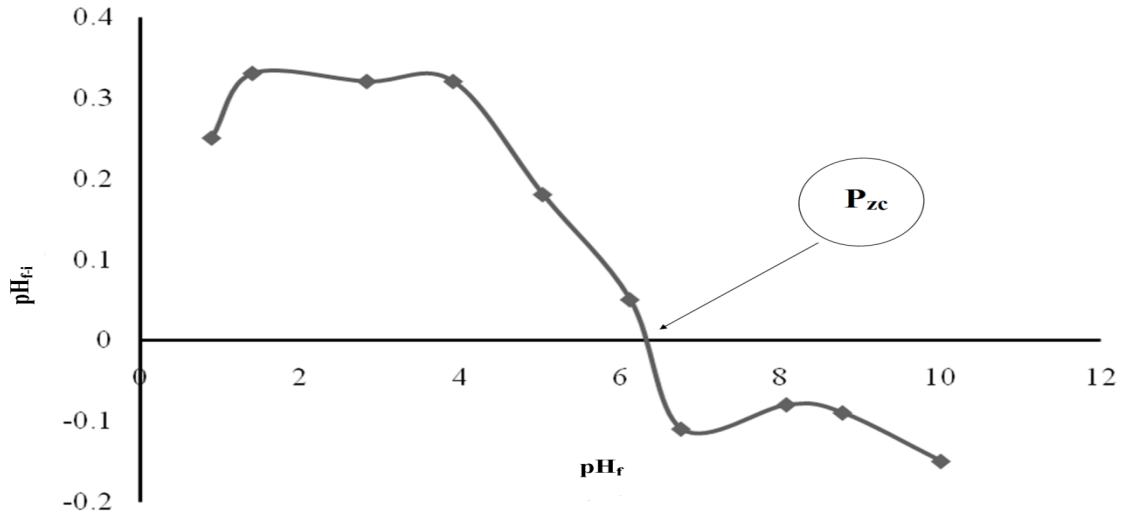

Figure 12. Plot of pH_f versus pH_{f-i} of titanium(IV) tungstomolybdate cation exchenger

4.4.4. Effect of pH on Photocatalytic Activities

The pH of solutions greatly affects the rate of reaction taking place on semiconductor surfaces due to its influences on surface-charge properties of the photocatalysts. The effect of pH in the range of 2.0 to 12.0 on the photocatalytic degradation rate of MB was investigated. The photodegradation efficiency of MB with an initial concentration of 10 ppm and photocatalyst (0.1 g) as a function of time is depicted on Appendix Table 4 and the corresponding plot is presented in Figure 13. The phtodegradation of MB is found to be 44.44 %, 47.61 %, 50 %, 60 %, 52.63 % and 47.05 % at pH 2, 4, 6, 8, 10 and 12, respectively. These results show that the photodegradation efficiency of MB was increased from 44.44 % (pH=2) to 60% (pH=8) and decreased to 47.05 % when pH is increased to 12. This indicates the degradation efficiency is higher in basic (i.e. negatively charged ions) than acidic (i.e. positively charged ions) conditions. The strong effect of pH on the photodegradation efficiency of MB was observed at pH = 8 with percent degradation of 60 %. Net charge on the photocatalyst surface is pH dependent. The cation exchanger has point of zero charge (p_{ZC}) at pH = 6.12. Below the p_{ZC} the photocatalyst has net positive charge and above the p_{ZC} the net charge on the

photocatalyst is negative. Less photocatalytic degradation at a lower pH than pHp_{zc} is due to the less availability of OH^- ions to form highly active •OH radicals. At higher pH than pHp_{zc}, adsorption of positively charged MB on the negatively charged photocatalyst increases due to ion-ion attraction and hence high photocatalytic degradation of MB at high pH than pHp_{zc}.

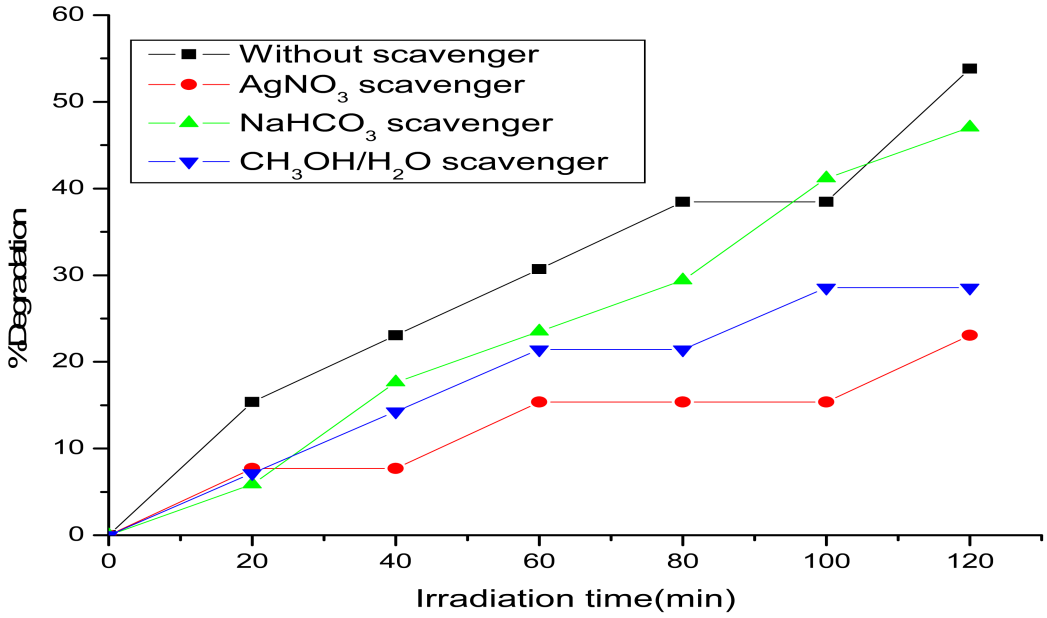

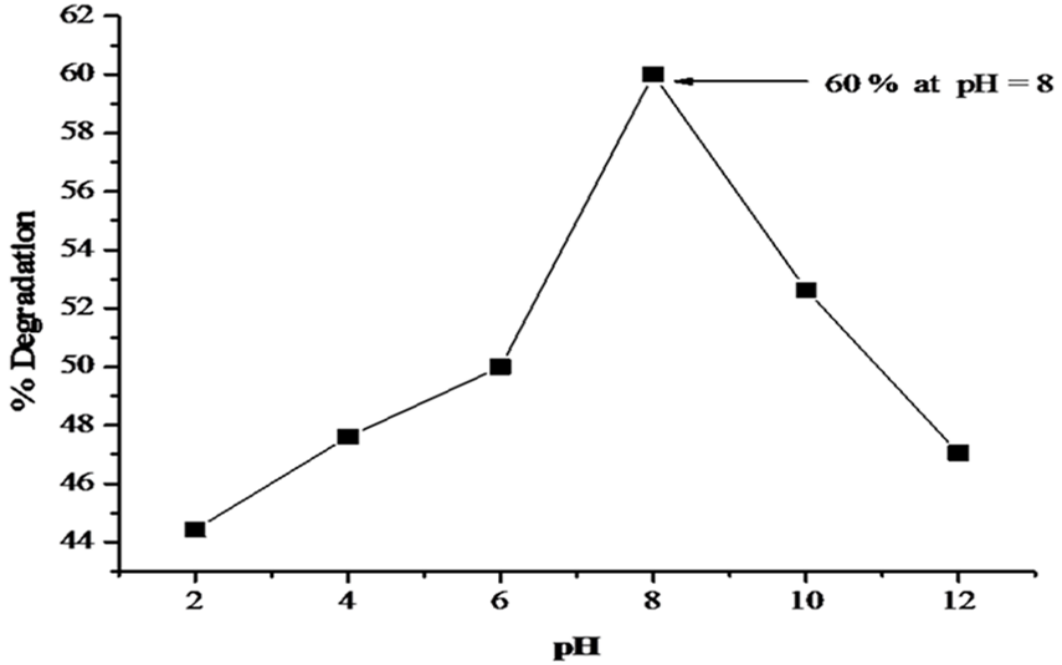
% Degradation
pH
60 % at pH = 8

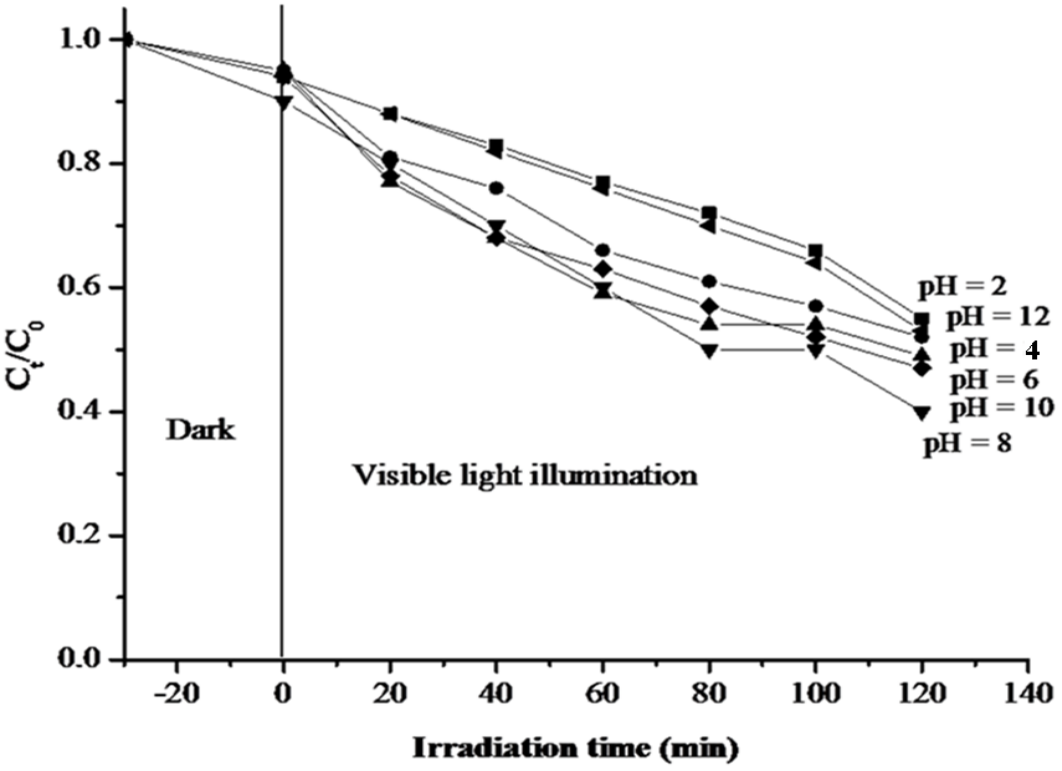
C_t/C_0
Irradiation time (min)
Dark
Visible light illumination
pH = 2
pH = 12
pH = 4
pH = 6
pH = 10
pH = 8

Figure 13. Plot of C_t/C_0 as a function of time for photocatalyzed degradation of MB dye under visible light irradiation by varying the pH of the solution and keeping both dye and photocatalyst amount constant (MB = 10 ppm, TTM = 0.1 g)

4.4.5. Effect of Initial dye Concentration on Photocatalytic Activities

The effect of the dye initial concentration on the photodegradation of MB was studied by varying the dye initial concentration from 10 ppm to 30 ppm . The other parameters such as catalyst load and pH were kept at 0.1 g and 8, respectively. The experimental results showed that; the rate of degradation efficiency decreased when the concentration of MB increased from 10 to 30 ppm, which is from 57.14 %, to 30.76 % upon 120 min visible light irradiation. The degradation efficiency of MB at different concentrations as a function of time under visible radiation is presented on Appendix table 5. The corresponding plot of the degradation efficiency of MB as a function of time with the same amount of photocatalyst (0.1g) and pH = 8.0 is depicted in Figure13. The highest degradation efficiency was obtained at the initial dye concentration, 10 ppm resulting in percent degradation of 57.14 %. As the dye concentration increases and the catalyst amount kept constant, fewer active sites are available per the substrate (dye) to interact with. Thus, resulting in decreased rate of photocatalytic degradation (Davis *et al*., 1994). Further, at higher initial dye concentration, the approach of the radiation photons to the catalyst surface was hindered and screened off, thereby, reducing the photocatalytic activity in the system (Epling and Lin, 2002). Moreover, at the higher dye concentration, the number of collisions between dye molecules increases at the cost of required collisions between dye molecules and ·OH radical and therefore, the rate of reaction was retarded (Lodha *et al*., 2007).

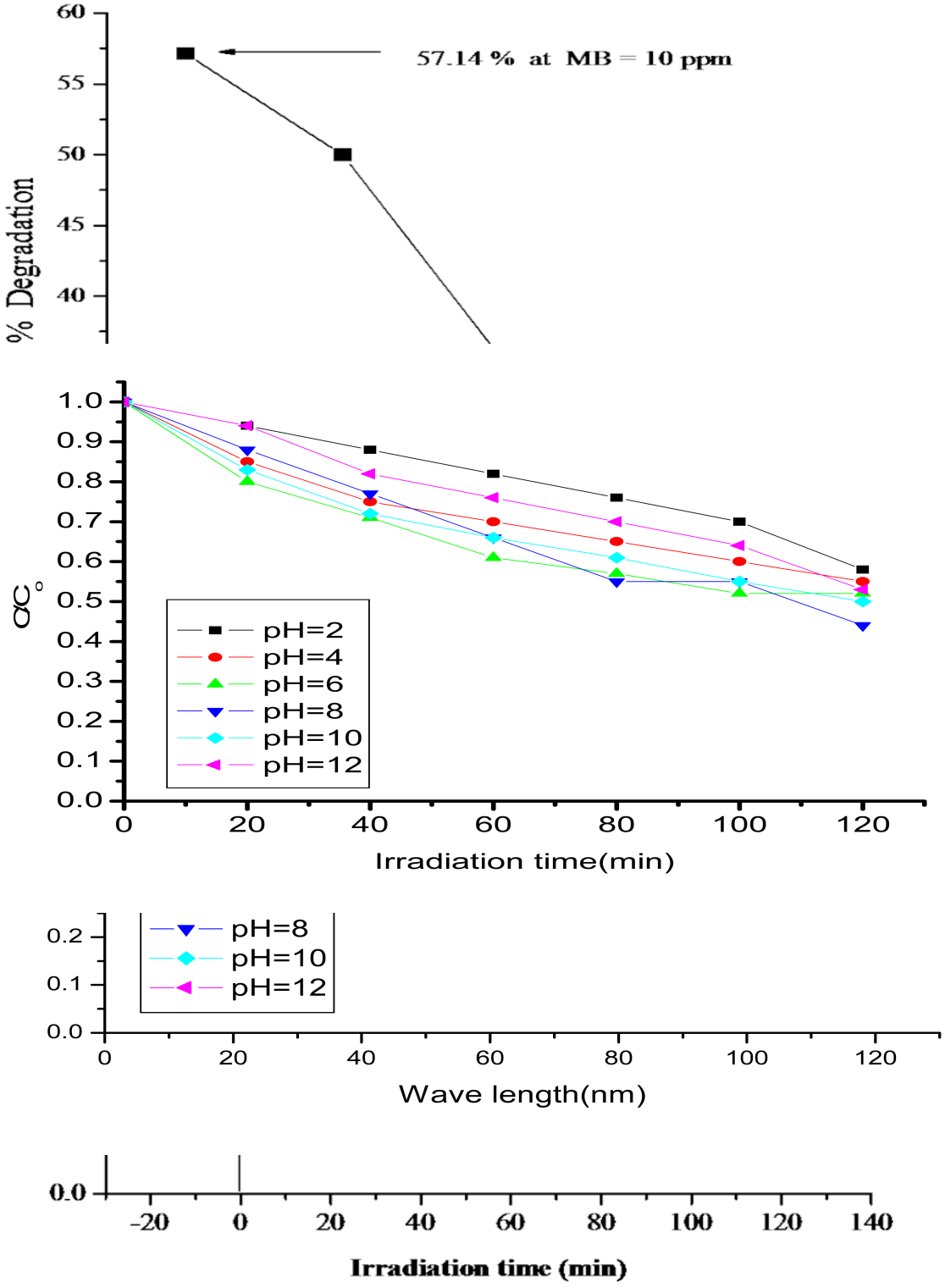
% Degradation
57.14 % at MB = 10 ppm
C/C°
pH=2
pH=4
pH=6
pH=8
pH=10
pH=12
Irradiation time(min)
Wave length(nm)
Irradiation time (min)

Figure 14. Plot of C_t/C_0 as function of time for photocatalyzed degradation of different concentration of MB under visible light irradiation by keeping the photocatalyst and pH constant (Catalyst = 0.1 g, pH = 8 and λmax = 664 nm

4.4.6. Effect of Visible light Irradiation

In order to investigate the effect of visible light irradiation on the catalyst-MB interaction, the following experimental sets (i.e., MB-visible-catalyst tests, blank tests and dark tests) were done using the above optimum values (Cat. = 1.0 g, MB = 10 ppm, pH = 8). Blank tests were performed under visible light without the addition of catalyst and almost no degradation was observed when the light was turned off. Some results (4 %) may be due to the solutions bubbled with $O_2\cdot$ In addition, the dark tests were also realized in dark condition to understand the effect of the light source when the catalyst added into the MB solution. The degradation results (7.14 %) may be due to adsorption mechanism. Generally, MB degradation rate was found to be increasing with irradiation time and visible light presence (i.e., 4 %, 7.14 % and 57.14 % degradations rates were achieved for the 'MB-visible', 'MB-dark-catalyst' and 'MB-visible-catalyst', respectively) as indicated in Figure 14.

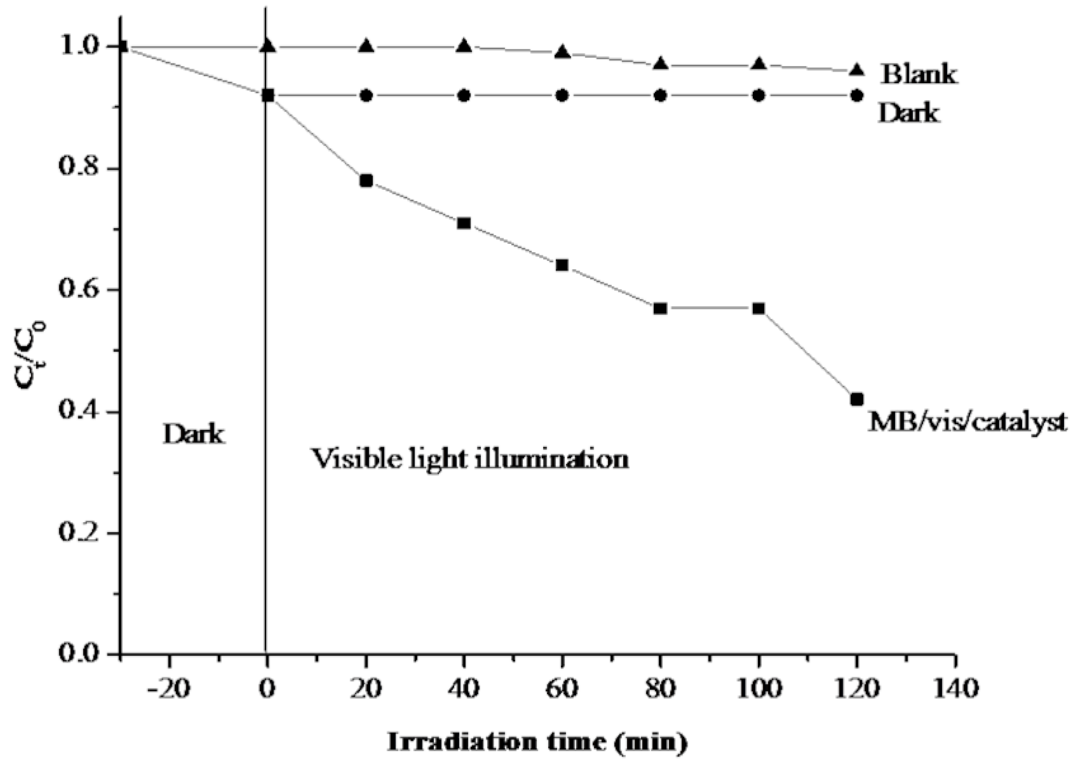

Figure 15. Plot of C_t/C_0 as a function of time for percent degradation of MB under visible light irradiation by keeping the photocatalyst, pH and MB constant (Catalyst = 0.1 g, pH = 8, MB = 10 ppm and λmax = 664 nm

4.4.7. Effect of Scavengers

To investigate the mechanism for photodegradation of the MB, influence of active species such as superoxide radical ($\cdot O_2^-$), hole (h^+) and hydroxyl radical ($\cdot OH$) in the process was studied. Different scavengers were employed individually to remove the corresponding active

species so that the function of different active species in the photodegradation process based on the change of photocatalytic conversion of MB was understood. The rate of photodegradation efficiency of MB is found to be 28.57%, 33.33%, 50%, when $AgNO_3$, CH_3O/H_2O and $NaHCO_3$ scavengers are employed respectively and 57.14% in the absence scavengers. The plot of degradation efficiency of MB in absence and presence of different scavengers with the same amount of photocatalyst (0.1 g) is presented in Figure 16. The scavengers used in this study were $NaHCO_3$ for h^+, CH_3O/H_2O for ·OH and $AgNO_3$ for superoxide radical ($\cdot O_2^-$) (Liu *et al,* 2011). The presence of $AgNO_3$ and CH_3OH influenced more the performance of the photocatalyst evidencing the prominent role played by hydroxide and superoxide radicals in the degradation process.

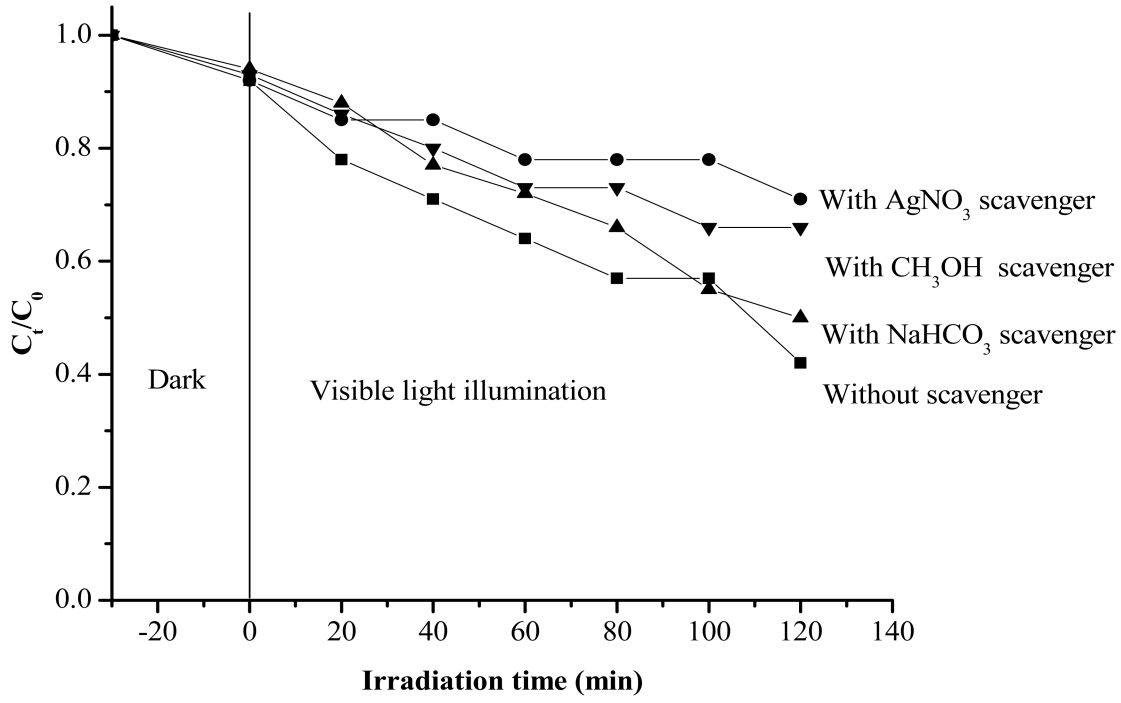

Figure 16. Plot of C_t/C_0 as a function of time for photocatalyzed degradation of MB dye under visible light irradiation in the absence and presence of different scavengers (photocatalyst = 0.1 g, MB = 10 ppm and PH = 8)

4.5. Real Sample Treatment Under Visible Light Irradiation

The real sample from Bahirdar textile share campany, was treated using the selected photocatalyst, titanium(IV) tungstomolybdate, under optimized conditions and visible light irradiation. It was conducted by taking 100 mL of the sample of waste water in 250 mL beaker by adjusting its pH at 8.0. Then 0.1 g of TTM was added in to the solution and the suspension was kept in the dark for 30 minute with continuous stirring to make sure the establishment of adsorption/desorption equilibrium. Finally, the suspension was irradiated with visible light upon continuous stirring and its absorbance was measured at 20 minute intervals for 120 minute.

4.5.1. UV-Visible Absorption Spectra of the Real Sample.

UV-visible absorption spectra of the real sample is depicted in Figure 17. One peak was observed in the UV range at λ = 298 nm.

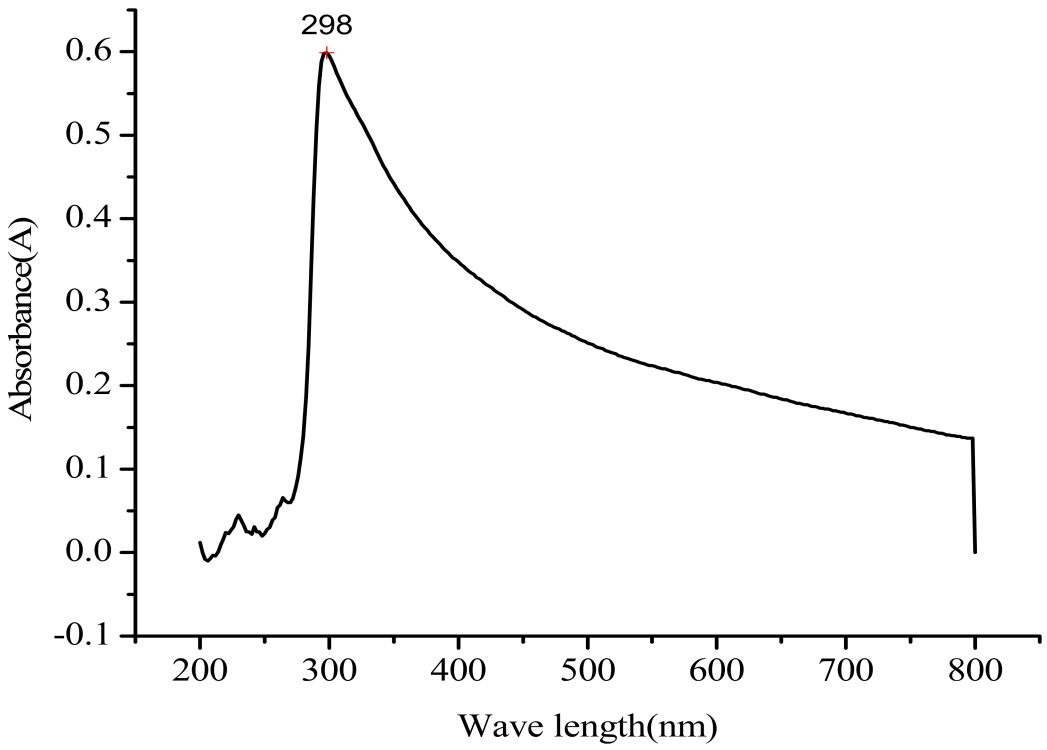

Figure 17. UV– visible absorption spectra of Real Sample

Perce
that
Figur
57.14
real
becau
conc
toget
degra
negat
it wo

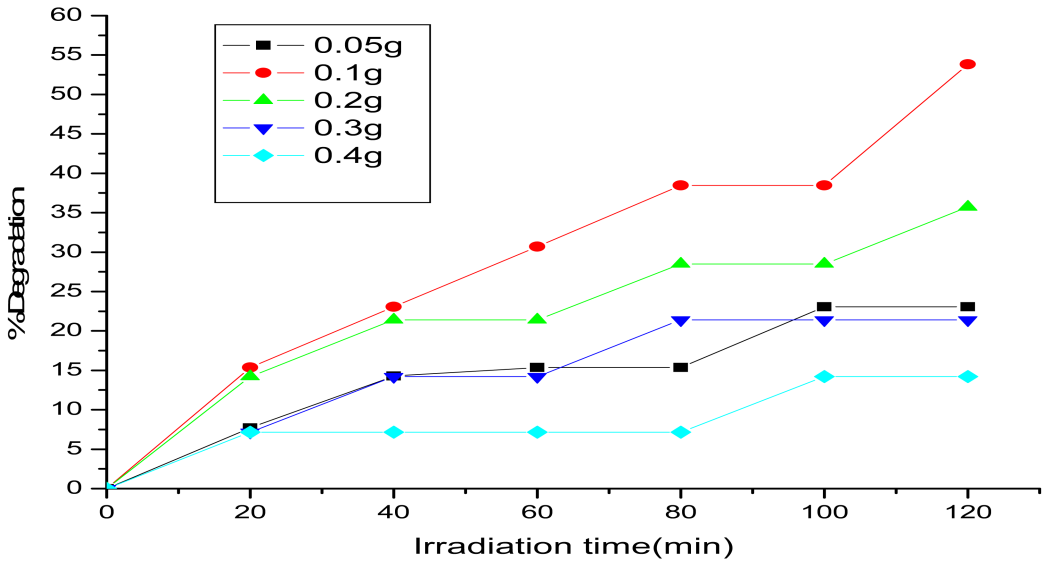

both types of dyes in the real sample reduces the degradation efficiency of the catalyst due to the prevention of visible light from reaching the surface of the catalyst by particles of dyes that results in reduced number of active sites (photogenerated holes and electrons) of the catalyst (Jing *et al.*, 2014). Thus, the degradation efficiency of the catalyst for model sample (MB) was higher than for the real sample.

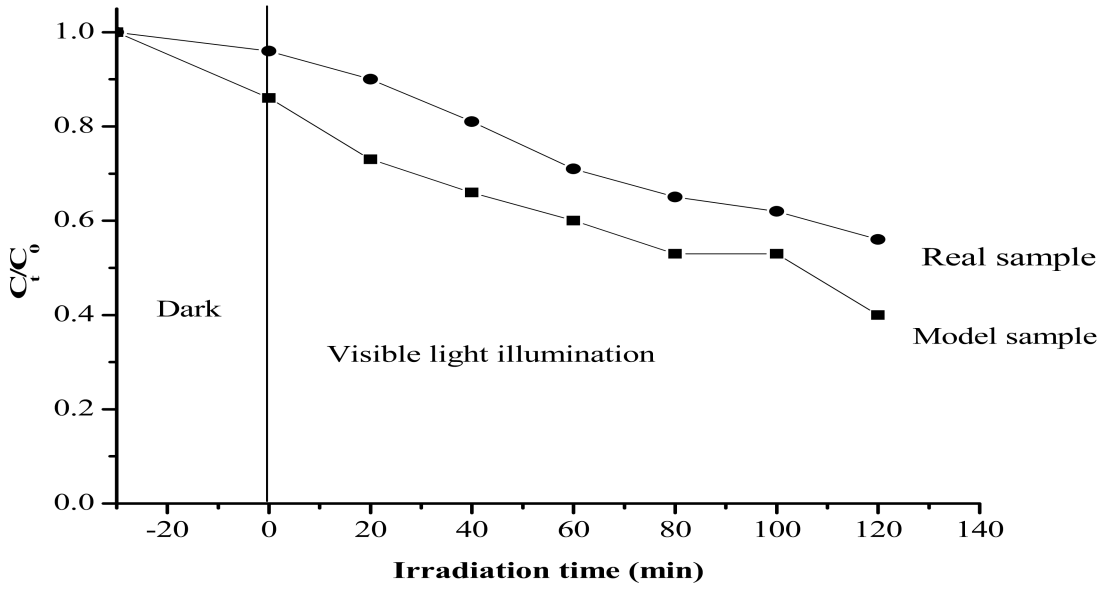

Figure 18. Plot of C_t/C_0 as function of time for real and model sample (MB) under visible light irradiation (photocatalyst = 0.1 g, MB = 10 ppm and PH = 8)

Table 9. Comparison on Photodegradation efficiency of some inorganic ion exchangers towards of methylene blue

S. No	Ion exchange Materials	Percent degradation (%)	Refences
1	supported-ZnO-Fe_2O_3-MnO_2	93	Tedla *et al.,* 2015
2	Pectin–thorium (IV) tungstomolybdate	76	Gupta *et al.,* 2013
3	Silver co-doped Zinc oxide / Ag-ZnO	72.4	Samuel *et al*., 2014
4	Zinc oxide / ZnO	56.2	Samuel *et al*., 2014
5	Titanium(IV) tungstomolybdate	57.14	Present work

4.6. Antimicrobial Activities of the as-Synthesized Photocatalyst

Inhibition zones produced by the as-Synthesized Photocatalyst is presented in Figure 20. In this case 1, 2 and 3 represent the Photocatalyst against the studied bacteria at concentrations of 150 µg/mL,100 µg/mL and 50 µg/mL respectively, whereas 4 and 5 represent deionized water and commercially available drug Chloramphnicol respectively. It was clearly observed that TTM acts as strong antibiotics against Gram-negative bacteria (*Salmonella thyphei* and *Escherichia coli*) than Gram-positive bacteria (*Staphylococcus aureus* and *Streptococcus*) bacteria. Order of antimicrobial activities of TTM against the studied bacteria is:

Salmonela thyphei > *Escherichia coli* > *Staphylococcus aureus* > *Streptococcus.*

The antimicrobial efficiency of TTM was evaluated using Gram-negative (*Escherichia coli*, *Salmonela thyphei*) and Gram-positive (*Streptococcus*, *Staphylococcus auras*) bacteria (Wang *et al.,* 2010): The effect of photocatalyst concentrations on bacterial inhibition is indicated on Table 10. In this case, the photocatalyst with concentrations 150 µg/mL, 100 µg/mL and 50 µg/mL have showed inhibition zones on the studied bacteria to a different extent. Furthermore, the order of inactivation follows 150 µg/mL > 100 µg/mL > 50 µg/mL. This evidences that the photocatalyst with 150 µg/mL has high performance than 100 µg/mL and 50 µg/mL indicating that as concentration increase, the antimicrobial activities of the photocatalyst against the selected bacteria increases. This result confirmed that as concentration increase the number of reactive species that can bind to the surface increases. Consequently, bacterial cells that adhere to the surface of the photocatalyst react with the free radicals causes the loss of membrane integrity (Gogniat *et al.,* 2006). As can be seen from table 10, the performance of the TTM is relatively low as compared to the reference drug, Chloramphnicol. The results of average inhibition zones of TTM at different concentration, deionized water and Chloramphnicol on different bacteria is depicted on Table 10.

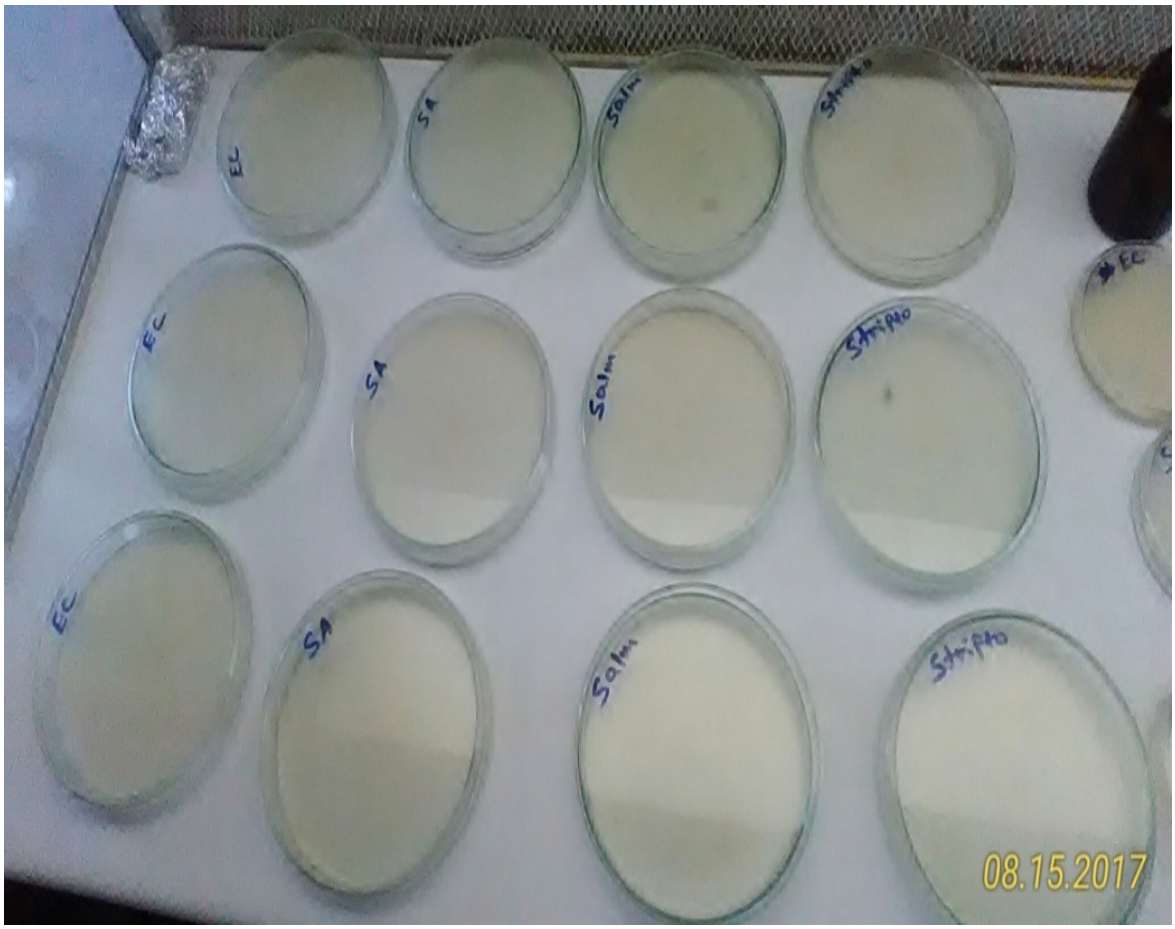

Figure 19. Antibacterial test for visible light irradiation (without photocatalyst)

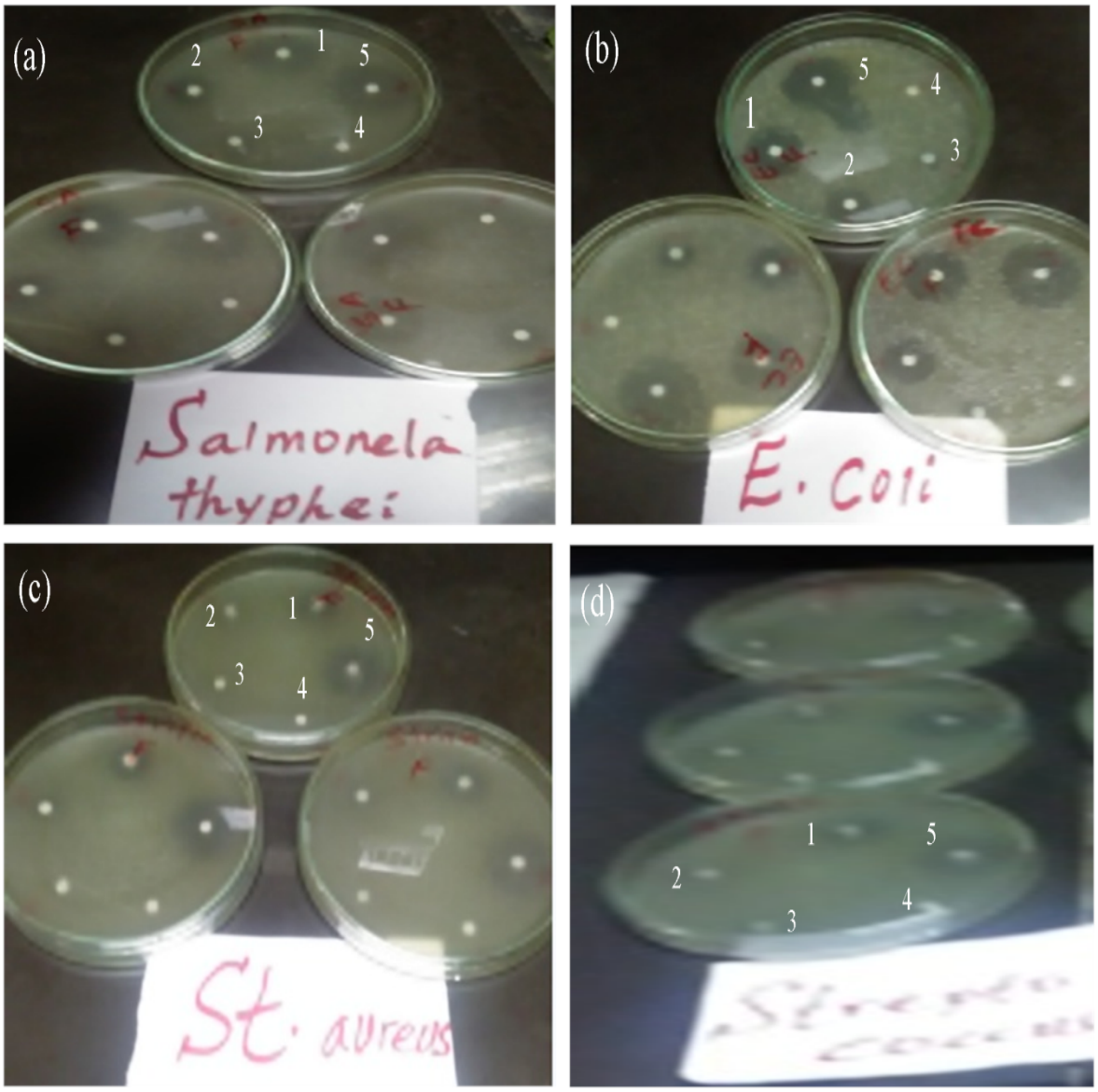
(a)
1
2
5
3
4
Salmonela thyphei
(b)
5
4
1
2
3
E. Coli
(c)
2
1
5
3
4
St. aureus
(d)
1
5
2
4
3

Figure 20. Inhibition zones of as-synthesized nanoparticle against both Gram-negative (*Salmonella thyphei*(a) and *Escherichia coli* (b)) and Gram-positive (*Staphylococcus aureus*(c) and *Streptococcus* (d)) bacteria in the presence of visible light irradiation. Where, 1 = 150 µg/mL, 2=100 µg/mL, 3 = 50 µg/mL of TTM, 4 = Deionized water and 5 = Reference Drug (Chloramphnicol)

Table 10. Inhibition Zones produced by different concentrations of TTM against both Gram-positive (*Staphylococcus aureus* and *Streptococcus*) and Gram-negative (*Escherichia coli* and *Salmonella thyphei*) bacteria (n = 3, mean ± SD)

Bacteria	**Gram positive bacteria**						**Gram negative bacteria**					
	Staphylococcus aureus (µg/ mL)			***Streptococcus*** (µg/ mL)			***Escherichia coli*** (µg/ mL)			***Salmonella thyphei*** (µg/ mL)		
Antibiotics	50	100	150	50	100	150	50	100	150	50	100	15
(TTM)	14.33±2.51	18.33±2.07	29.67±0.98	9.33±0.49	14.00±1.47	24.00±1.16	19.33±0.49	25.17±0.68	30.17±0.92	20.00±0.45	27.33±1.12	33.
DIW	-			-			-			-		
Chloramph	150 µg/mL			150 µg/mL			150µg/mL			150 µg/mL		
nicol	37.67 ± 0.49			33.83±0.68			41 ± 1.16			46.83 ± 2.25		

5. SUMMARY, CONCLUSION AND RECOMMENDATIONS

5.1. Summary and Conclusion

In this study, an inorganic cation exchanger: nano-sized titanium(IV) tungstomolybdate was synthesized, characterized and evaluated for its cation exchange capacity (CEC) and other properties. The exchanger had been synthesized through urea assisted homogenous precipitation technique by mixing 0.1 M sodium tungstate dihydrate, 0.1 M sodium molybdate dihydrate, 0.1 M titanium isopropoxide ($Ti(OCH(CH_3)_2)_4$ in (250 mL of ethanol, 1 mL of concentrated HCL 2 mL of deionized water) and 0.3 M urea at the mixing volume ratio of 1 : 2 : 2 : 3 respectively. To convert the as-synthesized amorphous cation exchanger into its nanocrystalline form, the sample was calcined at 300, 400, 500 and 600 C for 3 h. The sample calcined at 600 C showed the highest IEC. Finally, the sample calcined at the temperature of 600 ^{o}C was characterized and evaluated. The batch equilibrium method was applied to determine the IEC of the exchanger. The IEC of the as-synthesized sample was found to be 1.34 meq/g for Na^{+} ion. The XRD study revealed that the exchanger pre-calcined at 600 ^{o}C for 3 h had particle size: 41.35 nm, as calculated using Scherer formula. The FTIR spectrum approved that the synthesized exchanger is associated with adsorbed water and hydroxyl group in addition to the major functional groups, Mo−O, Ti−O and W−O. The nano-sized cation exchanger sample had the specific surface area of 4.416 ± 0.003 m^2/g as determined by BET adsorption isotherm equation. Based on separation factor α, as a guiding measures binary separations have been carried out for four sets of metal ions : Pb(II)-Ni(II), Pb(II)-Cu(II), Cr(III)-Ni(II) and Cr(III)-Cu(II). Photocatalytic activities and antimicrobial efficiency of the nanomaterial were evaluated using Methylene blue as a model organic pollutant and Gram-negative and Gram-positive bacteria as test microbes respectively.

5.2. Recommendations

The study showed that the exchanger has the promising features regarding its synthesis, characterization and other properties for which the exchanger was evaluated. Therefore, the author recommends researchers to pay attention for advancing further research on the following particular areas.

- To investigate further about the effects or influences of the exchanger's particle size (morphological study) and thermal property that influences the ion exchange process using DSC.
- To determine the separation capacity of the exchanger for treatment of radio-nucleotides other than uranium like Th(IV), Eu(III), Ce(III) *etc.*
- To apply the same material for practical industrial waste water treatment as well as radioactive waste treatment.
- To regenerate as well as to work on safe disposal of the spent ion exchanger.
- To further improve exchanger's ion exchange capacity by modifying its specific surface area.
- To improve thermal stability, chemical resistivity, distribution coefficient *etc*. through devising new preparation methods or coupling with organic substances.
- To further investigate the CEC and other behaviors of the exchanger calcined at temperatures higher than 600 ^{o}C.
- To investigate the application of nano-titanium(IV) tungstomolybdate on other dyes
- Involve photocatalytic parameters on antibacterial activity, such as the influence of time, and effect of light intensity.
- To investigate cytotoxic effects and the bactericidal effects of nano-titanium(IV) tungstomolybdate nanoparticle against different types of bacteria.

6. REFERENCES

Abd El-Latif, M.M. and El kady, M.F. 2008. Developing & characterization of a new zirconium vanadate ion exchanger and its novel organic- inorganic hybrid. *Journal of Applied Sciences Research*, 4 : 1–13.

Abd El-Latif, M.M. and El kady, M.F. 2011. Synthesis, characterization and evaluation of nano-zirconium vanadiate ion exchanger by using three different techniques. *Material Research bulletin,* 46 : 105–118.

Abdullah, M., Low, C. and Matthews, R.W. 1990. 'Effects of common inorganic anions on rates of photocatalytic oxidation of organic carbon over illuminated titanium dioxide. *Journal of Physical Chemistry, 94* : 6820–6825.

Abou-Mesalam, M.M. 2003. Sorption kinetics of copper, zinc, cadmium and nickel ions on synthesized silico-antimonate ion exchanger. *Colloids and Surfaces A: Physicochemical and Engineering Aspects*, 225 : 85–94.

Ahmed, S., Rasu, M.G., Wayde, N., Martens, R.B. and Hashib, M.A. 2010. Heterogeneous photocatalytic degradation of phenols in wastewater: A review on current status and developments. *Desalination,* 261 : 3–18.

Airoldi, C. and Oliveira, S.F. 1992. Preparation, properties and ionic exchange behavior of titanium (IV) arsenophosphate. *Journal of the Brazilian Chemical Society*, *3* : 47 – 51.

Akhtar, A., Khan, M.D.A. and Nabi, S.A., 2015. Synthesis, characterization and photolytic degradation activity of poly-o-toluidine–thorium (IV) molybdophosphate cation exchanger: Analytical application in metal ion treatment. *Desalination*, *361* : 1-12.

Akieh, M.N., Lahtinen, M.,Visnen, A. and Sillan,M. 2008. Preparation and characterization of sodium iron titanate ion exchanger and its application in heavy metal removal from waste waters. *Journal of Hazardous Materials*, 152 : 640–647.

Anischik, V.M., Borisenko, V.E., Zhdanok, S.A., Tolochko, N.K. and Fedosyuk, V.M. 2008. Nanomaterials and Nanotechnologies. Minsk: Izd. BGU. nano-zirconium vanadiate ion exchanger by using three different techniques. *Material Research bulletin,* 46 : 105–118.

Bamlaku Semagn, Tesfahun Kebede, Isabel D and Abi Taddesse. 2016. Synthesis, characterization and analytical application of polyaniline tin(IV) molybdophosphate composite with nanocrystalline domains, *Reactive and Functional Polymers*, 98 : 17–23.

Banerjee, S., Gopal, J., Muraleedharan, P., Tyagi, A.K. and Raj, B. 2006. Physics and chemistry of photocatalytic titanium dioxide: Visualization of bacterial activity using atomic force microscopy. *Current Science*, 90 : 1378–1383.

Belver, C., Bellod, R., Stewart, S.J., Requejo, F.G. and Fernandez Garcia, M. 2006. Nitrogen containing TiO_2 photocatalysts: Part 2. Photocatalytic behavior under sunlight excitation, *Applied Catalysis B: Environmental,* 65 : 309–314.

Bezabih Kelta, Abi Taddesse, Yadav, O.P., Isabel D and Mayoral, A., 2017. Nano-crystalline titanium (IV) tungstomolybdate cation exchanger: Synthesis, characterization and ion exchange properties. *Journal of Environmental Chemical Engineering*, *5* : 1004-1014.

Binti-Jubri, Z., Bin Hussein, M. Z., Yahaya, A. H. and Zainal, Z. 2007. Zinc-aluminum pamoate nanocomposite using direct co-precipitation and ion-exchange methods. *The Malaysian Journal of Analytical Sciences,* 11 : 48–56.

Bloomfield, S.F. 2002. Significance of biocide usage and antimicrobial resistance in domiciliary environments. *Journal of Applied Microbiology,* 92 : 144–157.

Bonetta, S., Bonetta, S., Motta, F., Strini, A. and Carraro, E. 2013. Photocatalytic bacterial inactivation by TiO_2 coated surfaces. *AMB Express*, 59 : 1–8.

Borisenko, V.E., and Tolochko N.K., 2008. Nanotechnologies : Stages of Development. *Naukai innovatsii (Minsk),* 12 : 66–68.

Bradley, D. C. 1989. Metal alkoxides as precursors for electronic and ceramic materials, *Chemical Reviews*, 89 : 1317–1322.

Buasri, A., Singpracha, C., Junprasert, C. and Chotwatcharin, T. 2008. Synthesis and Characterization of Sol-Gel Processed Organic/ Inorganic Composite Materials. *Kasetsart Journal (* Nature and Science*)* 42 : 367 –372.

Bushra, R., Shahadat, M., Ahmad, A., Nabi, S.A., Umar, K., Oves, M., Raeissi, A.S. and Muneer, M., 2014. Synthesis, characterization, antimicrobial activity and applications of polyaniline Ti(IV) arsenophosphate adsorbent for the analysis of organic and inorganic pollutants. *Journal of hazardous materials*, *264* : 481-489.

Byarugaba, D.K. 2004. A view on antimicrobial resistance in developing countries and responsible risk factors. *Internal Journal of Antimicrobial Agents,* 24 : 105–110.

Byrappa, K. and Yoshimura, M. 2001. Handbook of hydrothermal technology: A technology for crystal growth and materials processing. *Noyes Publications/William Andrew Publishing, LLC., USA,* 891.

Cao J., Luo, B.D., Lin, H.L., Xu, B. and Chen, S. 2012. Aluminum salt slag characterization and utilization. Review article, *Journal of Hazardous Materials*, 217–218 : 1–458.

Chand, S., Seema, Arti and Chahal, C.V. 2011. Synthesis, characterization and ion exchange properties of a new ion exchange material: Bismuth(III) iodophosphate. *Recent Research in Science and Technology*, 3 : 01–08.

Chen, C., Liu, J., Liu, P. and Yu, B. 2011. Investigation of photocatalytic degradation of methyl orange by using nano-sized ZnO catalysts. *Advances in Chemical Engineering and Science*, 1: 9–14.

Chira, R., Bhattacharjee, D. and Abhijit, N. 2011. *Physical Science Technology*, 7 : 122.

Chong, M.N. Jin, B., Chow, C.W.K., and Saint, C. 2010. Recent developments in photocatalytic water treatment technology: *A review, Water Research*, 44 : 2997–3027.

Claudia, M., Felinto, F.C., Paganini, P.P.and Abrao, A. 2005. Inorganic ion exchanger based on tin oxide for heavy metals separation. International Nuclear Atlantic Conference Santos, SP, Brazil, August 28 to September 2, 2005, *Institute of Brasilian Nuclear Energy,* 8.

Clive, E.H. 1994. Discovery and structure of solid inorganic ion exchange materials. *John wiley & sons, inc., New York,* 277.

Cohen, Z.Z., Eiden, C.and Lober, M.N. 1986. Evaluation of pesticide in ground water, in: W.Y. Gerner (Ed.), ACS Symp. Ser. 315, *American Chemical Society, Washington, DC,* 170–196.

Coleman, H.M., Marquis, C.P., Scott, J.A., Chen, S.S. and Amal, R., 2005. Bactericidal effects of titanium dioxide-based photocatalysts. *Chemical Engineering Journal*, 113 : 55–63.

Davis, R.J., Gainer, J.L., Neal, G.O. and Wu, I.W. 1994. Photocatalytic Decolorization of Waste water Dyes. *Water Environment Research,* 66 : 50–53.

Dhara, S., Sarkar, S., Basu, S.and Chattopadhyay, P. 2009. Separation of the 90Sr - 90Y pair with cerium(IV) iodotungstate cation exchanger. *Applied Radiation and Isotopes*, 67 : 530–53.

Ditta, I.B., Stelle, A., Liptrot, C., Tobin, J., Tyler, H., Yates, M.H., Sheel, D.W. and Foster, H.A. 2008. Photocatalytic antimicrobial activity of thin surface films of TiO_2, CuO and

TiO_2/CuO dual layers on *Escherichia coli* and bacteriophage T4. *Applied microbiology and biotechnology*, 79 : 127–133.

Dorfner, K. 1991. Ion exchangers. Walter de Gruvter, Berlin, Germany, 492p.

El-Naggar, I.M., Mowafy, E.A., El-Aryan, Y.F. and Abd El-Wahed, M.G. 2007. Sorption mechanism for Cs^{+}, Co^{2+} and Eu^{3+} on amorphous zirconium silicate as cation exchanger. *Journal of Solid State Ionics*, 178 : 741–747.

Epling, G.A. and Lin, C. 2002. Photoassisted bleaching of dyes utilizing TiO_2 and visible light. *Chemosphere*, 46 : *56*1–570.

Fisseha, G. 2010. Synthesis, characterization and analytical application of a new inorganic cation exchanger–titanium (IV) tungstomolybdate. *An Academic Thesis Submitted to the School of Graduate Studies, Department of Chemistry, Haramaya University, Ethiopia*.

Fletcher, P. and Townsend, R.P. 1981. Natural zeolites and their applications. *Journal of Chemical Society, Faraday Trans,* 2 : 77–955.

Gebru Hailemariam., Abi Taddesse., Kaushik, J. and Yadav, O.P. 2003. Distinct antimicrobial effects of synthesized ZnS, Ag-N co-doped ZnS and ZnS-Fe_2O_3 composite particles against some pathogenic bacteria strains. *Journal of surface science and Technology,* 29 : 1–20.

Gebru Hailemariam., Yadav, O.P. and Abi Taddesse. 2013. Green Synthesis of Silver Nanoparticles and their antibacterial activities. *Journal of surface science and Technology,* 29 : 47–66.

Gogniat, G., Thyssen, M., Denis M., Pulgarin, C. and Dukan, S. 2006. The bactericidal effect of TiO_2 photocatalysis involves absorption onto catalyst and the loss of membrane integrity. *FEMS microbiology letters*, 258 : 18–24.

Goncalves, M.S.T., Oliveira-Campos, A.M.F., Pinto, E.M.M.S., Plasencia, P.M.S. and Queiroz, M.J.R.P. 1999. Photochemical Treatment of Solutions of Azo Dyes Containing TiO_2. *Chemosphere*, 39 : 781–786.

Gupta, A.P., Verma, G.L.and Saiqa Ikram. 2000. Studies on a new heteropolyacid-based inorganic ion exchanger; zirconium (IV) selenomolybdate. *Journal of Reactive & Functional Polymers*, 43 : 33–41.

Gupta, V.K., Agarwal, S., Pathania, D., Kothiyal, N.C. and Sharma, G., 2013. Use of pectin–thorium (IV) tungstomolybdate nanocomposite for photocatalytic degradation of methylene blue. *Carbohydrate polymers*, 96 : 277–283.

Gupta, V.K., Singh, P.and Rahman, N. 2005. Synthesis, characterization, and analytical application of zirconium(IV) selenoiodate, a new cation exchanger. *Analytical and bioanalytical chemistry*, 381 : 471–476.

Haghi, M. Hekmatafshar, M. Janipour, M.B. Gholizadeh, S.S Faraz, M.K. Sayyadifar, F. and Ghaedi, M. 2012 . "Antibacterial effect of TiO_2 nanoparticles on pathogenic strain of E. coli." *International Journal of Advanced Biotechnology and Research*, 3: 621–62.

Harjula, R. and Lehto, J. 1987. Separation of cesium from nuclear waste solutions with hexa cyano ferrate(II) and ammonium phosphomolybdate. *Solvent Extraction and Ion Exchange*, 5 : 343.

Helfferrich, F. 1962. Ion exchange: McGraw-Hill Series in Advanced Chemistry. *New York: McGraw-Hill Book Company, Inc.,* 322.

Hendricks, N.R. 2005. The application of high capacity ion exchange adsorbent material, synthesized from fly ash and acid mine drainage, for the removal of heavy and trace metals from secondary co-disposed process waters. *Academic Thesis Presented to University of Western Cape, South Africa,* 287.

Hong, R.Y., Li, J.H., Chen, L.L., Liu, D.Q., Li, H.Z., Zheng, Y. and Ding, J., 2009. Synthesis, surface modification and photocatalytic property of ZnO nanoparticles. *Powder Technology*, *189* : 426–432.

Hu, E. L., Shaw, D. T., Siegel, R. W., Cox, D. M., Goronkin, H., Jelinski, L., Koch, C. C., Mendel, J. and Roco, M. C. 1999. R&D status and trends in nanoparticles, nano-structured materials,and nanodevices (final report). WTEC Panel on Nanostructure Science and Technology. Loyal college, Maryland, USA.

Ibanez, J.A., Litter, M.I. and Pizarro, R.A. 2003. Photocatalytic bactericidal effect of TiO_2 ON Enterobacter cloacae Comparative study with other Gram (-) bacteria. *Journal of Photochemistry and photobiology A: Chemistry*, 157 : 81–85.

Ilisz, I., Laszlo, Z. and Dombi, A. 1997. Investigation of the photodecomposition of phenol in near-UV-irradiated aqueous TiO_2 suspensions. I. Effect of charge-trapping species on the degradation kinetics. *Applied Catalysis A: General,* 180 : 25–33.

International Atomic Energy Agency (IAEA), 2002. Application of ion exchange processes for the treatment of radioactive waste and management of spent ion exchangers. Technical report series No. 408. Vienna, Austria, 115p.

Jian-Xiao, L.V., Ying, C., Guo-hong, X., Ling-yun, Z. and Su-fen, W., 2011. Decoloration of methylene blue simulated wastewater using a UV-H_2O_2 combined system. *Journal of Water Reuse and Desalination*, *1* : 45-51.

Jing, L., Wang, D. Wang, B., S.Li, Xin, B., H.Fu and Sun, J. 2006. Effects of noble metal modification on surface oxygen composition, charge separation and photocatalytic activity of ZnO nanoparticles. *Journal Molecular Catalysis A: Chemical,* 244 : 193–200.

Juang, R.S., Kao, H.C. and Chen, W. 2006. Column removal of Ni(II) from synthetic electroplating wastewater using a strong acid resin. *Separation and Purification Technology,* 49 : 36–42.

Kamat, P.V. and Meisel, D. 2002. Nanoparticles in advanced oxidation processes. *Current Opinion in Colloid & Interface Science,* 7 : 282–287.

Karkare, M.M. 2014. Choice of precursor not affecting the size of anatase TiO_2 nanoparticles but affecting morphology under broader view. *International Nano Letters*, *4* : 111.

Katsumata, H., Hayashi, T., Taniguchi, M., Suzuki, T.and Kaneco, S. 2014. Highly efficient visible lightdriven AgBr/Ag_3PO_4 hybrid photocatalysts with enhanced photocatalytic activity *Materials Science in Semiconductor Processing*, 25 : 68–75

Khider, K., Akretche, D.E. and Larbot, A. 2004. Purification of water effluent from a milk factory by ultrafiltration using Algerian clay support. *Desalination,* 167 : 147–151.

Kiros Guesh, Abi Taddesse and Yadav, O.P. 2013. Effect of Ag-N co-doping in Nanosize TiO_2 on Photocatalytic Degradation of Methyl Orange Dye. *Journal of surface science and Technology,* 29 : 1–14.

Komarneni and Katsuki, H. 2002. Nanophase materials by a novel microwave hydrothermal Process. *Journal of Pure and Applied Chemistry*, 74 : 1537–1543.

Kooti, M. and Matturi, L. 2011. Microwave-assisted fabrication of γ-Fe2O3 nanoparticles from tris (acetylacetonato) iron (III). *International Nano Letters,* 1 : 38–42.

Koseki, H., Shiraishi, K., Asahara, T., Tsurumoto, T. and Shindo, H. 2009. Photocatalytic bactericidal action of fluorescent light in a titanium dioxide particle mixture: an in vitro study. *Biomedical Research,* 30 : 189–192.

Kubelka, P.and Munk, F. 1931. Use of diffuse reflectance spectroscopy for optical characterization of unsupported nanostructures. *Journal of Applied Physics*, 98 : 4301.

Kuhn, K.P., Chaberny, I.F., Massholder, K., Stickler, M., Benz, V.W., Sonntag, H.G. and Erdinger, L. 2003. Disinfection of surface by photocatalytic oxidation with titanium dioxide and UVA light. *Chemosphere*, 53 : 71–77.

Lalena, J.N., Cleary, D.A., Carpenter, E.E. and Dean, N.F. 2008. Inorganic materials synthesis and fabrication. *A john wiley & sons, inc., publication, Canada,* 314.

Ledakowicz, S., Solecka, M.and Zylla, R. 1999. Biodegradation, decolourisation and detoxification of textile waste water enhanced by advanced oxidation processes, *Journal of Biotechnology*, 89 : 175–184.

Lee, K., Seo, W. S. and Park, J. T. 2003. *Journal of American Chemical Society*,125 : 3408.

Li, W., Shah, S. I., Sung, M. and Huang, C.P. 2002. Structure and size distribution of TiO_2 nanoparticles deposited on stainless steel mesh. *Journal of* Vocational *Sciences technology* B, 20(6) : 2303–2308.

Linsebigler, A., Lu, G. and Yates, J. 1995. Photocatalysis on TiO_2 surfaces: principle, mechanisms, and selected results. *Chemical Review,* 95 : 735–758.

Liu, L., Lv, J., Xu, G., Wang, Y., Xie, K. Chen, Z.and Wu, Y. 2013. Uniformly dispersed CdS nano particle sensitized TiO_2 nanotube arrays with enhanced visible-light photocatalytic activity and stability. *Journal of Solid State Chemistry,* 208 : 27–34.

Livage, J., Henry, M. and Sanchez, C. 1988 Sol-gel chemistry of transition metal oxides, *Progress in Solid State Chemistry*, 18 : 259–341.

Lodha, B. and Chaudhari, S. 2007. Optimization of Fenton-biological treatment scheme for the treatment of aqueous dye solutions. *Journal of Hazardous Materials*, *148* : 459–466.

Lovestam, G., Rauscher, H., Roebben, G., Klüttgen, B.S., Gibson, N., Putaud, J. and Stamm, H. 2010. Considerations on a definition of nanomaterial for regulatory purposes. *Europian Joint Research Centre (*EU*JRC) Reference Reports*, 40.

Mahmood, T., Saddique, M.T., Naeem, A., Westerhoff, P., Mustafa, S. and Alum, A. 2011. Comparison of different methods for the point of zero charge determination of NiO. *Industrial & Engineering Chemistry Research*, *50* : 10017–10023.

Maness, P.C., Smolinski, S., Blake, D.M., Huang, Z., Wolfrum E.J. and Jacoby,W.A. 1999. Bactericidal activity of photocatalytic TiO_2 reaction: toward an understanding of its killing mechanism. *Applied and environmental microbiology*, 65 : 4094–4098.

Matsunaga, T.R., Tomoda, Y., Nakajima, T. and Wake, H. 1985. Photochemical Sterilization of Microbial Cells by Semiconductor Powders. *FEMS microbiology letters*, 29 : 211–214.

Michael, J.W., Hawker, C.J., and Wooley, K.L. 2009. The advantages of nanoparticles for PET, focusing on molecular imaging. *Journal of nuclear medicine,* 50 : 1743–1746.

Mohanty, R.P. 2012. Fabrication and characterization of metal organic framework based membrane. Doctoral *Dissertation, National Institute of Technology, Rourkela.*

Moller, T. 2002. Selective crystalline inorganic materials as ion exchangers in the treatment of nuclear waste solutions. *An Academic Dissertation Presented to University of Helsinki,* 66.

Munnik, P., Petra, E., de Jongh and Krijn, P. *2015. Inorganic* nanocomposite. *Journal of Environmental Chemical Engineering*, 3 : 1586–1591.

Nabi, S.A. and Khan, A.M. 2006. Synthesis, ion exchange properties and analytical applications of stannic silicomolybdate: Effect of temperature on distribution coefficients of metal ions. *Reactive & Functional Polymers,* 66 : 495–508.

Nabi, S.A. and Naushad, M. 2008. Synthesis, characterization and analytical applications of a new composite cation exchanger cellulose acetate-Zr(IV) molybdophosphate. Colloids and Surfaces A: *Physicochemical and Engineering Aspects*, 316 : 217–225.

Nabi, S.A. and Shalla, A.H. 2009. Synthesis, characterization and analytical application of hybrid; Acrylamide zirconium (IV) arsenate a cation exchanger, effect of dielectric constant on distribution coefficient of metal ions. *Journal of Hazardous Materials*, 163 : 657–664.

Nabi, S.A., Naushad, M. and Inamuddin, 2007a. Synthesis and characterization of a new inorganic cation exchanger Zirconium(IV) tungstomolybdate: Analytical application for metal content determination in real sample and synthetic mixture. *Journal of Hazardous Materials*, 142 : 404–411.

Nabi, S.A., Shalla, A.H., Khan, A.M. and Ganie, S.A. 2007b. Synthesis, characterization and analytical applications of titanium(IV) molybdosilicate: A cation ion-exchanger. *Journal of colloids and surfaces A*, 302 : 241–250.

Nabi, S.A., Usmani, S.and Rahman, N. 1996. Synthesis, characterization and analytical applications of an ion-exchange material: zirconium(IV) iodomolybdate. *In Annales de chimie Science Materials,* 21 : 521–257.

Naushad, M. 2009. Inorganic and composite ion exchange materials and their applications (Review). *Ion Exchange Letters*, 2 : 1–14.

Nawar, N. and Hosny, N.M. 2000. Synthesis, spectral and antimicrobial activity study of o-aminoacetophenone o-hydroxybenzoylhydrazone complexes. *Transition Metal chemistry*, 25 : 1–8.

Nibret Alebel., Yadav, O.P., Isabel D and Abi Taddesse. 2015. "Cr-N co-doped ZnO nanoparticles: synthesis, characterization and photocatalytic activity for degradation of thymol blue." *Bulletin of the Chemical Society of Ethiopia,* 29 : 247–258.

Okeke, I.N., Laxminarayan, R., Bhutta, Z.A., Duse, A.G., Jenkins, P., O'Brien, T.F., Pablos-Mendez, A. and Klugman, K.P. 2005. Antimicrobial resistance in developing countries. Part I: recent trends and current status. *The Lancet infectious diseases*, *5*(8) : 481–493.

Pathania, D., Sharma, G., Kumar, A. and Kothiyal, N.C., 2014. Fabrication of nanocomposite polyaniline zirconium (IV) silicophosphate for photocatalytic and antimicrobial activity. *Journal of Alloys and Compounds*, *588* : 668–675.

phuruangrat,A.,Ham, D.J., Thongtem, S., and Lee, J.S. 2009. Electrochemicalhydrogen evolution over MoO_3 nanowires produced by microwave-asssisted hydrothermal reaction. Electrochemical commun., 11: 1740–1743.

Pouretedal, H.R., Norozi, A., Keshavarz, M.H. and Semnani, A. 2009. Nanoparticles of zinc sulfide doped with manganese, nickel and copper as nanophotocatalyst in the degradation of organic dyes. *Journal of Hazardous Material,* 162 : 674–681.

Raichur, A. 2009. Nano scale water treatment needs innovative engineering. *Science and Development Network, Indian,* 6 : 141.

Rao,V.S.,Rao, K.S., Rao, M.N. and Bora1, U.S., 2011. Studies on the surface characterization of newly prepared activated kaza's carbons. *Asian journal of biochemical and pharmaceutical research,* 2 : 567–584.

Rashad, M.M., Elsayed, E.M., Moharam, M.M., Abou-Shahba, R.M. and Saba, A.E. 2009. Structure and magnetic properties of $Ni_xZn_{1-x}Fe_2O_4$ nanoparticles prepared through co-precipitation method. *Journal of Alloys and Compounds*,486 : 759–767.

Rauf, M.A. and Ashraf, S.S. 2009. Application of Advanced Oxidation Processes (AOP) to dye degradation an overview. In: Arnold R. Lang (Ed.), Dyes and Pigments: New Research. *Nova Science Publishers, Inc*., 70 : 231–345.

Robinson, T., McMullan, G. and Marchant, R.P. 2001. Nigam and Remediation of dyes in textile effluent: a critical review on current treatment technologies with a proposed alternative, *Bio resource Technology,* 77 : 247–255.

Sakthivela, S.B., Neppolianb, M.V., Shankarb, B., Arabindoob, M., Palanichamyb, V. and Murugesanb, V. 2003. Solar photocatalytic degradation of azo dye: comparison of photocatalytic efficiency of ZnO and TiO_2, *Solar Energy Materials* and *Solar Cells*, 77 : 65–82.

Saquib ,M. and Muneer, M. 2003.TiO_2 mediated photocatalytic degradation of triphenyl methane dye (gentian violet), in aqueous suspensions. *Dyes and Pigments,* 56 : 37–49.

Sasirekha, N., Rajesk, B. and Chen, W. 2009. Synthesis of TiO_2 sol in a neutral solution using $TiCl_4$ as precursor and H_2O_2 as an oxidizing agent. Thin Solid Films, 518 : 36–42.

Sears, W.G. 1956. Determination of Specific surface area of colloidal silica by titration with sodium hydroxide. *Journal of Analytical chem*istry, 28 : 1981–1983.

Sepehrian, H., Ahmadia, S.J., Waqif-Husainb, S., Faghihianc, H. and Alighanbari, H. 2010. Adsorption studies of heavy metal ions on mesoporous aluminosilicate, novel cation exchanger. *Journal of Hazardous Material,* 176 : 252–256.

Sharma, G., Pathania, D., Naushad, M. and Kothiyal, N.C., 2014. Fabrication,characterization and antimicrobial activity of polyaniline Th(IV) tungstomolybdophosphate nano composite material: efficient removal of toxic metal ions from water. *Chemical Engineering Journal*, *251* : 413–421.

Siddiqi, Z.M. and Pathania, D. 2003. Titanium(IV) tungstosilicate and titanium(IV) tungstophosphate: two new inorganic ionexchangers. *Journal of Chromatography A*, 987 : 147–158. `

Siddiqui, W.A. and Khan, S.A. 2007. Synthesis, characterization and ion exchange properties of zirconium(IV) tungstoiodophosphate, a new cation exchanger. *Bulletin of Materials Science*, 30 : 43–49.

Silva, G.L.J.P, Da Silva, M.L.CP. and Cartano, T. 2002. Preparation and characterization of hydrous zirconium oxide formed by homogeneous precipitation. *Material Research*, *5* : 149–153.

Singh, N.J. and Tandon, S.N. 1979. Zirconium arsenophosphate as an ion exchanger. *Journal of Radioanalytical Chemistry, 49 : 195–203.*

Srinivasan, C. and Somasundaram, N., 2003. Bactericidal and detoxification effects of irradiated semiconductor catalyst, TiO_2. *Current Science*, 1431-1438.

STARA (Society for Technology and Action for Rural Advancement), 2010. Access to safe water for the bottom of pyramid: strategies for disseminating technology research benefits. Secondary Research Report, November 2010. Department for International Development, East Kilbride, Canada, 38p.

Sumej, C. and Raveendran, B. 2008. Synthesis and characterization of tin(IV) phenyl phosphonate in nano form. *Bulletin of Materials Science*, 31 : 613–617.

Sun, J., Qiao, L. Sun, S. and Wang, G. 2008. Photocatalytic degradation of Orange G on nitrogendoped TiO_2 catalysts under visible light and sunlight irradiation. *Journal of Hazard. Mater.* 155 : 312–319.

Tachikawa, S., Noguchi, A., Tsuge, T., Hara, M., Odawara, O. and Wada, H. 2011. Optical properties of ZnO nanoparticles capped with polymers. *Journal of Hazardous Materials*, *4* : 1132–1143.

Tang, H., Berger, H., Schmid, P. E. and Levy, F. 1993. Solid State Communication, 87 : 847–850.

Tang, J., Zou, Z., Yin, J. and Ye, J. 2003. Photocatalytic degradation of methylene blue on $CaIn_2O_4$ under visible light irradiation. *Chemical Physics Letters,* 382 : 175–179

Tedla Haileyesus., Isabel Diaz., Tesfahun Kebede and Abi Taddesse. 2015. Synthesis, characterization and photocatalytic activity of zeolite supported $ZnO/Fe_2O_3/MnO_2$ nanocomposites, *Journal of Environmental Chemical Engineering,* 3 : 1586–1591.

Tesfay Wolderufael., Yadav, O.P. and Abi Taddesse. 2013. Synthesis, characterization and photocatalytic activity of AgN-codoped ZnO nanoparticles towards methyl red degradation. *Bulletin of the Chemical Society of Ethiopia*, 27 : 221–232.

Thakkar, R. and Chudasama,U. 2009. Synthesis and characterization of zirconium titanium phosphate and its application in separation of metal ions. *Journal of Hazardous Materials*, 172 : 129–137.

Thembela, H., Mohan, M., Mbhuti H. and Yvani, D. 2006. Nanotechnology, water development, global dialogue on nanotechnology and the poor: opportunities and risk. *Meridian Institute, Chennai.*

Toyo zawa, Y. 1976. *Journal of* Luminescence, 13.

Toyozawa,Y. 1980. In relaxation of elementary Excitation (Edited by R. Kubo & E. Hanamura),p.3 Springer-Verlag, *New York*.

Wang X., Hu, Z., Chen, Y., Zhao, G., Liu, Y. and Wen, Z. 2009. A novel approach towards high performance composite photocatalyst of TiO_2 deposited on activated carbon. *Applied Surface Science*, 255 : 3953–3958.

Wang, B.,. Li, Q., Wang, W., Li, Y. and Zhai, J. 2010. Preparation and characterization of Fe^{3+}doped TiO_2 on fly ash cenospheres for photocatalytic application. *Applied Surface Science.* 257 : 3473–3479.

Wong, C.C. and Chu, W. 2003. The direct photolysis and photocatalytic degradation of alachlor at different TiO_2 and UV sources. *Chemosphere, 50* : 981–987.

Xu, S. and Lin, M. C. 2007. Theoretical study on the kinetics for OH reactions with CH_3OH and C_2H_5OH. *Proceedings of the Combustion Institute,* 31 : 159-166

Yavari, R., Ahmadi, S.J., Huang, Y.D., Khanchi, A.R., Bagheri, G. and He, J.M. 2009. Synthesis, characterization and analytical application of a new cation exchanger – titanium(IV) molybdophosphate. *Talanta*, 77 : 1179–1184.

Yavuz, C.T., Mayo, J.T., Yu, W.W., Prakash, A., Falkner, J.C., Yean, S., Cong, L., Shipley, H. J., Kan, A., Tomson, M., Natelson, D. and Colvin, V.L. 2006. Low-field magnetic separation of monodisperse Fe_3O_4 nanocrystals. *Science,* 314 : 964–967.

Zainal, Z., Hui, L.H., Hussein, M.Z. and Ramli, I. 2005. Removal of dyes using immobilized titanium dioxide illuminated by fluorescent lamps. *Journal of Hazardous Materials,* 125 : 113–120.

Zhang, L., Huang, T., Zhang, M., Guo X. and Yuan, Z. 2008. Studies on the capability and behavior of adsorption of thallium on nano-Al_2O_3. *Journal of Hazardous Materials,* 157 : 352–357.

Zhen, M. and Francisco, Z. 2006. Heterogeneous Catalysis by Metals in Encyclopedia of Inorganic Chemistry, John Wiley. doi:10.1002/0470862106.ia084.

7. APPENDIX

7.1. Appendix Tables

Appendix Table 1. Ion exchange capacity and Physical appearance of the as-synthesized exchanger and the exchanger samples calcined at varying temperatures for 3 h with different volume ratios

TIP	ST	SM	UR	Calcination Temperature (^{0}C)	Tim (hr)	IEC (meq.g^{-1})	Appearance of the sample after calcination
4	1	1	3	300	3	0.38	Dark gray
4	1	1	3	400	3	0.42	Dark gray
4	1	1	3	500	3	0.46	Dark Greene
4	1	1	3	600	3	0.56	Light gray
2	1	2	3	300	3	0.62	Dark gray
2	1	2	3	400	3	0.77	Dark gray
2	1	2	3	500	3	1.02	Gray
2	1	2	3	600	3	1.34	Light gray

Note:- TIP - Titanium isopropoxide, UR-Urea, SM-sodium molybdate dihydrate,
ST - Sodium tungstate dihydrate.

Appendix Table 2. C_t/C_0 as a function of time by varying the photocatalyst keeping both dye initial concentration and pH constant under visible light irradiation (MB = 10 ppm, pH = 8)

Time (min)	C_t/C_0 0.05 g	C_t/C_0 0.1 g	C_t/C_0 0.2 g	C_t/C_0 0.3 g	C_t/C_0 0.4 g
-30	1	1	1	1	1
0	0.92	0.92	0.93	0.93	0.93
20	0.85	0.78	0.8	0.86	0.86
40	0.78	0.71	0.73	0.80	0.86
60	0.78	0.64	0.73	0.80	0.86
80	0.78	0.57	0.66	0.73	0.86
100	0.71	0.57	0.66	0.73	0.80
*120	0.71	0.42	0.60	0.73	0.80

*% Degradation = 28.57 %, 57.14 %, 40 %, 26.66 %, 20 % respectively.

Appendix Table 3. Plot of pH_f versus pH_{f-i} for Nano-titanium(IV)tungstomolybdate

S. No	pH_i	pH_f	pH_{f-i}
1	0.64	0.89	0.25

2	1.07	1.40	0.33
3	2.51	2.83	0.32
4	3.59	3.91	0.32
5	4.85	5.03	0.18
6	6.07	6.12	0.05
7	6.87	6.76	-0.11
8	8.16	8.08	-0.08
9	8.87	8.78	-0.09
10	10.16	10.01	-0.15

Appendix Table 4. C_t/C_0 as a function of time by varying the pH of the solution keeping both dye and photocatalyst amounts constant with visible irradiation (MB = 10 ppm, Catalyst = 0.1 g)

Time (min)	C_t/C_0 PH = 2	C_t/C_0 PH = 4	C_t/C_0 PH = 6	C_t/C_0 PH = 8	C_t/C_0 PH = 10	C_t/C_0 PH = 12
-30	1	1	1	1	1	1
0	0.94	0.95	0.95	0.90	0.94	0.94
20	0.88	0.81	0.77	0.80	0.78	0.88
40	0.83	0.76	0.68	0.70	0.68	0.82
60	0.77	0.66	0.59	0.60	0.63	0.76
80	0.72	0.61	0.54	0.50	0.57	0.70
100	0.66	0.57	0.54	0.50	0.52	0.64
*120	0.55	0.52	0.49	0.40	0.47	0.53

*% Degradation = 44.44 %, 47.61 %, 50 %, 60 %, 52.63 %, 47.05 % respectively.

Appendix Table 5. C_t/C_0 as a function of time by varying the amounts of initial dye concentration keeping both pH and photocatalyst constant with visible irradiation (pH = 8, Catalyst = 0.1 g)

Time (min)	C_t/C_0 10 ppm	C_t/C_0 15 ppm	C_t/C_0 20 ppm	C_t/C_0 25 ppm	C_t/C_0 30 ppm
-30	1	1	1	1	1
0	0.92	0.92	0.92	0.93	0.92
20	0.78	0.85	0.85	0.86	0.84

40	0.71	0.78	0.85	0.8	0.84
60	0.64	0.71	0.78	0.8	0.84
80	0.64	0.71	0.78	0.8	0.84
100	0.5	0.57	0.71	0.73	0.76
*120	0.42	0.50	0.64	0.66	0.69

*% Degradation = 57.14 %, 50 %, 35.71 %, 33.33 %, 30.76 %, respectively.

Appendix Table 6. C_t/C_0 as a function of time for percent degradation of MB dye under visible light irradiation by keeping the photocatalyst, pH and MB concentration constant (Catalyst = 0.1 g, pH = 8, MB = 10 ppm and λmax = 664 nm)

Time (min)	C_t/C_0 MB-visible-catalyst	C_t/C_0 MB-dark-catalyst	C_t/C_0 MB-visible
-30	1	1	1
0	0.92	0.92	1
20	0.78	0.92	1
40	0.71	0.92	1
60	0.64	0.92	0.99
80	0.57	0.92	0.97
100	0.57	0.92	0.97
*120	0.42	0.92	0.96

*% Degradation = 57.14 %, 7.14 %, 4% respectively

Appendix Table 7. C_t/C_0 as a function of time for percent degradation of MB in the absence and presence of different scavenges (Catalyst = 0.1 g, MB = 10 ppm and PH = 8) under visible light

Time (min)	C_t/C_0 Without scavenger	C_t/C_0 With $AgNO_3$ scavenger	C_t/C_0 With CH_3OH scavenger	C_t/C_0 With $NaHCO_3$ scavenger
-30	1	1	1	1
0	0.92	0.92	0.93	0.94
20	0.78	0.85	0.86	0.88
40	0.71	0.85	0.80	0.77
60	0.64	0.78	0.73	0.72
80	0.57	0.78	0.73	0.66

100	0.57	0.78	0.66	0.55
*120	0.42	0.71	0.66	0.50

*% Degradation = 57.14 %, 28.57%, 33.33%, 50%, respectively

Appendix Table 8. C_t/C_0 as a function of time for percent degradation of Real sample vs Model sample with visible light irradiation (MB = 1ppm, Catalyst = 0.1 g and pH = 8)

Time(min)	C_t/C_0 Model sample	C_t/C_0 Real Sample
-30	1	1
0	0.86	0.93
20	0.73	0.87
40	0.66	0.78
60	0.60	0.69
80	0.53	0.63
100	0.53	0.60
*120	0.40	0.54

*% Degradation = 57.14 %, 43.75 %

Appendix Table 9. Diameters of Zones of inhibition produced by different concentrations of TTM against both Gram-positive (*Staphylococcus aureus* and *Streptococcus*) and Gram-negative (*Escherichia coli* and *Salmonella thyphei*) bacteria (n = 3, where n indicates diameters of zones of inhibition in mm)

Bacteria		Gram positive						Gram negative					
		Staphylococcus aureus (µg/ mL)			*Streptococcus* (µg/ mL)			*Escherichia coli* (µg/ mL)			*Salmonella thyphei* (µg/ mL)		
Antibiotics (TTM)	Tr.№	50	100	150	50	100	150	50	100	150	50	100	150
	1	17.5	21	31	10	13	25.5	20	26	29	20.5	28.5	33
	2	12	16.5	29	9	16	23.5	19	24.5	31	20	27.5	33.5
	3	13.5	17.5	29	9	13	23	19	25	30.5	19.5	26	33
Average		14.33	18.33	29.67	9.33	14.00	24.00	19.33	25.17	30.17	20.00	27.33	33.17
Max.		17.50	21.00	31.00	10.00	16.00	25.50	20.00	26.00	31.00	20.50	28.50	33.50
Min.		12.00	16.50	29.00	9.00	13.00	23.00	19.00	24.50	29.00	19.50	26.00	33.00
SD		2.51	2.07	0.98	0.49	1.47	1.16	0.49	0.68	0.92	0.45	1.12	0.25
	1	-	-	-	-	-	-	-	-	-	-	-	-
DIW	2	-	-	-	-	-	-	-	-	-	-	-	-
	3	-	-	-	-	-	-	-	-	-	-	-	-
	Tr.№	150 µg/mL			150 µg/mL			150 µg/mL			150 µg/mL		
Chloram-phnicol	1	38			33			40			44.5		
	2	38			34			42.5			49.5		
	3	37			34.5			40.5			46.5		
Average		37.67			33.83			41			46.83		
Max.		38			34.5			42.5			49.5		
Min.		37			33			40			44.5		
SD		0.49			0.68			1.16			2.25		

7.2. Appendix Figure

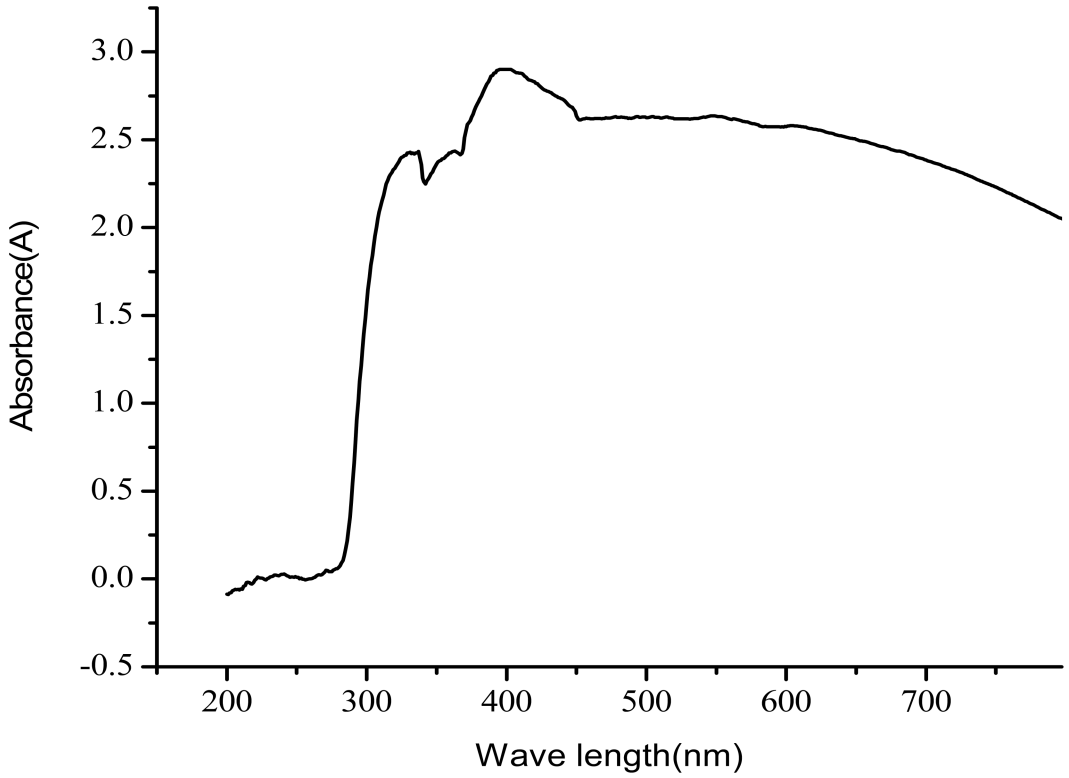

Appendix figure 1. UV-Visible absorption spectra of the as-synthesized titanium(IV) tungstomolybdate